Megakaryocyte Whole Genome Duplication and Cancer Evolution



Antonio Rodríguez Romera

Balliol College

University of Oxford

A thesis submitted for the degree of

Doctor of Philosophy

Michaelmas term, 2025

Supervised by Prof. Beth Psaila and Prof. Ketan J Patel

Abstract

Whole genome duplication (WGD) occurs rarely in healthy human cells but frequently in cancer. Uniquely, megakaryocytes (MKs) achieve functional maturation through repeated rounds of endomitosis and WGD, reaching ploidies up to 128N. How MKs tolerate such extensive genome amplification —and with what consequences— has been unclear. By deeply interrogating the biology of healthy MKs, I show that polyploid MKs accumulate DNA damage and exhibit marked chromosomal instability (CIN), yet continue to cycle through successive WGDs despite an intact p53 pathway. Consequently, after each WGD round, MKs adopt a transcriptional programme marked by inflammatory signalling, likely due to cGAS–STING activation via cytosolic DNA sensing. Critically, MKs preferentially engage the non-canonical NF-κB pathway while avoiding type I interferon and senescence programmes, an adaptation to CIN previously described in tumour cells.

Mechanistically, I identified ANKRD26 as a central determinant of WGD tolerance. During megakaryopoiesis, ANKRD26 is selectively repressed, preventing detection of centrosome amplification, PIDDosome assembly, and p53 activation. In patients with a rare inherited thrombocytopenia, in which mutations in the 5'-UTR region of ANKRD26 block this repression, ANKRD26 overexpression reinstates the tetraploid checkpoint in maturing MKs, constraining their polyploidization, and resulting in inefficient platelet production. Extending these insights, analyses of >1000 cancer cell lines revealed that downregulation of the ANKRD26–PIDDosome axis commonly accompanies polyploidisation, suggesting a shared strategy between MKs and tumours for tolerating centrosome amplification after WGD. This highlights how understanding unusual aspects of rare cell types can be of broad relevance to human physiology.

Acknowledgements

First, I would like to thank my primary supervisor, Beth Psaila, for her unwavering support, for the opportunity to join the project that forms this thesis, and for making the ever-challenging DPhil experience so enjoyable. I am also grateful to my secondary supervisor, Ketan Patel, for his insightful guidance.

Thank you to Alan Cantor for stopping at my poster at the Gordon Research Conference in 2022 and offering a fruitful collaboration from which I have learned so much. I would like to thank the many collaborators who made this thesis possible —especially Stefan Constantinescu, Harsh Goyal, and Neil Morgan- for their support, and the WIMM principal investigators, Ross Chapman, Jim Hughes, and Hashem Koohy, for insightful conversations about my project.

Thanks to my funders: the Medical Research Council, the Clarendon Fund, and the Foley-Béjar Fund; for supporting my studies at the University of Oxford and Balliol College.

I am most grateful to the incredible members of the Psaila and Mead labs, past and present, for their invaluable help and for making me love science even more than when I started. Thank you, Abs, for always having a moment to talk about our shared love of megakaryocyte biology. To Natalie, Yuqi, Zoë, Ramy, and Rupen, among many others, thank you for the laughs and support during the toughest times. And to Camelia, for being the best science and gym buddy.

Thanks to Simone, Brynelle, Anna María, Luca, and Claire for being the best companions during my time in the UK; I will always appreciate your long-lasting friendship. To my housemates, Andrew and Sharvi, thank you for your support and the many fun dinners.

Lastly, to my partner, Guopeng Chen, whose kindness and selfless support (and Lao Gan Ma fried rice) were all I needed after long days of failed experiments in the lab.

A mi hermano, José, el otro Dr. Rodríguez Romera, y a mis padres, Carmen y Antonio, por las largas conversaciones por videollamadas que sirvieron para mantener un trozo de mi hogar cerca de mí durante todo este tiempo.

This thesis is dedicated to all of you.

Declaration

I declare that this thesis is entirely my own work, and except where otherwise stated, describes my own research.

Contents

List of Figures **xi**

List of Tables **xiv**

Abbreviations **xv**

1 Introduction **1**

1.1 The Origin And Functions of Megakaryocytes 2

1.1.1 Embryonic And Foetal Megakaryopoiesis 2

1.1.2 Adult Megakaryopoiesis 3

1.1.3 Platelet Production 6

1.1.4 Megakaryocytes Are More Than Just Platelet-producing Cells 8

1.2 Whole Genome Duplication, a Blessing And a Curse 10

1.2.1 Physiological Routes to Scheduled Polyploidy 10

1.2.2 Physiological Whole Genome Duplication 13

1.2.3 Megakaryocyte Whole Genome Duplication: Multiple Paths to Multiple Ploidies 17

1.2.4 Pathological Alterations of Megakaryocyte Ploidy 19

1.2.5 Inappropriate Use of Doubled Genomes: WGD And Cancer 21

1.3 Consequences of Whole Genome Duplication 22

1.3.1 The Burden of Multiple Genomes 22

1.3.2 Mechanisms of Ploidy Control 24

1.4 Hypotheses And Aims 26

2 Materials And Methods **28**

2.1 Cell Line Work 29

2.1.1 Cell Line Maintenance 29

2.1.2 Virus Work 29

2.1.3 Generation of Isogenic Tetraploid Clones by Cytokinesis Failure 30

2.1.4 In Vitro Cell Line Drug Treatments 31

2.2 Human Induced Pluripotent Stem Cells 31

2.3 Human Samples 31

2.4 Isolation of Megakaryocytes From Mouse Bone Marrow 32

2.5 In Vitro Differentiation of Megakaryocytes 33

2.5.1 Megakaryocyte Differentiation From Primary Mouse cKIT+ Cells 33

2.5.2 MK Differentiation From Primary Human Haematopoietic Stem And Progenitor Cells 34

2.5.3 MK Differentiation From Human Induced Pluripotent Stem Cells 34

2.6 Flow Cytometry Analysis 35

2.6.1 Antibody Staining for Flow Cytometry 35

2.6.2 DNA Content Analysis by Flow Cytometry 36

2.6.3 EdU Incorporation Assay by Flow Cytometry 36

2.7 Fluorescence-Activated Cell Sorting 37

2.8 Imaging Analysis 37

2.8.1 Immunofluorescence 37

2.8.2 Live Cell Imaging 39

2.9 Imaging Flow Cytometry 39

2.10 Molecular Biology 40

2.10.1 Reverse Transcription Quantitative PCR 40

2.10.2 Single Cell RNA Sequencing Analysis of In Vitro Megakaryopoiesis by SmartSeq-3 40

2.10.3 Single Cell Whole Genome Sequencing 42
2.11 Single Cell RNA Sequencing Data Processing 44
2.11.1 Data Pre-processing 44
2.11.2 Data Analysis 44
2.11.3 Cell Cycle Analysis 45
2.11.4 Pathway Analysis 45
2.11.5 Trajectory Analysis 46
2.12 Single Cell Whole Genome Sequencing Analysis 46
2.13 Cancer Cell Line Encyclopedia Analysis 47
2.14 Statistical Analysis 47

3 Impact of Whole Genome Duplication on Megakaryocyte Genome Integrity 48
3.1 Introduction 48
3.1.1 Genomic Integrity in Scheduled Polyploidy 49
3.1.2 DNA Damage in Megakaryocytes 50
3.1.3 Chapter Aims 51
3.2 Results 52
3.2.1 Megakaryocytes Accumulate DNA Damage 52
3.2.2 Primary Polyploid Megakaryocytes Are Genetically Unstable 57
3.2.3 Copy Number Alterations on Primary Megakaryocytes . . 59
3.3 Discussion 63

4 Interrogation of the Megakaryocyte Cell Cycle And Tetraploid Checkpoint 66
4.1 Introduction 67
4.1.1 Intrinsic Ploidy Control in Somatic Cells 67
4.1.2 Ploidy Is a Hallmark of Adult But Bot Embryonic Megakaryocytes 69
4.1.3 Inherited Thrombocytopenias Associated With Germline ANKRD26 Mutations 70

4.1.4 Chapter Aims 72
4.2 Results 74
4.2.1 Single Cell RNAseq Allows Accurate Study of The Cell Cycle of Polyploid Cells 74
4.2.2 p53 Remains Functional During Megakaryocyte Polyploidization 81
4.2.3 ANKRD26 is Downregulated During Megakaryocyte Maturation 82
4.2.4 Whole Genome Duplication Tolerance on ANKRD26-Related Thrombocytopenia 84
4.2.5 Whole Genome Duplication Tolerance During Megakaryocyte Ontogenesis 90
4.2.6 Understanding of Ploidy Differences Across Megakaryocyte Ontogeny 90
4.3 Discussion 93

5 Role of ANKRD26 on WGD tolerance in solid tumours 97
5.1 Introduction 98
5.1.1 Genetic Strategies That Favour Whole Genome Duplication in Cancer 98
5.1.2 Therapeutic Strategies for the WGD Status 99
5.1.3 Chapter Aims 100
5.2 Results 102
5.2.1 CCLE Analysis Reveals ANKRD26–PIDDosome Downregulation After Whole Genome Duplication 102
5.2.2 Unscheduled WGD Prevents ANKRD26 Protein Recruitment to The Centrosome in a p53-Dependent Manner . . . 102
5.3 Discussion 106
5.4 Summary Findings 107

6 Conclusions And Future Work **108**

6.1 Outcomes And Broad Implications of This Research 109

6.1.1 Genome Doubling Shapes Megakaryocyte Biology 109

6.1.2 ANKRD26 Plays a Key Role in WGD Tolerance 110

6.2 Limitations of This Work 112

6.3 Future Work 114

6.3.1 Other Forms of DNA Damage on MKs 114

6.3.2 What is the Role of ANKRD26 Dysregulation in the Predisposition to Acute Myeloid Leukaemia? 114

6.3.3 Can we Harness ANKRD26 as a Therapeutic Target for p53 Proficient WGD+ Cells? 116

6.4 Conclusion 117

7 Publications **118**

7.1 Published Articles 119

7.2 Manuscripts in Preparation 120

Appendices

A Supplementary Information **122**

A.1 Supplementary Figures 123

A.2 Supplementary Tables 124

References **130**

List of Figures

1.1 Classical and revised models of haematopoiesis 4
1.2 Polyploidization mechanisms 11
1.3 Megakaryocyte endomitosis 18
1.4 Mechanisms of ploidy control 24

2.1 Selection of TP53 targeting shRNA guides 30
2.2 Optimisation of *in vitro* mouse megakaryocyte differentiation . . 33
2.3 Optimisation of *in vitro* human megakaryocyte differentiation . . 35
2.4 PCR cycle optimisation for SmartSeq-3 41
2.5 Representative cDNA traces of pooled SmartSeq-3 libraries 42
2.6 Representative cDNA traces of pooled scDNAseq libraries 43
2.7 scRNAseq quality control metrics 44

3.1 Validation of imaging flow cytometry for γH2AX detection 53
3.2 γH2AX detection on HEL cells by ploidy 54
3.3 Analysis of γH2AX on iMKs 55
3.4 Study of DNA damage repair dynamics on iMKs 56
3.5 Primary mouse MKs accumulate DNA damage 58
3.6 Evidence of micronuclei formation in primary mouse megakaryocytes 59
3.7 Megakaryocyte micronuclei are a source of DNA damage 60
3.8 Preparation and quality control of single cell whole genome sequencing libraries 61
3.9 Megakaryocytes are aneuploid 62

4.1 Pathways for centrosome amplification control 68

4.2 Common somatic mutations associated with ANKRD26-related thrombocytopenia 71
4.3 *In vitro* derived MKs can complete endomitosis 74
4.4 Experimental layout for *in vitro* study of the polyploid megakaryocyte cell cycle by scRNAseq 75
4.5 Cell cycle correction for polyploid cells 76
4.6 Single Cell characterization of *in vitro* differentiated megakaryocytes 77
4.7 Properties of cycling megakaryocytes 78
4.8 Functional validation of the FUCCI system on UT7 cells 79
4.9 mRNA expression scaling with ploidy 79
4.10 Transcriptional changes of megakaryocytes across ploidy 81
4.11 p53 is functional in megakaryocytes 82
4.12 ANKRD26 is downregulated during megakaryopoiesis 83
4.13 Haematopoietic Stem Cell and Progenitor Cells are expanded in the bone marrow of patients with ANRKD26-RT 85
4.14 ANKRD26 mutant megakaryocytes are low polyploid 85
4.15 Mutations on ANKRD26 activate the p53 pathway 86
4.16 Mutations in ANKRD26 activate the p53 pathway 87
4.17 Mutations in ANKRD26 do not block megakaryocyte lineage commitment. 88
4.18 Sustained ANKRD26 expression triggers p53 on polyploid MKs . 89
4.19 Unlike ANKRD36mut MKs, low ploidy embryonic MKs do not activate p53. 91
4.20 Embryonic MKs do not express ANKRD26 or activate p53 in response to WGD 92

5.1 Cancer Cell Line Encyclopaedia analysis of diploid and polyploid cells 103
5.2 Experimental layout for *in vitro* evolution experiment 104
5.3 Dihydrocytochalasin D treated p53 proficient cells downregulate PIDDosome components 105

5.4 Tetraploid HCT116 cells loose ANKRD26 at their centrosomes in a p53-dependent manner. 105

A.1 p53 does not affect ploidy of *in vitro* differentiated megakaryocytes 123

List of Tables

A.1 Details of human TP53 targeting shRNA guides 124
A.2 Details of reagents utilised for human megakaryocyte differentiation.124
A.3 Reagents used for iPSC-derived megakaryocyte differentiation . . 124
A.4 Details of flow cytometry reagents 125
A.5 i7 and i5 primer sequences 125
A.6 Lysis Buffer reagents used for SmartSeq-3 protocol 126
A.7 Retro-transcription reagents used for SmartSeq-3 protocol 126
A.8 cDNA PCR reagents used for SmartSeq-3 protocol 126
A.9 Tagmentation reagents used for SmartSeq-3 protocol 127
A.10 Library Indexing reagents used for SmartSeq-3 protocol 127
A.11 Reagents used for immunostaining experiments 127
A.12 Secondary antibodies used for immunostaining experiments . . . 127
A.13 Nuclei isolation buffer reagents for scDNAseq. 128
A.14 Nuclei wash buffer reagents for scDNAseq 128
A.15 Nuclei lysis buffer reagents for scDNAseq 128
A.16 PCR reagents for scDNAseq 128
A.17 Manually curated gene sets 129
A.18 Information of ANKRD26 patient samples used 129

List of Abbreviations

AMKL	Acute Megakaryoblastic Leukaemia
AML	Acute Myeloid Leukaemia
ANKRD26	Ankyrin Repeat Domain Containing 26
ANKRD26-RT	ANKRD26-related Thrombocytopenia
CALR	Calreticulin
CCNE1	Cyclin E1
CDK	Cyclin-Dependent Kinase
cDNA	Complementary DNA
cfDNA	Cell Free DNA
CIN	Chromosomal Instability
CNV	Copy Number Variation
DAPI	4',6-diamidino-2-phenylindole
DCD	Dihydrocytochalasin D
DMS	Demarcation Membrane System
DS	Down Syndrome
ecDNA	Extrachromosomal DNA
EdU	Ethynyl-2'-deoxyuridine
EoBaMa	Eosinophils, Basophils, Mast cell
ER	Endoplasmic Reticulum
FACS	Fluorescence-Activated Cell Sorting
FISH	Fluorescence *In Situ* Hybridization

G1	Gap 1
G2	Gap 2
GATA1	GATA binding factor 1
GEF	Guanine Nucleotide-Exchange Factor
HSC	Haematopoietic Stem Cell
HSPC	Haematopoietic Stem/Progenitor Cell
iMK	Induced Pluripotent Stem Cell-Derived Megakaryocyte
iPSC	Induced Pluripotent Stem Cell
LNP	Lipid Nanoparticle
M	Mitosis
MDS	Myelodysplastic Syndrome
MK	Megakaryocyte
MKL1	Megakaryoblastic Leukemia 1
MkP	Megakaryocyte Progenitor
MOI	Multiplicity Of Infection
MPN	Myeloproliferative Neoplasms
MYH10	Mon-Muscle Myosin IIB
PCA	Principal Component Analysis
PF4	Platelet Factor-4
PI	Propidium Iodide
RT-qPCR	Reverse Transcription Quantitative Polymerase Chain Reaction
S	Synthesis
SAC	Spindle Assembly Checkpoint
scRNAseq	Single Cell RNA Sequencing
scWGS	Single Cell Whole Genome Sequencing
TGC	Trophoblasts Giant Cells
TPO	Thrombopoietin

UMAP	Uniform Manifold Approximation and Projection
UTR	Untranslated Region
WGD	Whole Genome Duplication
WPC	Weeks Post Conception

1 Introduction

Contents

1.1 The Origin And Functions of Megakaryocytes 2
1.1.1 Embryonic And Foetal Megakaryopoiesis 2
1.1.2 Adult Megakaryopoiesis 3
1.1.3 Platelet Production 6
1.1.4 Megakaryocytes Are More Than Just Platelet-producing Cells 8
1.2 Whole Genome Duplication, a Blessing And a Curse 10
1.2.1 Physiological Routes to Scheduled Polyploidy 10
1.2.2 Physiological Whole Genome Duplication 13
1.2.3 Megakaryocyte Whole Genome Duplication: Multiple Paths to Multiple Ploidies 17
1.2.4 Pathological Alterations of Megakaryocyte Ploidy 19
1.2.5 Inappropriate Use of Doubled Genomes: WGD And Cancer 21
1.3 Consequences of Whole Genome Duplication 22
1.3.1 The Burden of Multiple Genomes 22
1.3.2 Mechanisms of Ploidy Control 24
1.4 Hypotheses And Aims 26

1.1 The Origin And Functions of Megakaryocytes

Megkaryocytes (*mega-* 'large' *-karyo-* 'cell nucleus' and *-cyte* 'cell') are the largest and rarest cells in the bone marrow, accounting for <0.05% of nucleated cells and measuring 50-100 μm in size [1]. From their differentiation process to platelet production, megakaryocytes (MKs) show unique characteristics that distinguish them from any other cell lineage.

1.1.1 Embryonic And Foetal Megakaryopoiesis

During human development, blood production occurs in three waves, sequentially staged at distinct anatomical sites of the developing embryo. The first (primitive) haematopoietic cells appear in the blood islands of the yolk sac 2-3 weeks post conception (WPC) [2], and is formed by erythroid, MK, and macrophage progenitors rather than fully potent haematopoietic stem cells (HSCs) [3]. A second (pro-definitive) haematopoietic wave occurs just before the onset of circulation and generates the first multipotent haematopoietic progenitors. The first HSCs originate during the third (definitive) wave at the Aorta-Gonad-Mesonephros, 3 to 5 WPC, where they arise from an specialised subset of vascular cells called haemogenic endothelial cells [2, 4]. Migration of cell progenitors to the fetal liver marks the start of definitive haematopoiesis, making the liver the main fetal haematopoietic organ. The final transition to bone marrow haematopoiesis starts at 10 to 12 WPC and culminates shortly after birth when the bone marrow becomes the main and final site of haematopoiesis [4].

The first MKs are found in the human yolk sac as early as 4 WPC, and platelets are first observed in circulation at 8-9 WPC [5]. Recent studies have characterized embryonic and foetal megakaryopoiesis at the single cell level [6]. Notably, human yolk sac MKs showed high expression of the embryonic haemoglobin subunit ϵ1, in line with previous studies suggesting that MK and erythroid lineages might not be completely separated at early developmental stages [6, 7]. Perhaps most interesting, single cell analyses revealed a subset

of haemogenic endothelial cells marked by THBS1 expression that were biased towards MK production, suggesting that MK lineage specification might happen at the haemogenic endothelium [6].

Neonatal MK progenitors are very proliferative and generate MKs at a 10-fold higher rate when compared to adult megakaryopoiesis on *in vitro* settings [8]. Although several factors can alter MK production from HSCs, thrombopoietin (TPO) signalling through its receptor MPL (also know as TPO-R) is the main stimulatory axis for megakaryopoiesis. Neonatal MKs show higher *ex vivo* response to recombinant TPO which has been attributed to higher activity of the transcription factor GATA1 and its known targets, MPL, and Cyclin D1 [8].

Unlike adult MKs, the first platelet-producing cells in the yolk sac are mostly diploid and become progressively more polyploid in the fetal liver (1.7% $\geq$ 8N in the yolk sac, compared to $\sim$ 15% in the fetal liver) [5]. Despite their small size, fetal MKs show classic signs of maturation, including a developed cytoplasmic demarcation membrane system (DMS), and abundant protein-rich granules [8, 9]. However, platelet production by fetal MKs is less efficient compared to adult MKs. This is thought to be, at least partially, due to their lower ploidy [10].

1.1.2 Adult Megakaryopoiesis

Adult megakaryopoiesis starts from the pluripotent HSC. The classic haematopoiesis paradigm represents HSC differentiation as a step-wise model, where pluripotent progenitors become increasingly more committed through a series of discrete steps at the expense of loosing self-renewal potential. This model follows a tree-like structure, where HSCs reside at the root of the tree and are responsible for indirectly repopulating the entire haematopoietic system through the production of oligopotent and unipotent progenitors (Fig. 1.1A).

The ability to study haematopoiesis at the single cell level challenged this model of blood cell production, and the application of single cell multiomic techniques (i.e. transcriptome, epigenome, metabolome or proteome) has shown that HSC maturation is more accurately represented by a continuous differentiation model,

with smooth transitions across cell stages, rather than a discrete multi-step process [11, 12] (Fig. 1.1B).

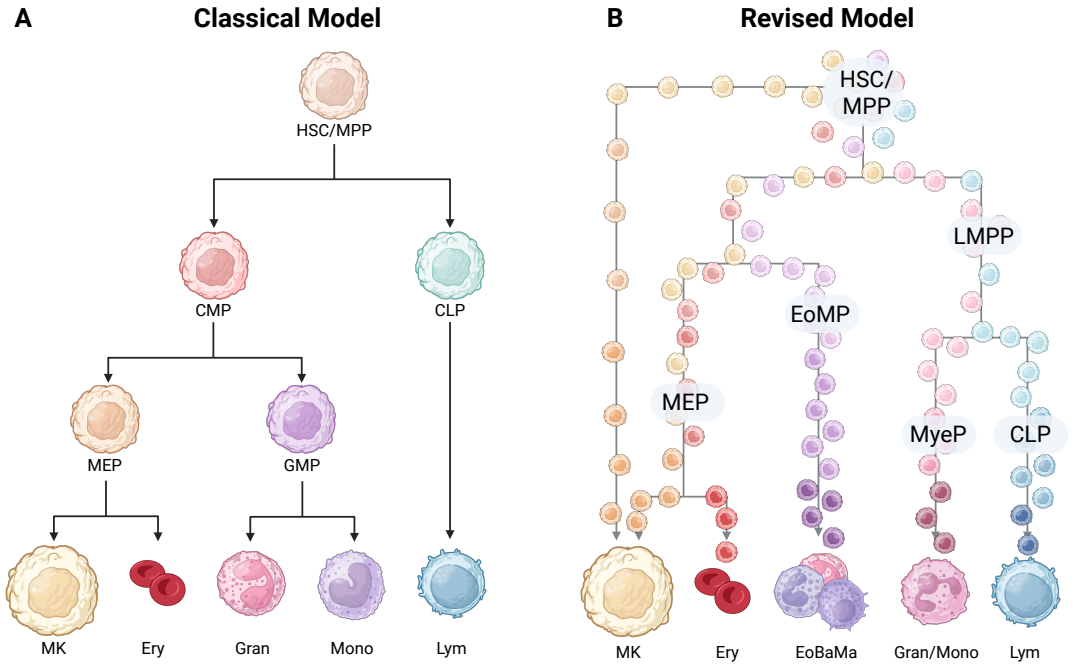


Figure 1.1: Classical and revised models of haematopoiesis. **A**, the classical model describes haematopoiesis as a step-wise process where HSCs become increasingly more committed after each differentiation step. **B**, the current model of haematopoiesis represents HSC differentiation as a continuous process and introduces a direct differentiation route from HSCs to MKs. HSC: haematopoietic stem cell, MPP: multipotent progenitor, CMP: common myeloid progenitor, CLP: common lymphoid progenitor, MEP: myeloid erytrhoid progenitor, GMP: granulocyte-monocyte progenitor, LMPP: lymphoid-myeloid primed progenitor, EoMP: eosinophil-basophil-mast cell progenitor. MyeP: myeloid progenitor. Adapted from [5, 13]. Created in https://BioRender.com.

The first bifurcation step in haematopoiesis delineates two major developmental paths: one giving rise to lympho-myeloid progenitors, and the other to megakaryocyte-erythroid-myeloid progenitors [14]. Along this trajectory, monocyte and neutrophil progenitors diverge from the shared MK-erythroid lineage, while eosinophils, basophils, and mast cells (EoBaMa) remain associated with the erythro-megakaryocytic axis. After separating from EoBaMa cells, the last lineage specification event involves uncoupling of the closely affiliated MKs and erythroid lineages, producing unipotent MK progenitors that will terminally differentiate into MKs [13] (Fig. 1.1B).

In addition to a gradual commitment from HSCs to MKs, an increase body of evidence shows that MK production can happen directly at the HSC level. Fundamental studies performing over 1000 single cell mouse transplants demonstrated that HSCs can stably restore megakaryopoiesis without contributing to any other cell lineage [15]. Follow up work using transposon-based lineage tracing models -which permits the study of naive haematopoiesis *in vivo* avoiding the confounding factors of transplant-based assays [16]- revealed that direct MK differentiation from HSCs might be the preferred route for naive megakaryopoiesis, with little contribution from other trajectories through common progenitors [17]. Importantly, while other cell types shared at least one multi/oligo potent progenitor, direct differentiation from HSC appears to be an exclusive property of MKs [17].

The study of megakaryopoiesis in humans is limited to *in vitro* liquid or semi-solid systems which are inherently biased by the selection of the culture conditions. Also, technical and ethical considerations restrain human *in vivo* studies to xenotransplantation models [13]. Thus, although multiple lines of evidence demonstrate the existence of a direct HSC-MK differentiation path in mice, this remains to be as convincingly proven in normal human haematopoiesis [13]. *In vivo* single cell lineage tracing of unperturbed human haematopoiesis is now possible by following mitochondrial mutations [18, 19] or stochastic epimutations at CpG sites [20]. These methods have revealed HSC lineage biases during healthy young and aged haematopoiesis, but haven not yet been applied to demonstrate the existence of MK-restricted human HSCs. Importantly, these techniques are limited to the study of MK progenitors since fully mature polyploid MKs are too fragile to survive common human sample processing techniques, and platelets do not have a nucleus [13]. Combination of lineage tracing techniques with dedicated methods for MK isolation might help us unpick the role of HSC MK restriction in human adult megakaryopoiesis.

1.1.3 Platelet Production

Once fully matured, MKs are responsible for the sustained production of platelets in a process called thrombopoiesis. In contrast to other cell lineages where, for example, one erythroblast will give rise to a single red cell, it is estimated that one mature MK will produce up to 3000 platelets [21]. This production feat is possible thanks to two main cellular adaptations (1) the development of an intracellular membrane system called the demarcation membrane system (DMS), and (2) the systematic duplication of the MK whole genome without cell division, resulting in polyploidization. The DMS is an elaborate membrane network that takes up the entire cytoplasm of the mature MK, and supplies the large demand for cell membrane required for platelet production. Polyploidization is thought to help the synthesis of platelet components by scaling up the protein production machinery [22]. Importantly, small diploid MKs are also able to produce platelets, albeit at a smaller scale, suggesting that polyploidization is not necessary for platelet formation but is required to sustain the platelet demand [23].

Four distinct and non-exclusive mechanisms for thrombopoiesis have now been proposed: in the classic model, immobilized MKs sitting in the bone marrow sinusoidal vessels extend long microtubule-driven protrusions called pro-platelets into the flowing blood. Subjected to shear forces inside the vascular lumen, these extensions separate from the MK body and break up into smaller fragments known as platelets in the blood stream [21, 24]. Notably, this model highlights the importance of shear forces for thrombopoiesis, and informed the design of better strategies for *in vitro* production of platelets beyond static cell cultures [21].

Alternatively, MKs can engage in "cytoplasmic fragmentation" for thrombopoiesis. On this model, platelets are made within the MK in regions called platelet territories, and are released by rupture of the MK body [25]. This mechanism has also been observed *in vivo* and is thought to be relevant for acute and rapid platelet supply [26].

In later studies, MKs were proposed to generate platelets via membrane budding. Detailed *in vivo* imaging showed that platelets can pinch off directly

from the plasma membrane of "inactive" MKs lacking long pro-platelet extensions [27]. This phenomenon was more frequent than pro-platelet formation, and it was estimated that membrane budding could produce 89% of the platelet mass [27]. However, whether this process is able to produce functional platelets or just microvesicles is still a subject of debate [28, 29].

Most recently, it was suggested that circulating neutrophils can reinforce platelet production by "plucking" on peri-sinusoidal MK extensions in the mouse bone marrow, although the relevance of this process in steady state human thrombopoiesis remains to be elucidated [30, 31].

In most studies, intravital visualization of platelet formation has focused on the bone marrow compartment. However, MKs have been observed outside the bone marrow niche, particularly in the spleen and the lung [32]. Direct visualization of the murine lung vasculature demonstrated that the lung is a site of platelet biogenesis. This study (controversially) suggested that pulmonary thrombopoiesis might contribute to up to 50% of the total platelet production [33]. Follow-up investigations challenged these conclusions, highlighting that the paucity of MKs in perfused murine lungs, and their inability to produce pro-platelets *in vitro* could not justify the production of half of the circulating platelets [34]. Notably, the origin of lung MKs, whether they are trapped in the lung vasculature after migrating from the bone marrow or they are generated *in situ* from tissue resident HSCs (or a combination of the two), is still not known [32].

In summary, thrombopoiesis appears to involve multiple mechanisms and anatomical sites, yet the extent to which each contributes to the total platelet pool remains highly contested. Redundancy is a hallmark of mammalian physiology, especially if the process is essential for life, and several systems might function concurrently to ensure platelet production under physiological and pathological conditions.

1.1.4 Megakaryocytes Are More Than Just Platelet-producing Cells

MKs have been proposed to participate in other processes such as HSC regulation and, more recently, the immune response. A major leap in our understanding of the multifaceted biology of MKs came from the use single cell transcriptional profiling, revealing that MKs don't exist as a uniform population, but instead consist of diverse cell subtypes with specialized functions that span beyond platelet production [35]. However, the extent to which this functional variation represents distinct maturation stages, cell types, or transient phenotypes of the same mature MK rather than functionally distinct cellular subsets is not known.

Megakaryocytes Modulate The Haematopoietic Niche

MKs are rare and sparsely distributed in the bone marrow, yet over 60% of the HSCs reside within 3 cell diameters of an MK [36]. Inside this "niche", MKs induce HSC quiescence through secretion of platelet factor-4 (PF4) and transforming growth factor beta 1 (TGFβ1) [37]. In line with this, direct MK ablation or targeted deletion of TGFβ1 or PF4 results in active HSC cycling and expansion [38, 39]. Importantly, in murine bone marrow transplants, MK-derived IGF1 and IGFBP3 can promote HSC long-term multi-lineage reconstitution, and transplanted HSCs home preferentially near MKs [40]. Therefore, MKs can form an haematopoietic niche that controls HSC proliferation.

Immune Properties of Megakaryocytes

Platelets are the first barrier to form at sites of injury and play key roles in immunity including leukocyte and endothelial activation, promotion of neutrophil extracellular trap formation, and pathogen sensing and clearing [37]. During thrombopoiesis, MKs load platelets with immune receptors and cytokines, however MKs are not just protein production factories for platelets and can utilize these factors themselves to participate in immune responses.

In line with this, MKs express molecules that can modulate the adaptative immunity. This includes CD40L, which stimulates macrophages, B and T cells via its receptor CD40 [37]. Additionally, plasma cells (antibody-producing B lymphocytes) reside closer to MKs in the bone marrow than it would be expected by chance, and MK-derived interleukin 6 can promote plasma cell survival [37].

The role of MKs in immunity was highlighted in recent studies that demonstrated the existence of a dedicated MK sub-population with immune properties in the bone marrow and the lung [41, 42]. This MK subset was substantially different than other MK types identified (i.e. cycling, niche-supporting and platelet-producing MKs). Morphologically, they are significantly smaller and mostly diploid, and transcriptionally they show a monocytic-like mRNA expression program. In the bone marrow, immune MKs are capable of engulfing and digesting bacteria, and stimulate T cell expansion *in vitro* [41]. In the lung, immune MKs express class II major histocompatibility complex, an antigen presenting molecule usually restricted to professional antigen presenting cells (i.e. dendritic cells, macrophages or B cells) and were shown to promote antigen presentation and CD4-T cell activation *in vivo* and *in vitro* [43]. Notably, immune MKs were not able to produce proplatelets upon TPO stimulation *in vitro*, indicating that immune MKs might not be responsible for the immune function of platelets and raising questions regarding whether these small, non-polyploid, non platelet-producing cells should be classified as MKs at all [41].

The origin of immune MKs is still debated. Their transcriptional and morphological properties indicate that they might develop from a separate, monocyte-related, differentiation path [44]. However, direct transplantation of bone marrow MKs into the lung of healthy mice showed that exposure to non-aseptic hyperoxic environments can induce an immune phenotype in MKs [43]. On the other hand, immune MKs were also observed on fetal megakaryopoiesis and could be produced *in vitro* from human embryonic stem cells, suggesting a developmental origin [6]. Further studies, perhaps applying lineage tracing

techniques, might shed some light on the developmental relationships between the newly described MK subtypes.

1.2 Whole Genome Duplication, a Blessing And a Curse

Whole Genome Duplication (WGD) refers to the balanced replication of the entire chromosome makeup, producing cells with two or more copies of each chromosome. Hence, this process is fundamentally different to aneuploidy where cells gain or loose only some chromosomes (or parts of them). Although polyploidization is developmentally programmed in MKs and other cell types, aberrant (i.e. non-programmed- WGD) is the commonest copy number alteration in cancer, and it fuels oncogenesis [45]. On this section I will discuss the scheduled and unscheduled paths towards WGD and the role of tetraploidy in physiological and pathological contexts.

1.2.1 Physiological Routes to Scheduled Polyploidy

How does a cell become polyploid? Under physiological conditions, WGD is achieved by programmed adaptations of the cell cycle - such as endomitosis, endocycling or cytokinesis failure - or the controlled fusion of diploid cells. During development, or in response to challenges such as tissue regeneration, cells can employ one or more of these mechanisms to achieve ploidy (Fig.1.2).

Cell Fusion

Cell fusion can happen between the same cell type (homotypic) or between different cell types (heterotypic) and is key in tissue development and homeostasis. Examples for this include the fusion of myoblasts to form myotubules in the muscle, monocyte/macrophage fusion to generate osteoclasts, the formation of syncytiotrophoblasts via cytotrophoblast fusion in the placenta or the fusion between sperm and oocyte during fertilization, which constitutes the major heterotypic cell fusion event. This process is generally mediated by proteins

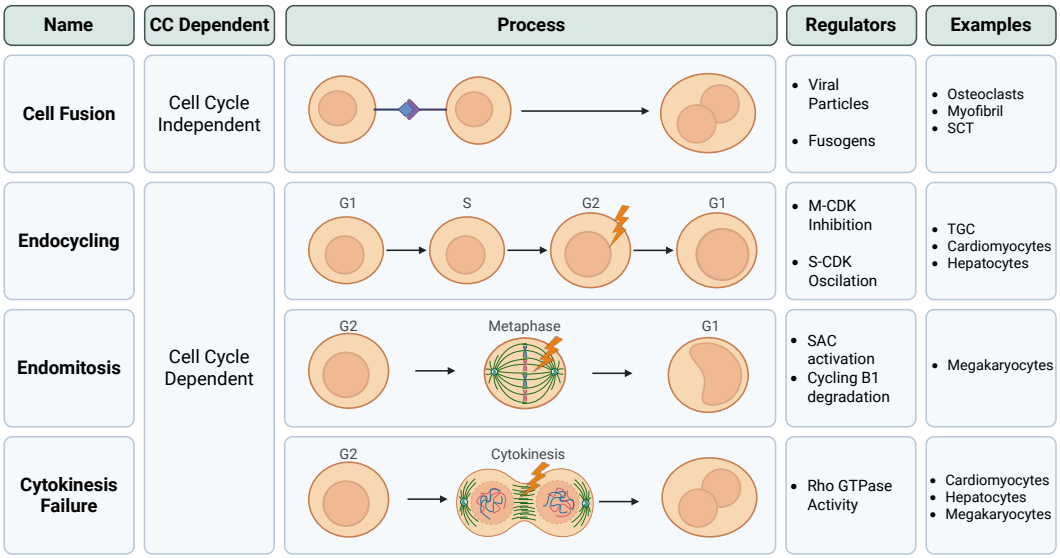


Figure 1.2: WGD can be achieved via several mechanisms which can be dependent or independent of cell cycle progression. Cell types may utilise several paths to become polyploid. CC: cell cycle, TGC: trophoblast giant cell, SCT: syncytiotrophoblast. Adapted from [46]. Created in https://BioRender.com.

named "fusogens" localized in the membrane of one or both of the fusing cells [47] (Fig.1.2).

In response to tissue injury, bone marrow–derived cells have the capacity to fuse with differentiated cells, giving rise to hybrid cells with regenerative potential [48]. This form of heterotypic cell fusion has been documented across multiple organs —including muscle, brain, retina, intestine, and liver— where it contributes to the restoration of tissue function [49, 50].

Endocycling

The mammal cell cycle is divided in four phases, Gap 1 (G1), Synthesis (S), Gap (G2) and Mitosis (M). The ordered progression through these stages is regulated by cyclin-dependent kinases (CDKs) and their association with non-catalytic subunits called cyclins. CDK-cyclin complexes phosphorylate specific substrates to promote DNA replication (S-phase CDKs or S-CDK) and mitosis (mitotic CDKs or M-CDK). Endocycling is a variation of this process where cells are unable to enter mitosis and instead alternate between S- and

G-phases. This results in the production of a single mononucleated cell with twice the genomic content [46] (Fig.1.2).

In mammals, endocycling -also known as endoreplication or endoreduplication- requires two key events to happen (1) inhibition of mitosis progression by M-CDK activity suppression, and (2) periodical inactivation of S-CDK activity to enable G phase entry, and subsequent reactivation to initiate a new endocycle [51]. In trophoblasts giant cells (TGC) M-CDK inhibition is induced by programmed overexpression of the CDK inhibitors p57 and p21 [52]. In hepatocytes and TGCs, the transcription factor family E2F controls a unique G2/M transcriptional program that is critical for mitosis, and is essential to regulate endocycle progression [53].

Endomitosis

In contrast to endocycling cells, endomitotic cells can enter mitosis but abort before the start of cytokinesis. In particular, endomitosis is caused by changes to the metaphase–anaphase transition triggering mitosis exit before chromosome segregation. Extended mitosis delay owing to the activation of the spindle assembly checkpoint can either result in cell death (also known as mitotic catastrophe), or mitotic slippage, in which cells exit mitosis and produce a mononucleated tetraploid cell [54]. Notably, MKs are the only human somatic cell known to utilise endomitosis as a mechanism for programmed polyploidization. However, mitotic slippage and endomitosis are commonly observed in cancer cells, including those treated with spindle poisons (such as taxol drugs) [54, 55]. MK polyploidization is discussed in detail in Section 1.2.3.

Cytokinesis Failure

Cytokinesis is the final step in the cell cycle and is composed by four key steps: (1) establishment of a division plane, (2) contraction of the actomyosin ring, (3) ingression of the cleavage furrow and (4) formation of the intercellular bridge and midbody. Alterations on any of these events can cause cytokinesis failure preventing cell abscission and producing a single, generally binucleate,

polyploid cell. This process has been documented in several cell types including hepatocytes and cardiomyocytes [46].

In hepatocytes, insulin-mediated PI3K-AKT signalling can trigger the reorganization of the cytoskeleton during mitosis, impeding the correct location of RhoA -the master orchestrator of cytokinesis- at the division site, and blocking the formation of the contractile ring [46, 56]. In hepatocytes and cardiomyocytes the transcription factor family E2F, in particular the atypical cell cycle repressors E2F7 and E2F8, are also essential. Indeed, E2F7/8 double-knockout mice show increase of diploid hepatocytes and cardiomyocytes and altered expression of cytokinesis-related transcripts such as Ect2, Mklp1 and Racgap1 [57].

Physical obstruction of the cleavage furrow by chromatin or lagging chromosomes can promote cytokinesis failure. In cardiomyocytes, the expression of the telomere-maintenance enzyme telomerase decreases sharply at birth. Shortened telomeres can undergo non-homologous end joining, which can cause DNA to bridge between cell poles during chromosome segregation. On this situation, the abscission checkpoint halts cytokinesis and causes polyploidization [58]. Of note, this mechanism has been demonstrated telomerase-null zebra fish and in human cardyomyocytes *in vitro*, but the relevance of this phenomenon in human physiology requires further research [58].

1.2.2 Physiological Whole Genome Duplication

WGD is encoded within the developmental program of several human cell types, and it is proposed to confer these cells unique properties that better enable them to perform their cellular functions. Importantly, WGD is associated with terminal differentiation in somatic tissues and cell cycle arrest. Several benefits have been attributed to WGD although their implications on human biology have not always been demonstrated [59].

The most intuitive advantage of doubling the genetic material could be an increase of the total protein output. WGD allows somatic cells to grow larger and can permit cells to be metabolically more active [60]. A good example of this are

the secretory alveolar cells in the mammary glands which become binucleated through cytokinesis failure and WGD inhibition in genetically engineer mice results in significant decrease of milk production during breast feeding [61].

Polyploidization might also protect against genotoxic stress. Harbouring multiple gene copies can buffer against deleterious gene-inactivating mutations such as the lost of a tumour suppressor gene, by providing extra copies of the essential elements [62]. In the liver, for example, early tumour lesions emerge preferentially from diploid cells as shown in human patients and carcinogen-induced murine models, suggesting that polyploid cells are shielded against tumour formation [46].

Hepatocytes

At birth, all hepatocytes in mammals are diploid and polyploidization occurs during postnatal growth [46]. In the adult liver, roughly 30% of the human hepatocytes are polyploid, in contrast with mice where up to 90% of hepatocytes undergo WGD [46].

Polyploid hepatocytes exist as mono-nucleate or binucleate cells. Thus, a tetraploid hepatocyte can be either mono-nucleated (with four genome copies contained in the same nucleus) or binucleated (with each nuclei harbouring two genome copies) and octoploid hepatocytes contain either a single 8N nucleus or two tetraploid nuclei [46]. This source of hepatocyte variability was proposed to play a role in the functional specialization of hepatocytes. However, detailed single cell transcriptomic and spatial profiling of hepatocytes showed little differences between diploid and tetraploid liver cells and suggested that hepatocyte functional specification is mostly driven by their spatial location rather than their DNA content [63, 64].

One unique aspect of the liver is its regenerative capacity. Several groups have demonstrated that, upon partial hepatectomy, both diploid and polyploid hepatocytes contribute to the full restoration of the liver mass. However, whether ploidy is needed for this process is not clear, and studies on E2F7/8 double

knockout mice (which mostly produce diploid hepatocytes) show similar liver regenerative capacity compared to wild-type polyploid controls [57].

Liver regeneration is possible through mitosis and endocycles of both, diploid and polyploid cells. This has two important consequences: hepatocytes can increase their ploidy during liver regeneration and cycling polyploid hepatocytes can reduce their DNA content through ploidy reversal. Ploidy-reduced hepatocytes can then re-enter the cell cycle and in some cases produce a new polyploid cell. The loop between polyploid and ploidy reversal is called the "ploidy conveyor" and has been demonstrated *in vivo* using elegant multicolour lineage-tracing systems [65].

Cardiomyocytes

Cardiomyocte polyploidization is highly conserved across species which suggests that WGD might assist on cardiac function. An interesting example is the giraffe heart, which generates twice the blood pressure compared to similar-sized mammals and is form predominantly by polyploid cardiomyocytes [66].

Most cardiomyocytes are diploid at birth and WGD occurs postnatally. The emergence of polyploid cardiomyocytes is thought to be an adaptation necessary to cope with an increase blood pressure and cardiac wall stress that accompany postnatal development [67]. Indeed, in neonatal mice, WGD coincides with the expression of sarcomere genes and fatty acid oxidation [68] although these differences reduce in adulthood where the mono- and multi-nuclear cardiomyocyte transcriptional profiles become indistinguishable [69].

The heart responds to physiological and pathological changes in mechanical workload with size expansion. Thus, during hypertrophic growth cardiomyocytes increase in volume rather than in numbers which correlates with polyploidization [70]. Of note, hypertrophy is also induced in pathological settings and ploidy increase has been reported after myocardial infraction [71]. Importantly, this form of tissue growth is preferred since mitotic cell proliferation would disrupt

the structural integrity, contractile ability, and electrical coupling necessary for the correct function of the heart [67].

In contrast to hepatocytes, WGD correlates with cell cycle arrest and general cytokinesis defects which precludes polyploid cardiomyocyte proliferation, even when exposed to mitogenic signals [58]. Although, hypertrophy can serve as a compensatory mechanism for increased mechanical workload, cell division is required for cardiac regeneration. In line with this, cardiomyocyte polyploidization at birth correlates with a block in cardiac regeneration [59] and targeting diploid cardiomyocytes or reduction of cardiomyocyte ploidy have been proposed as mechanism to enhance cardiac regeneration [58].

Osteoclasts

Osteoclasts are multinucleated bone-resorbing cells formed by the gradual fusion of diploid monocyte-derived progenitors in the bone marrow [72]. Osteoclast increased nuclear content improves their bone resorption capabilities. Careful balance between mineral deposition and resorption is essential to maintain the bone structure, hence osteoclast multinucleation needs to be tightly controlled [73]. Osteoclast fusion is regulated by the "fusogens" DC-STAMP, OC-STAMP and the RNA-binding protein La [73, 74]. Concordantly, overexpression of DC-STAMP in transgenic mice causes osteoclast hyper-nucleation and a osteoporotic phenotype [75]. Importantly, osteoclast multi-nucleation is independent of terminal cell differentiation and mono-nucleated osteoclasts retain low levels of bone resorption abilities, suggesting that therapies targeting cell fusion, rather than general osteoblast suppression, may be a better alternative to control bone resorption activity [72].

Polyploid Tissue Barriers

In some developmental contexts increasing tissue size via polyploidization rather than cell number can be advantageous. One large cell, as opposed to two (or more) smaller ones produces a seamless barrier, which can block processes

such as cell migration since they require cell junctions to happen. An important example of this can be found at the maternal-fetal interface. TGCs in the placenta form a continuous layer between the maternal blood supply and the fetus and achieve a ploidy up to 512N via endocycling. Also in the placenta, the large multinucleate syncytiotrophoblast controls the maternal-fetal nutrient exchange at the same time that shields the fetus from the maternal immune system [60, 76].

1.2.3 Megakaryocyte Whole Genome Duplication: Multiple Paths to Multiple Ploidies

During the later stages of MK maturation, MK progenitors switch from classical mitosis to polyploidization, producing the largest cells in the bone marrow. This process is encoded within the differentiation program of MKs and pathologies affecting MK maturation frequently result in the production of diploid MKs, that usually have lower capacity to produce platelets. The MK polyploidization cycle is commonly referred to as endomitosis, which suggests an abortive mitosis without chromosome segregation or cytokinesis. However, efforts over the last decades have demonstrated that MKs employ multiple mechanisms on their journey to polyploidy [55].

The first *in vitro* studies of the MK cell cycle confirmed that MKs can enter mitosis and suggested that WGD was achieved by abortive mitoses [77]. Follow up work showed that MKs were able to segregate chromosomes and start cytokinesis as evidenced by the ingression of the cleavage furrow. However, in endomitotic MKs, there is a rapid regression of the furrow and the two daughter cells fuse back together [78]. Later studies validated these observations and suggested that MKs have a defective contractile ring due to impaired Rho/Rock signalling [79]. Abortive cytokinesis is evident in the progression from 2N to 4N, and multipolar mitoses with partial furrow ingression can be observed during 4N-8N transition [79]. However, cytokinesis failure is not always the chosen mechanism for MK polyploidization, and direct visualization of chromosome dynamics showed that high ploidy MKs (≥8N) abort mitosis without entering cytokinesis,

and suggested that progression to cytokinesis only happens between the 2N-8N stages [80]. Thus, MKs employ a form of cytokinesis failure at low ploidy stages (2N-8N) but increase their ploidy further via endomitosis. Of note, classic forms of cytokinesis failure give rise to binucleated cells. However, during cytokinesis the MK nuclei are incompletely separated and remain attached by nucleoplasmic bridges that cross through the division plane [81]. Hence, cytokinesis failure in MKs produces a single polylobulated nuclei.

Importantly, recent reports have demonstrated that exiting mitosis at the mitotic stage (endomitosis) can impair the formation of the nuclear envelope and compromise nuclear stiffness, causing prominent nuclear deformations in MKs and cell lines after pharmacologically-induced endomitosis [82]. These observations explain the link between the polyploidization mechanism and the complex nuclear architecture observed in MKs. A schematic illustration of the MK endomitotic process is shown in Fig.1.3.

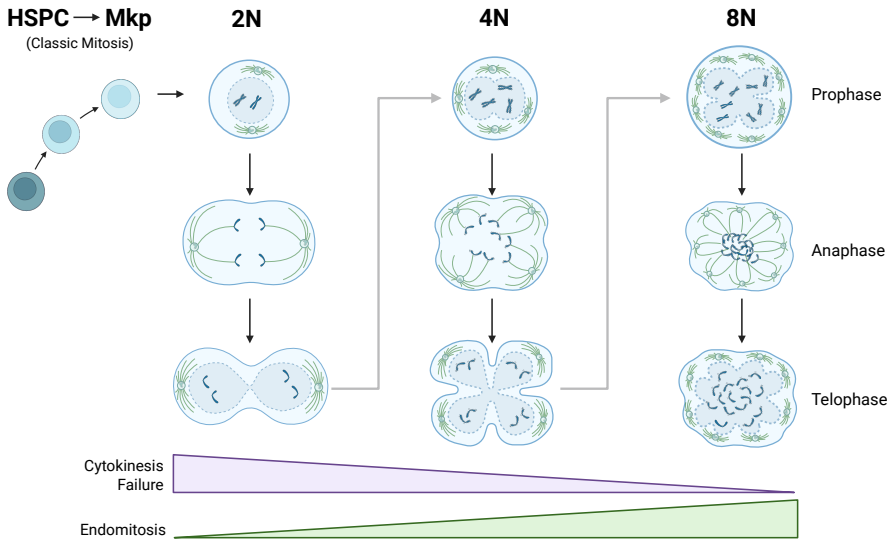


Figure 1.3: MKs utilize different mechanisms to become polyploid. During transitions between 2N-4N and 4N-8N MKs show clear furrow ingression and cytokinesis abortion, indicating polyploidization via cytokinesis failure. From 8N onwards, MKs show little chromosome segregation during anaphase and no cytokinesis progression, akin to an endomitotic cycle. Adapted from [55]. Created in https://BioRender.com.

Interestingly, MKs can harness other mechanisms to become polyploid.

Elegant studies using KO mouse models showed that, when MKs are prevented from entering mitosis by genetic depletion of CDK1, they can utilise endocycles to become polyploid without affecting steady state thrombopoiesis, demonstrating that the path to ploidy does not impact MK function [83].

MK Cell Cycle Regulation

The endomitotic process is regulated by the same transcription factors that are required for MK differentiation. These include GATA-1, RUNX1 and FLI1, and knocking out these transcription factors in mouse models leads to major defects in MK ploidy and differentiation [55].

During cytokinesis, RhoA signalling is required to establish the actomyosin ring at the cleavage furrow and generates the contraction force necessary to complete cell abscission. Correct positioning and activation of RhoA is controlled by guanine nucleotide-exchange factors (GEFs). In MKs, the transcription coactivator megakaryoblastic leukemia 1 (MKL1) downregulates GEF-H1 - allowing the first 2N to 4N transition- and ECT2, which enables polyploidization to higher ploidy levels [84]. In parallel, RUNX1-mediated transcriptional repression of the non muscle myosin IIB (MYH10) is required to the formation of a defective contractile ring and induce failure of cytokinesis [85].

1.2.4 Pathological Alterations of Megakaryocyte Ploidy

Several examples of pathologies that show modified MK ploidy exist, and the mechanistic drivers of the ploidy alterations are diverse and not always fully understood. [55].

The 5q- syndrome is a subtype of myelodysplastic syndrome (MDS) characterized by a macrocytic anemia and, in some cases, thrombocytosis. Interestingly, MKs in patients with 5q- MDS are polyploid but hypolobulated. The clinical phenotype of 5q- MDS is attributed to genetic haploinsufficiency of genes located in the missing region of chromosome 5, including RPS14 and CSNK1A1,

although the precise mechanism by which this prevents polyploidization remains unclear [86, 87].

Acute megakaryoblastic leukaemia (AMKL) is a subtype of acute myeloid leukemia (AML) characterised by an accumulation of diploid MKs, which is attributed to a differentiation blockage at the MK progenitor stage. The genetic origin of AMKL is complex. In infants is associated with down syndrome (DS) and GATA1 mutations. In adults and non-DS infants is frequently driven by chromosome translocations and the formation of chimeric oncogenes such as RBM15-MKL1 [88].

BCR-ABL-negative myeloproliferative neoplasms (MPNs) are a group of haematologic malignancies driven by the acquisition of activating mutations of the MPL-JAK2-STAT signalling pathway, mimicking the signalling effects of the megakaryopoietic cytokine TPO. Essential thrombocythemia, is a form of MPN characterised by the overproduction of large polyploid MKs and marked increase in the number of circulating platelets. In contrast, myelofibrosis -the most aggressive form of MPN- presents with a pathological deposition of scarring tissue in the bone marrow, and a characteristic production of clusters of small aberrant hypoploid MKs. The mechanisms behind the discordant MK ploidy phenotypes between MPN manifestations are not clear, but might be related to defective expression of the full length isoform of GATA-1 in myelofibrosis and pre-fibrotic states [89, 90].

Lastly, familial thrombocytopenias are a group of disorders where somatic mutations affect the production of MKs and/or platelets. Mutations associated with these disorders are as diverse as the mechanism involved in platelet production but defects on MK ploidy are frequently associated with transcription factors such as GATA1 (x-linked macrothrombocytopenia), RUNX1 (familial platelet disorder with propensity to AML) and FLI1 (Paris-Trousseau syndrome) [91].

1.2.5 Inappropriate Use of Doubled Genomes: WGD And Cancer

The effects of WGD on human physiology depend on whether the cell is programmed to undergo ploidy, and while some cells utilize WGD as part of their differentiation program, unscheduled access to tetraploidy -particularly by proliferating cells- can cultivate malignancy.

The first evidence of the oncogenic potential of doubled genomes came from the demonstration that tetraploid p53 -/- mouse mammary epithelial cells were capable of tumour formation while their genetically matched diploid counterparts were not [92]. Subsequent studies demonstrated that unscheduled WGD is oncogenic on diverse cell types, irrespective of the mechanism of origin [45].

Non-programmed WGD can arise via multiple mechanisms, but failure of cell division is thought to be the most common. Persistent DNA damage via replication stress and telomere crisis -distinctive hallmarks of early cancer genomes- can induce polyploidization via endomitosis and cytokinesis failure [93, 94]. Persistent inhibition of mitosis progression by the spindle assembly checkpoint (SAC) can also lead to mitotic slippage and WGD [95]. Certain oncogenes can also promote genome duplication such as $BRAF^{V600E}$, which promotes cytokinesis failure by RhoA deregulation, or $H\text{-}RAS^{V12}$ and cyclin E1 overexpression which can enhance polyploidization by endocycles or re-replication (an abnormal form of DNA replication where failure of cell-cycle control allows DNA segments to be copied more than once during the same cycle) [96, 97]. Lastly, viral-mediated cell fusion can cause unscheduled polyploidization and promote tumour formation [98].

Large pan-cancer studies have shown that WGD is a highly common genetic lesion, and it is estimated that approximately 30% of all solid tumours experience a WGD event during their evolution [99–101]. WGD frequently arises as an early oncogenic event, fuelling chromosomal instability and accelerating cancer progression [100–102]. Concordantly, the emergence of WGD is associated with poor prognosis across cancer types [100]. Crucially, the incidence of WGD not only depends on the tumour type but also the tissue of origin. For example, while intraocular melanomas show very low WGD prevalence (~6%),

polyploidy is common in melanomas from cutaneous origin (~40%) [45]. These observations suggest that some tissues might be better adapted to undergo polyploidization and underlay the importance of understanding the mechanisms behind WGD tolerance.

Interestingly, the incidence of WGD increases on metastatic lesions and over half of the metastatic tumours are WGD+ [103]. The exact reasons why WGD+ is enriched in metastatic sites are not know. WGD can promote chromosome instability which has been shown to promote metastasis through DNA-sensing pathway and could explain the link between WGD and neoplastic dissemination [104]. Moreover, the extra set of centrosomes on polyploid cells can induce a cell invasive phenotype [105].

1.3 Consequences of Whole Genome Duplication

1.3.1 The Burden of Multiple Genomes

The occurrence of WGD creates obstacles to cell physiology. For instance, protein expression does not scale linearly with chromosome copy number which can limit certain cellular processes, particularly those related to genome homeostasis [106, 107]. Moreover, navigating polyploid mitoses is challenging and are prone to chromosome segregation errors [108]. These biological constraints can act as oncogenic drivers on transformed cells, but also impose unique vulnerabilities to the tetraploid stage, which can be exploited to target WGD+ tumours [108].

WGD results in the accumulation of extra centrosomes within cells. Centrosomes are the primary microtubule-organizing centres, and their number is normally subject to strict control. When supernumerary centrosomes are present during mitosis, cells can assemble multipolar spindles, producing three or more daughter cells that are highly aneuploid and often non-viable [109]. To counteract this, cells can cluster excess centrosomes to re-establish a bipolar spindle and thereby improve the fidelity of chromosome segregation. Nevertheless, this

process is inherently error-prone, as multi-centrosome divisions are susceptible to merotelic attachments, in which a single kinetochore engages with microtubules from both spindle poles [109]. Such errors frequently lead to chromosome lagging and micronuclei formation [109]. As a result, WGD sustains elevated rates of chromosome missegregation and accelerates the accumulation of both structural and numerical genomic abnormalities [110].

Mitotic errors were thought to be the main cause of chromosomal instability on WGD cells. However, detailed single cell tracking of the first cell cycle after polyploidization have shown that polyploid cells present massive DNA damage accumulation during the first S-phase after WGD, with multiple over- and under-replicated regions compared to diploid controls [111]. Importantly, this was independent of the mechanism used to achieve ploidy (endocycling, endomitosis or cytokinesis failure) [111]. The authors demonstrated that this phenomenon was due to improper scaling of DNA replication factors and the effects could be mitigated by increasing their expression via E2F1 overexpression or extending the length of the first G1 phase [111].

In multinucleated polyploid cells, individual nuclei can progress through the cell cycle asynchronously. Under these conditions, the lagging nucleus is urged into mitotic entry forcing premature chromosome condensation and resulting in DNA damage. [112]. This phenomenon, termed chronocrisis, has been reported in multinucleated polyploid Drosophila neuroblasts, mouse embryonic neural stem cells, and human cancer cell lines following cytokinesis inhibition [112, 113]. Interestingly, chronocrisis has also been observed in cells containing micronuclei, indicating that this process may not be exclusive to polyploid cells [113].

The consequences of WGD extend beyond mitotic defects, and recent studies have revealed that WGD can also disrupt chromatin architecture [114]. Under normal conditions, chromosomes are organized into distinct domains of transcriptionally active (compartment A) and repressed (compartment B) chromatin. However, analyses of p53-deficient WGD+ cells have shown that WGD induces alterations in chromatin segregation and impaired compartmentalization of A/B

domains [114]. These defects promote the repositioning of chromatin regions, shifting oncogene-associated loci into compartment A while relocating tumour suppressor regions into compartment B, thereby enhancing oncogenic potential [114]. Mechanistically, these changes result from insufficient levels of CTCF, which compromise the maintenance of A/B compartment boundaries. Consistent with observations reported by Gemble and colleagues [111], pharmacological prolongation of the G1 phase was sufficient to restore proper compartmentalization [114].

1.3.2 Mechanisms of Ploidy Control

Given the scarring nature of unscheduled WGD, it is not surprising that multicellular organisms have developed tumour-suppressive mechanisms to restrain WGD+ cell proliferation (Fig. 1.4).

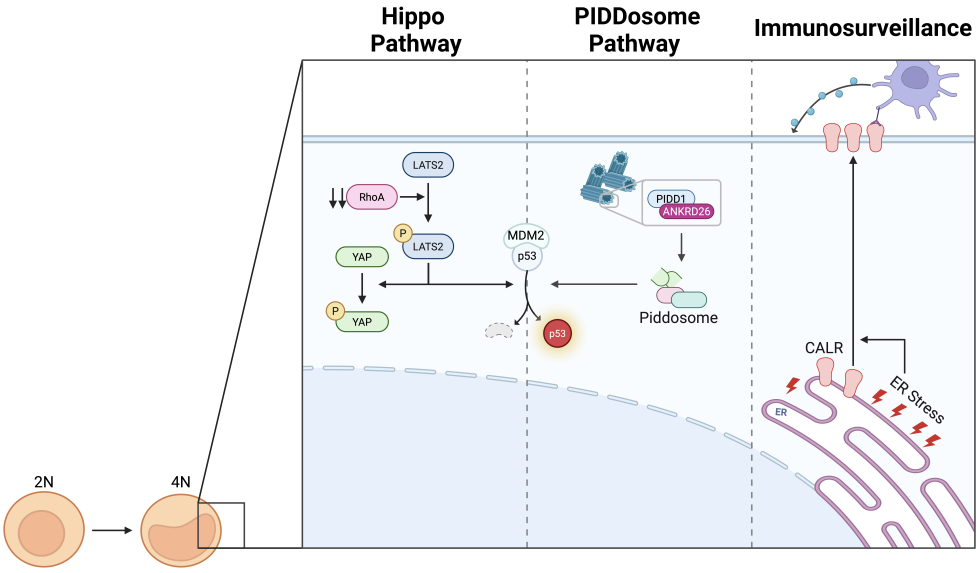


Figure 1.4: Successful elimination of WGD+ cells can be achieved via intrinsic and extrinsic mechanisms. Low RhoA activity leads to LATS2 kinase activation which phosphorylates and inactivates YAP, as well as stabilizes p53 through direct inhibition of MDM2. Accumulation of extra centrosomes can activate the PIDDosome which stabilizes p53 through Caspase 2-mediated MDM2 degradation. Additionally, WGD-induced ER stress promotes the translocation of calreticulin (CALR) to the cell surface, which can be detected by immunosurveillance mechanisms. Adapted from [92, 115, 116]. Created in https://BioRender.com.

Contrary to what their name suggest, ploidy-restricting pathways (also

referred to as tetraploid checkpoint pathways) do not detect additional chromosome copies but rather the concomitant centrosome amplification. Perturbation screenings on p53 proficient cells have demonstrated the presence of two main pathways of proliferation control after WGD.

Centrosome amplification following cytokinesis failure can trigger the Hippo tumour suppressor pathway [117]. In this context, cell proliferation is limited in two ways. First, Hippo signalling leads to the activation of the kinases LATS1 and LATS2, which phosphorylate and inactivate the oncogenic transcriptional co-activators YAP and TAZ. Secondly, active LATS2 also inhibits the key p53 suppressor MDM2, stabilising p53 and inducing cell cycle arrest [117].

Accumulation of extra centrosomes can also recruit PIDD1 to the mature centrioles and promote the formation the PIDDosome complex. Activation of this multi-protein complex promotes Caspase-2 activation which results in MDM2 cleavage and p53 stabilisation [118]. Follow up studies demonstrated that PIDD1 recruitment and subsequent PIDDosome activation was dependent on the presence of ANKRD26 at the centriole distal appendages and ANKRD26 removal via genetic manipulation was sufficient to abrogate the activation of PIDDosome pathway upon pharmacological induction of WGD [115, 119].

Lastly, polyploid cells can be detected and cleared by the immune system. Screening of 480 chemical compounds revealed that polyploidization-inducing agents cause cell surface exposure of the immunogenic cell death marker calreticulin (CALR) [116]. Mechanistically, polyploid cells show constitutive endoplasmic reticulum (ER) stress which leads to an aberrant translocation of CALR from the ER to the cell surface. Importantly, CALR-exposing polyploid cells were efficiently cleared in immunocompetent mice and reduction of DNA content, ER-stress or CALR exposure were required to scape the immunosurveillance system *in vivo*, demonstrating that the immune system can also play a role restraining polyploid cell generation [116].

1.4 Hypotheses And Aims

WGD is a unique process with broad implications in both physiological and pathological contexts. In MKs, WGD is essential to sustain the massive demand for platelet production and interruptions of this process are associated with multiple diseases. Unlike most somatic cells, which typically arrest after a single round of WGD, MKs engage in successive endomitotic cycles, reaching ploidy levels as high as 128N. Navigating mitoses with abnormally high chromosome numbers is inherently challenging, often resulting in chromosome missegregation and genomic instability. More over, improper scaling of the cell proteome can compromise the genomic integrity of polyploid cells. To avoid these detrimental effects, somatic cells possess tetraploid checkpoints that prevent proliferation of polyploid cells, which converge on p53 activation. Consistent with this, WGD in solid tumours frequently arises in the context of p53 mutations [100]. Intriguingly, around 40% of solid tumours tolerate WGD despite retaining functional p53, implying that they acquire specific adaptations to bypass tetraploid checkpoint activation and keep proliferating [100]. This raises an important parallel with MK biology: while being p53 proficient, MKs are also uniquely adapted to achieve extreme polyploidization without triggering cell-cycle arrest, suggesting a complete inability to activate tetraploid checkpoints.

Despite the increasing evidence of WGD's deleterious effects and the tumour-suppressive mechanisms that normally restrain it, little is known about the genomic integrity and the mechanisms for WGD tolerance of highly polyploid MKs. I therefore hypothesize that (1) WGD compromises MK genome stability, (2) MKs employ specialized pathways to bypass tetraploid checkpoints, and (3) p53 wild-type WGD+ tumours may hijack these adaptations to sustain proliferation under active p53 surveillance. To address these hypotheses I propose the following aims for this thesis:

1. To study DNA damage and genome integrity on polyploid MKs.

2. To describe the transcriptional adaptations of MKs across their ploidy spectrum.

3. To identify the plausible mechanisms MKs utilise to bypass the tetraploid checkpoint pathway.

4. To explore if these mechanisms are utilised by p53 wild-type polyploid tumours to avoid tetraploid checkpoint activation.

Please note that in addition to this broad introductory chapter, each results chapter contains a further, detailed introduction specific to each section.

2
Materials And Methods

Contents

2.1 Cell Line Work 29
2.2 Human Induced Pluripotent Stem Cells 31
2.3 Human Samples 31
2.4 Isolation of Megakaryocytes From Mouse Bone Marrow 32
2.5 In Vitro Differentiation of Megakaryocytes 33
2.6 Flow Cytometry Analysis 35
2.7 Fluorescence-Activated Cell Sorting 37
2.8 Imaging Analysis 37
2.9 Imaging Flow Cytometry 39
2.10 Molecular Biology 40
2.11 Single Cell RNA Sequencing Data Processing 44
2.12 Single Cell Whole Genome Sequencing Analysis 46
2.13 Cancer Cell Line Encyclopedia Analysis 47
2.14 Statistical Analysis 47

2.1 Cell Line Work

2.1.1 Cell Line Maintenance

The cell lines used for these project were: HCT116, HEL and UT7. All cells were cultured according to the recommendations from the German Collection of Microorganisms and Cell Cultures (DSMZ) and tested monthly for mycoplasma contamination. HEL and UT7 cells were cultured in RPMI 1640 medium (Gibco, 11875093) supplemented with 10% Foetal Bovine Serum (FBS, Merck F9665-500Ml), 100 U/mL penicillin and 100 µg/ ml streptomycin (Merck, P4333-100ML). UT7 cells were additionally supplemented with recombinant human thrombopoietin (hTPO, PeproTech, 300-18-100uG) at 10ng/mL. HCT116 cells were cultured in McCoy's 5A media (Merck, M9309-500ML) supplemented with 10% FBS, 100 U/mL penicillin and 100 µg/mL streptomycin (Merck, P4333-100ML). For cell passage, HCT116 cells were detached using trypsin 0.25% (Merck, 59429C-500ML) for 5 minutes at 37^{o}C followed by an equal volume of 100% FBS to quench the enzyme. All cells were maintained at 37°C with 5% CO_2.

Cell lines were preserved at 1-5x10^6 cells/mL in FBS supplemented with 10% dimethyl sulfoxide (DMSO, Merck D2650-100ML).

2.1.2 Virus Work

To perform lentiviral transduction, cell lines were cultured over night (~18h) with the appropriate cell media in the presence of Polybrene (Merck, TR-1003-G) at 8μg/mL and the lentiviral vector was added at a pre-tested Multiplicity Of Infection (MOI). Viral supernatant was removed after overnight incubation and cells were resuspended in virus-free media and incubated for another 24 hours. Transduced cells were purified 48h after transduction using Fluorescence-Activated Cell Sorting (FACS).

Using a pre-tested MOI = 1, UT7 cells were transduced with lentiviral particles packed with the pLenti-PGK-Neo-PIP-FUCCI vector [120] (Addgene #118616).

Transduced cells were FACS-selected based on mCherry and mVenus expression and expanded in culture using the appropriate cell media.

Using a pre-tested MOI = 5, HCT116 cells were transduced with a SMARTvector Lentiviral Human TP53 hEF1a-TurboRFP shRNA (Horizon, details on Appendix Table A.1) which contains a human TP53-targeting shRNA along with the fluorescent reporter TurboRFP. The SMARTvector Non-targeting hEF1a-TurboRFP was used as a non-targeting control (Horizon, VSC11716). Transduced cells were FACS-selected based on RFP expression and expanded in culture using the appropriate cell media. Three TP53-targeting guides were tested, and the most effective was chosen based on RT-qPCR knockdown efficiency (Fig. 2.1, Appendix Table A.1).

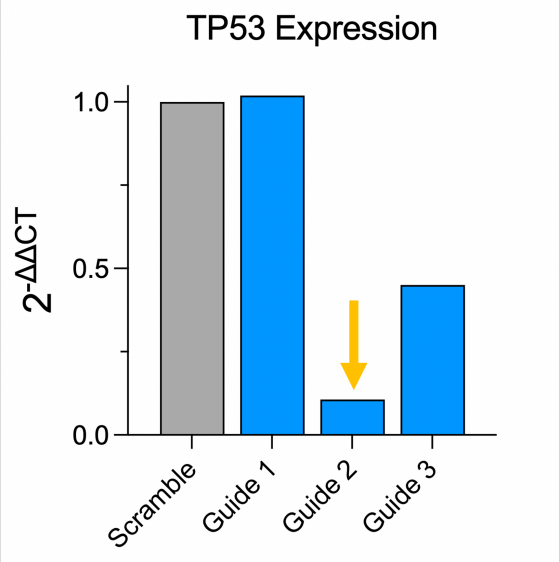


Figure 2.1: Selection of TP53 targeting shRNA guides. TP53 expression measured by RT-qPCR (ΔΔCt method) after shRNA targeting using three different guides. The arrow indicates the guide selected based on maximum silencing efficiency.

2.1.3 Generation of Isogenic Tetraploid Clones by Cytokinesis Failure

Isogenic tetraploid clones were generated using previously described methods [121]. In brief, HCT116 cells were treated with dihydrocytochalasin D (DCD, MP Biomedicals 0215077101) at 0.75 μM for 18h to induce tetraploidy via cytokinesis

failure. Cells were then washed, seeded at low density in 15 mm cell culture dishes (ThermoFisher, 150468), and cultured in DCD-free media for two weeks to generate single cell-derived colonies. Isogenic clones were isolated and screened by flow cytometry, confirming the presence of stable diploid and tetraploid cells.

2.1.4 In Vitro Cell Line Drug Treatments

The fidelity of the FUCCI system on UT7 cells was tested using a combination of drugs and cell culture regimes. Briefly, UT7 cells were seeded at $0.5x10^6$ cells/mL in 96 well plates (SLS, 3596) with the appropriate media supplemented with Nocodazole (MCE, HY-13520) , Aphidicolin (MCE, HY-N6733), Cisplatin (MCE, HY-17394), Hydroxyurea (MCE, HY-B0313) or 1.5% v/v dimethyl sulfoxide (DMSO, Merck D2650-100ML) as control. Serum starved cells were cultured with UT7 media without FBS. Cell cycle changes were assessed by flow cytomtery after 24h of incubation.

2.2 Human Induced Pluripotent Stem Cells

h-iPSC cell culture maintenance was carried out by Dr. Abdullah Khan.

Human Induced Pluripotent Stem Cells (h-iPSCs, ThermoFisher, #A18945) were maintained on plates coated with Geltrex (ThermoFisher, #A1569601) and StemFlex (ThermoFisher Scientific, #A3349401) medium. Cells were maintained during routine passaging in a 37^oC incubator at 5% CO_2. Routine clump passaging was performed using ReLeSR (Stem Cell Technologies, #100-0483). Cells were mycoplasma tested at 1-month intervals, and karyotyped every 12 months or if issues were noted on routine culturing.

2.3 Human Samples

Peripheral blood and bone marrow samples from patients with ANKRD26-RT were kindly shared by a collaborator, Dr. Alan Cantor (Harvard Stem Cell Institute, Boston Children's Hospital). These samples were collected and

biobanked by his team. In brief, patients and appropriate healthy control donors provided written informed consent in accordance with the Declaration of Helsinki for sample collection and use in research. Mononuclear cells were isolated by Ficoll gradient centrifugation (VWR Int, 17-1440-03). For some samples, CD34 enrichment was performed using immunomagnetic beads (Miltenyi, 130-100-453). Total mononuclear cells or CD34+ cells were cryopreserved in FBS supplemented with 10% DMSO.

2.4 Isolation of Megakaryocytes From Mouse Bone Marrow

Primary megakaryocytes (MKs) were isolated from mouse bone marrow samples using a previously established method [122]. Tibia, femur and hip join bones were dissected from euthanised mice from a C57BL/6 genetic background. To isolate the bone marrow, bone epiphysis was cut and bones were placed within a 0.5 mL microcentrifuge tube (Eppendorf, 0030120086) with a punched hole in the bottom and everything was placed inside a 1.5 mL microcentrifuge tube (Eppendorf, 0030125215) containing 100 μL of CATCH buffer: PBS (Life Tech, 10010056), HEPES 12.5 mM (Fisher, 15478749), EDTA 1.5 mM (ThermoFisher, AM9260G), Bovine Serum Albumin 1.75% (Miltenyi, 130-091-376) and FBS 2.5%. The nested tubes were spun down at 2600g for 1 minute and pelleted bone marrow cells inside were resuspended in 1 mL of CATCH buffer.

Bone marrow cell suspension was passed through a series of filters of decreasing pore size (70 µm, 20 µm, 15 µm, Pluriselect, 43-50070-51, 43-50020-03, 43-50015-03). MKs retained on the 20 µm and 15 µm filters were recovered using CATCH buffer into a 50mL falcon tube (SLS, 352070). When needed, non-retained cells (MK-depleted diploid bone marrow cells) were used as experimental controls. After isolation, MKs were centrifuged (300 g, 10 min), resuspended in 1 mL of CATCH buffer and kept at room temperature until needed.

2.5 In Vitro Differentiation of Megakaryocytes

2.5.1 Megakaryocyte Differentiation From Primary Mouse cKIT+ Cells

Primary mouse bone marrow cells were obtained from tibia, femur and hip join bones from euthanised mice from a C57BL/6 genetic background. Bone marrow cells were isolated using the centrifugation method described above, resuspended into FACS buffer (PBS, FBS 10% v/v) and counted using the Trypan blue (Merck T8154-100ML) and the LUNA II automatic cell counter (Logos Biosystem).

Mouse CD117 (also known as cKIT)-positive haematopoietic stem and progenitor cells (HSPCs) were labelled with MicroBead-conjugated anti-mouse CD117 antibodies (Miltenyi Biotec, 130-091-224) and purified using MACS magnetic separator columns (Miltenyi Biotec, 130-042-401). cKIT+ cells were seeded at 1x10^6 cells/mL in MK differentiation media containing StemSpan SFEM (StemCell Tech, 09650), recombinant human thrombopoietin (hTPO, PeproTech, 300-18-100uG) at 10ng/mL and recombinant mouse stem cell factor (mSCF, PeproTech, AF-250-03-100uG) at 5ng/mL. mSCF concentrations were titrated to produced the highest amount of total MKs (Fig. 2.2). Cells were differentiated over the course of five days and cultures were supplemented with fresh media every 2-3 days.

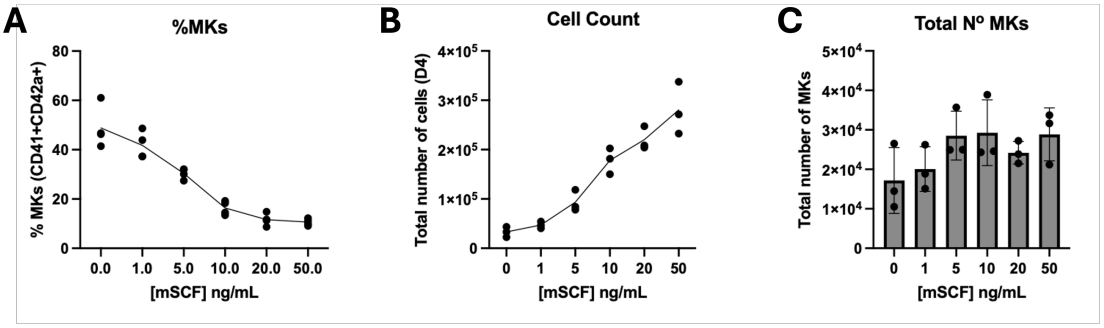


Figure 2.2: Optimisation of *in vitro* mouse MK differentiation. **A**, fraction of MKs obtained by *in vitro* differentiation determined by flow cytometry. **B**, total number of cells obtained determined by the Trypan blue method. **C**, total number of MKs obtained calculated from the total number of cells times the fraction of MKs. n = 3 mice per group

2.5.2 MK Differentiation From Primary Human Haematopoietic Stem And Progenitor Cells

Cryopreserved peripheral blood mononuclear cells were thawed by warming the vials briefly at 37^{o}C and gradually diluted into DMEM media (Gibco, #21056023) supplemented with 20% FBS and 0.1 mg/mL of DNase I (Merck, Cat. DN25), centrifuged at 300 g for 5 minutes and washed in FACS buffer.

Human HSPCs were selected based on CD34 positivity by FACS (Section 2.7). Purified CD34+ cells were cultured at 0.5x10^{6} cells/mL in human MK differentiation media. Media conditions previously used (Fig. 2.3, protocol 1) were optimised to maximize the fraction of MKs obtained (Fig. 2.3, protocol 2). Details of the cytokines used are in Appendix Table A.2. Cells were maintained at at 0.5-1x10^{6} cells/mL at 37°C with 5% CO_2 for 12 days and were supplemented with fresh media every 2-3 days.

2.5.3 MK Differentiation From Human Induced Pluripotent Stem Cells

MK production from human iPSC cells was carried out using a previously described method [123]. Details of the reagents used are in Appendix Table A.3. The protocol starts by h-iPSC clump dissociation (day -1) in StemFlex supplemented with RevitaCell and subsequent culture in ultra-low attachment 6-well plates (Life Tech, 174932) over night. To induce mesoderm formation, cell aggregates were seeded in collagen I + IV coated plates and cultured with APEL2, hBMP-4, hVGEF-A and hFGF-2 50 ng/mL for five days at 37°C with 5% O_2 (hypoxic conditions).

At day 5, media was replaced with APEL2 supplemented with hBMP-4, hSCF, hFLT3-L, hTPO at 25 ng/mL and hIL3, hIL6 at 10 ng/mL and cultured in normoxic conditions for five days to induce hemogenic endothelium formation.

At day 10, non-adherent HSPCs produced from the hemogenic endothelium were harvested, counted using Trypan blue and seeded at 0.2x10^{6} cells/mL in APEL2 supplemented with hFLT3-L, hSCF at 10 ng/mL and hTPO, hIL3 and hIL6

A

Protocol 1	Protocol 2
StemSpan SFEM II	StemSpan SFEM II
hTPO 5 ng/mL	hTPO 50ng/mL
hSCF 25ng/mL	hSCF 1ng/mL
	IL6 10ng/mL
	IL9 20ng/mL
	LDL 40µg/mL
Pen/Strep 100 U/ML	Pen/Strep 100 U/ML

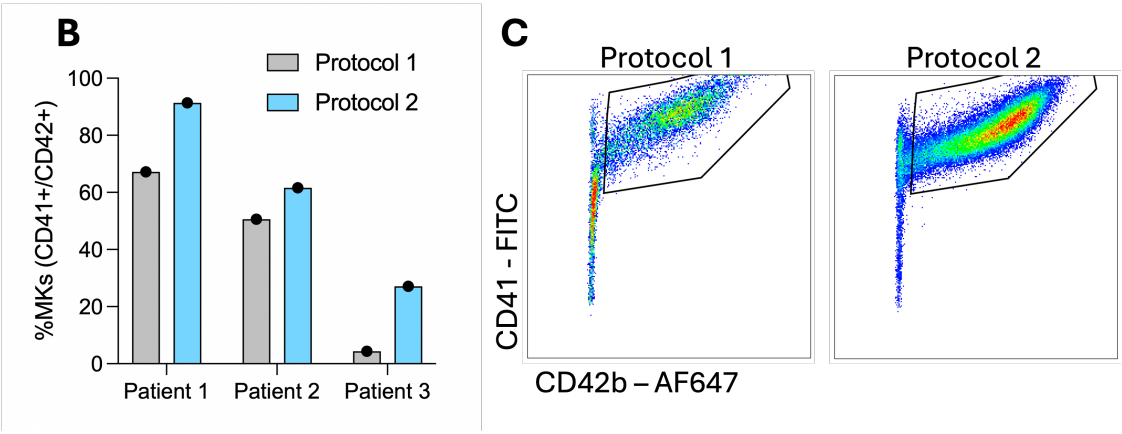


Figure 2.3: Optimisation of *in vitro* human MK differentiation. **A**, comparison of previous (protocol 1) and optimised (protocol 2) cytokine regimens for human MK differentiation. **B**, fraction of MKs obtained by *in vitro* differentiation determined by flow cytometry. **C**, exemplar flow cytometry plots of *in vitro* differentiated megakaryocytes using protocols 1 and 2. n = 3 donors.

at 5 ng/mL and 4% C/C Chemically Defined Lipids. Cells were cultured for seven days at 37°C with 5% CO_2 (normoxic conditions) to induce MK differentiation.

2.6 Flow Cytometry Analysis

2.6.1 Antibody Staining for Flow Cytometry

Cells used for staining were pelleted and resuspended in FACS buffer. Antibodies were added at pre-titrated concentrations (Appendix Table A.4) and cells were stained for 20 min at 4^{o}C. Cell suspensions containing MKs were stained for 20 min at room temperature. Antibodies were washed with FACS buffer and 4',6-diamidino-2-phenylindole (DAPI) or Propidium Iodide (PI) were

use for dead cell exclusion (Appendix Table A.4). Stained cells were kept at 4^{o}C, or at room temperature if they contained MKs, until analysed.

Laser calibration and population gating was carried out using Fluorescence Minus One (FMO), single stain and unstained controls. With the exception of DNA dyes (Hoechst, DAPI, PI), compensation beads (OneComp eBeads ThermoFisher, 01-1111-42) were use for single stain controls. Unless stated otherwise, analyses were carried out using the BD LSRFortessa X-20 Cell Analyser (BD Biosciences) and flow cytometry profiles were analysed using FlowJo (v.10.10.0, BD Biosciences).

2.6.2 DNA Content Analysis by Flow Cytometry

Prior antibody staining cells were resuspended at 0.5x10^6 cells/mL in FACS buffer with 10 μg/mL of Hoechst 33342 (ThermoFisher, cat. H3570) and incubated for 30 mins at 37^{o}C. Following incubation cells were washed and stained with antibodies when needed or directly prepared for flow analysis. PI was use for dead cell exclusion (Appendix Table A.4). For ploidy analysis, singlets were excluded based on Area vs Height plots from the Hoechst channel (laser: 405, Filter set: 450/50). MK average ploidy was calculated as previously described [124]:

$$(2 \times N_{2N\ cells} + 4 \times N_{4N\ cells} + 8 \times N_{8N\ cells}...)/N_{Total\ cells}$$

2.6.3 EdU Incorporation Assay by Flow Cytometry

EdU incorporation assay was performed using the iFluor 488 EdU Staining Proliferation Kit (Abcam, ab219801) and following the kit instructions. Briefly, live cells were incubated with 5-ethynyl-2'-deoxyruidine (EdU) 10 μM for 2 hours before fixing, permeabilisation, and Click chemistry labelled with iFluor 488. EdU-labelled cells were then stained with the appropriate antibody cocktail using the protocol described above. Lastly, when required, DNA was also stained for ploidy analysis using Hoechst 33342 using the protocol described above.

2.7 Fluorescence-Activated Cell Sorting

FACS was performed on labelled cells using the protocols described before. CD34+ cell sorting was performed using the FACSAria Fusion Cell sorter (BD Biosciences). Cells were sorted into 1.5 mL microcentrifuge tubes (Eppendorf, 0030125215) with 100 μL of MK differentiation media (nozzle 100 nm, sorting mode high purity bulk)

MK single cell sorting for SmartSeq-3 was performed using the FACSAria Fusion Cell sorter (BD Biosciences). Cells were single cell sorted into nuclease-free 96 well plates (Azenta, 4ti-0770/C) containing 3 μL of cell lysis media (Appendix Table A.6). To ensure the integrity of large cells, sorting was performed using the largest nozzle (130 nm) and low flow pressure (8 psi).

MK single cell sorting for Single Cell Whole Genome Sequencing was performed using the BD FACSDiscover S8 Cell Sorter (BD Biosciences). Cells were single cell sorted into nuclease-free 384 well plates (Azenta, 4TI-0384/C). To ensure the integrity of large cells, sorting was performed using the largest nozzle (130 nm) and low flow pressure (8 psi).

2.8 Imaging Analysis

2.8.1 Immunofluorescence

Prior preparation for imaging analysis of MKs derived from iPSCs and human CD34+ cells were adhered to glass coverslips (SLS, MIC3330) coated with 3.5 μg/cm^2 of Cell-Tak^{TM} (Corning, 354240) contained within a 24 well plates (Corning, 3526). Primary mouse MKs failed to bind to Cell-Tak coated slides and were stained in suspension instead, spinning cells at 300 g for 5 min to remove each reagent after the appropriate incubation time.

Cells were fixed in 4% paraformaldehyde (PFA, ThermoFisher, 11586711) for 10 min at room temperature and permeabilised with 0.1% Triton-X100 (Sigma Aldrich, T8787-50ML) for 5 min at room temperature. The cells were then blocked for 1 hour in block buffer (1% Bovine Serum Albumin, 2% Goat Serum in PBS) for

1 hour at room temperature. Primary antibodies were diluted in block buffer and cells were stained at 4^{o}C over night. Stained cells were washed three times with PBS and incubated for 1h at room temperature with the appropriate secondary antibody diluted in block buffer. Details of primary and secondary antibodies utilised can be found in Appendix Tables A.11 and A.12 respectively. After staining with the secondary antibody, the cells were washed three times with PBS. Lastly, to visualize the DNA, the cells were stained for 5 minutes with 10 μg/mL of Hoechst 33342 in PBS. Coverslips were retrieved and dipped in distilled water to remove excess salts before mounting with 5 μL of Hydromount (SLS, NAT1324) and kept at 4^{o}C over night to allow the mounting media to harden before imaging. Cells in suspension were seeded in imaging cell culture slides (Greiner, 543079) and were allowed to settle at the bottom of the chamber for 15 minutes before imaging.

For centrosome and ANKRD26 imaging analysis HCT116 cells were seeded in 24 well plates (Corning, 3526) containing autoclaved glass coverslips (SLS, MIC3330) with the appropriate cell media and incubated over night to allow cells to adhere. Cells were washed with PBS and pre-treated for 2 minutes at room temperature with with PTEM buffer: 0.2% Triton X-100, 20 mM PIPES pH 6.8 (Alpha Aesar J60300.AK), 1 mM $MgCl_2$ (Life Technologies Ltd, AM9530G) and 10 mM EGTA (ThermoFisher, A16086.18) in deionised H_2O. Cells were fixed with 4% PFA for 20 minutes at room temperature, and blocked for 1 hour at room temperature with triton block buffer: 2.5% FBS, 200 mM glycine (Life Tech, 15527013) and 0.1% Triton X-100 (Sigma Aldrich, T8787-50ML) in PBS. Primary antibodies were diluted in Triton Block and cells were stained for 1 hour at room temperature. Excess antibody was washed with PBS-T (PBS, 0.1% Triton X-100) before staining with secondary antibody diluted in triton block for 1 hour at room temperature. After washing three times with PBS-T, antibody Fc regions were blocked with Normal Rabbit IgG (Cell Signalling #2729) for 30 minutes at room temperature. Cells were then sequentially stained with an additional primary and secondary antibody using the same steps indicated above. Lastly, coverslips were retrieved and dipped in distilled water to remove excess

salts before mounting with 5 μL of Vectashield (2B Scientific Ltd, H-1900-10). Mounted coverslips were sealed with nail polish and kept at 4^{o}C over night to allow it to harden before imaging.

iPSC-derived and human CD34+ derived MKs and HCT116 cells were imaged using the Leica DMi8 THUNDER (Leica) inverted wide-field microscope. Primary mouse MKs were imaged using the ZEISS LSM 880 Inverted Confocal Microscope.

To ensure proper capture of the entire cell volume, z-stacks series were taken for all experiments. Max-projected images were analysed and quantified using Fiji [125] (v.2.16.0/1.54p) and custom analysis macros.

2.8.2 Live Cell Imaging

CD34+ HSPC-derived MKs were resuspended in fresh MK differentiation media (Appendix Table A.2) supplemented with 1 μM of SiR-DNA (SpiroChrome, SC007), seeded in imaging chambers (Ibidi, 80821) incubated at 37^{o}C for 20 min before imaging. Life cell imaging analysis was performed using the Leica DMi8 THUNDER (Leica) inverted wide-field microscope equipped with an Okolab incubation chamber and fitted with temperature and CO_2 control. Images were taken every 10 minutes over 18h. 4x pixel binning was used to increase detection sensitivity while reducing phototoxicity. Images were analysed using the integrated Leica Application Suite X (LAS X).

2.9 Imaging Flow Cytometry

Samples for Imaging Flow Cytometry were prepared using a similar protocol as described above with the following modifications: cells were only stained with fluorochrome-conjugated primary antibodies (Appendix Table A.4). DNA was stained with DRAQ5 (ThermoFisher, 65-0880-92) for 10 minutes at room temperature. After staining, cells were kept in FACS buffer until analysed. Cells were analysed using the BD FACSDiscover S8 Cell Sorter (BD Biosciences). Flow cytometry files and the corresponding images were analysed using FlowJo (v.10.10.0, BD Biosciences) using the plugging CellView Lens (v.2.0.15, BD

Biosciences). Quantification of imaging parameters was performed using Fiji [125] (v.2.16.0/1.54p).

2.10 Molecular Biology

2.10.1 Reverse Transcription Quantitative PCR

RNA was extracted from pellets of 0.5x10^6 cells using the RNeasy Mini Kit (Qiagen, 74104) following the instructions provided. A NanoDrop spectrophotometer was used to quantify RNA concentration and quality based on the 260/280 and 260/230 absorbance ratios. Equal RNA amounts were reverse-transcribed using the High-Capacity cDNA Reverse Transcription kit (Life Technologies, 4368814). Single-stranded cDNA abundance was quantified using TaqMan Real-Time PCR Assays and the TaqMan Universal PCR Master Mix (ThermoFisher, 4304437) on a StepOne Plus RT-PCR System (ThermoFisher). Ct values were determined using the integrated StepOne software and relative mRNA expression changes were estimated using the ΔΔCt method:

$$\Delta Ct = Ct_{Gene\ of\ interest} - Ct_{Houskeeping\ gene}$$

$$\Delta\Delta Ct = \Delta Ct_{Control\ sample} - \Delta Ct_{Test\ sample}$$

GAPDH was used as housekeeping control for all experiments.

2.10.2 Single Cell RNA Sequencing Analysis of In Vitro Megakaryopoiesis by SmartSeq-3

SmartSeq-3 analysis was performed as previously described [126, 127]. Cells were single cell sorted into nuclease-free 96 well plates (Azenta, 4ti-0770/C) containing 3 μL of Lysis Buffer (Appendix Table A.6). Plates were spun down, and kept at -80^{o}C until processed. Cells were lysed in a thermocycler (ProFlex PCR System, ThermoFisher) at 72^{o}C for 10 minutes. Retro-transcription (RT) was performed immediately after lysis by adding 1 μL of RT buffer per well (Appendix Table A.7) using a MANTIS Liquid Dispenser (FORMULATRIX) and

the published RT conditions [127]. Complementary DNA (cDNA) was amplified by adding 6 μL of PCR mix (Appendix Table A.8) to each well using the MANTIS Liquid Dispenser and the published PCR conditions [127]. As recommended, the number PCR cycles used was experimentally selected as the minimum number of PCR cycles required to produce enough cDNA material for tagmentation (Fig. 2.4). PCR products were stored at -20^{o}C until required for further processing.

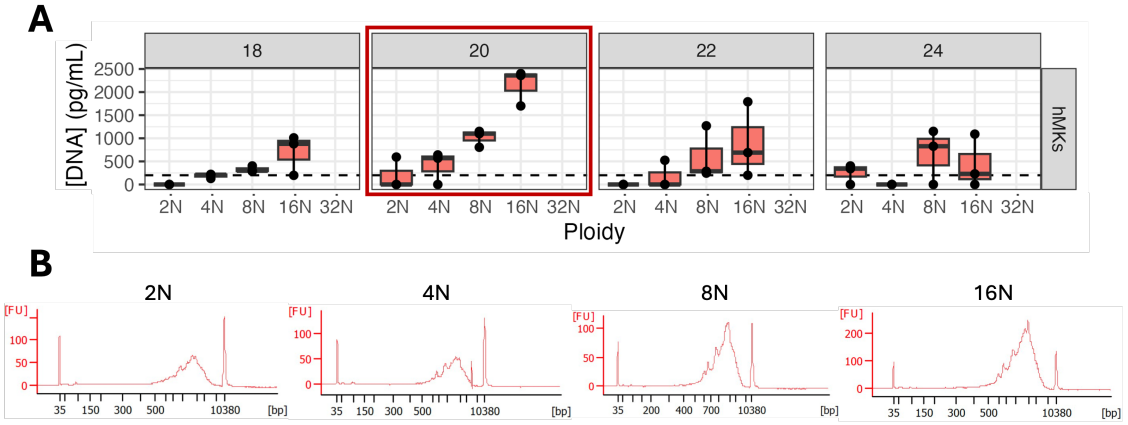


Figure 2.4: PCR cycle optimisation for SmartSeq-3. **A**, DNA concentration determined by Qubit of single cell cDNA libraries at increasing ploidy levels for 4 different number cycles tested. The red box indicates the number of cycles selected. The dashed line indicates the minimum amount of cDNA required to proceed to DNA tagmentation (100 pg/mL). Each dot represents a single cell library. **B**, representative single cell cDNA library traces for each ploidy class after amplification using 20 PCR cycles.

Amplified cDNA was diluted with 10 μL of nuclease free water (Life Technologies, AM9938) and purified using AMPure XP Beads (Beckman Coulter, A63882) at a 0.6:1 beads/library ratio using the automatic liquid handler Biomek FX (Beckman Coulter) and eluted with 12 μL of nuclease free water. Purified cDNA was quantified with QuantiFluor dsDNA (Promega, E2670) in black 384 well microplates (Greiner, 781076) using a CLARIOstar Plus microplate reader (BMG Labtech). cDNA libraries were normalised to 100 pg/μL. 1 μL of normalised cDNA libraries was added to 1 μL of tagmentation solution (Appendix Table A.9) before tagmentation at 55^{o}C for 10 minutes. Using the MANTIS, Tn5 was striped off the DNA by adding 0.5 μL of 0.2% Sodium Dodecyl Sulfate (SDS, Promega, V6551). Lastly, 3 μL of Index PCR mix (Appendix Table A.10) was added along with 1

μL of custom i7 and i5 primers (IDT, Appendix Table A.5) before amplifying the tagmented libraries using the published PCR conditions [127]. Barcode combinations were unique for every cell which permitted single-cell library demultiplexing after sequencing. Amplified libraries were pooled and purified using AMPure XP Beads (Beckman Coulter, A63882) at a 0.6:1 beads/library ratio and a 15 μL elution volume. Library concentration was estimated using the Qubit 1X dsDNA High Sensitivity Kit (ThermoFisher, Q33230) and library traces were inspected using Bioanalyzer High Sensitivity DNA Analysis kit (Agilent, 5067-4626) Fig. 2.5.

Libraries were sequenced at ~200x10^5 reads/cell using a v2.5 150 Cycles NextSeq 500/550 High Output Kit (Illumina, 20024907) and a NextSeq 550 System (Illumina). The following read distribution was used: R1=75, I1=8, I2=8, R2=75.

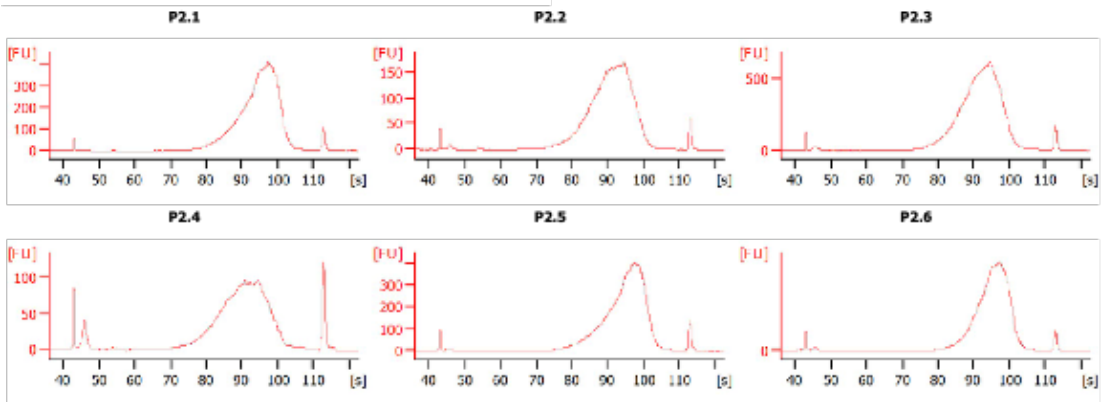


Figure 2.5: Representative cDNA traces of six pooled SmartSeq-3 libraries.

2.10.3 Single Cell Whole Genome Sequencing

Nuclei isolation was performed based on published protocols [128] and 10X Genomics Demonstrated Protocol: CG000169 (Rev E). Briefly, cells were spun down (300 g, 5 min) and resuspended in 100 μL of Nuclei Isolation Buffer (Appendix Table A.13) and incubated 3 minutes on ice before quenching the lysis reaction with 1 mL of Wash Buffer (Appendix Table A.14). Extracted nuclei were stained with Hoechst 33342 for 10 mins at RT and kept in Nuclei Buffer (PBS 0.5x, BSA 0.5 %, Nuclease-free Water) at 4^{o}C until sorted.

Single Cell Whole Genome Sequencing was performed as previously described [129]. Briefly, cells were single cell sorted into 384 well plates (Azenta, 4ti-0387) and stored at -20^{o}C until used. 0.2 μL of Lysis Buffer (Appendix Table A.15) was dispensed to each well using the mosquito LV liquid dispenser (SPT Labtech) and cells were lysed at 55^{o}C for 10 min followed by a 15 min incubation at 75^{o}C to deactivate the protease.

Direct cell tagmentation was performed using 0.6 μL of tagmentation buffer (TD:ATM buffers at 2:1 ratio, Illumina FC-131-1096) at 55^{o}C for 5 min. Tn5 was striped off the DNA by adding 0.2 μL of NT Buffer (Illumina, FC-131-1096).

Finally, tagmented DNA was amplified using 1 μL of custom i7 and i5 primers (IDT, Appendix Table A.5) and 4 μL of PCR buffer (Appendix Table A.16). DNA amplification was performed in a thermocycler (ProFlex^{TM} PCR System, ThermoFisher) using previously described settings [129]. Amplified libraries were pooled and purified using AMPure XP Beads (Beckman Coulter, A63882) at a 1.8:1 beads/library ratio and eluted with 20 μL nuclease free water. Library concentration was estimated using the Qubit 1X dsDNA High Sensitivity Kit (ThermoFisher, Q33230) and library traces were inspected using Bioanalyzer High Sensitivity DNA Analysis kit (Agilent, 5067-4626) Fig. 2.6.

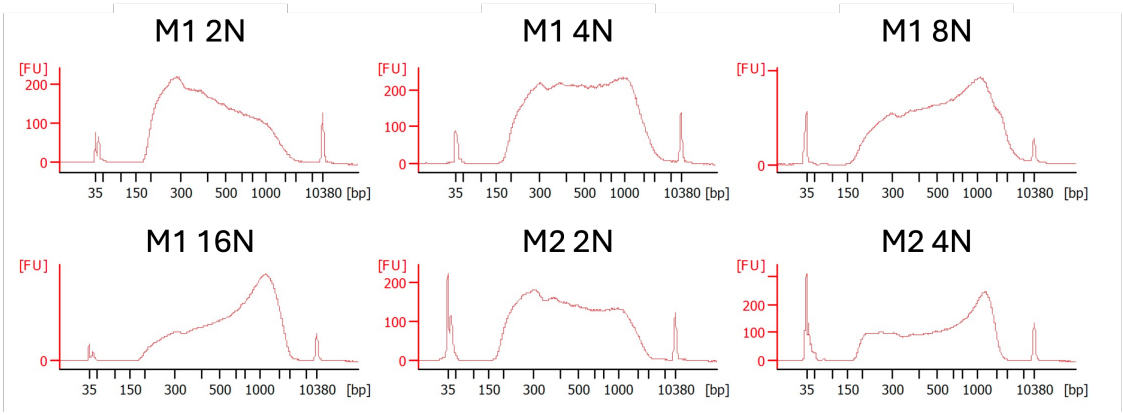


Figure 2.6: Representative cDNA traces of six pooled scDNAseq libraries.

Libraries were sequenced at ~0.05x coverage/cell using a v2.5 150 Cycles NextSeq 500/550 High Output Kit (Illumina, 20024907) in a NextSeq 550 System (Illumina) and the following read distribution: R1=75, I1=8, I2=8, R2=75.

2.11 Single Cell RNA Sequencing Data Processing

2.11.1 Data Pre-processing

Illumina binary base call (BCL) files were uploaded into a High Performance Computing server and demultiplexed into FASTQ files using bcl2fastq conversion software (v2.20.0.422, Illumina). FASTQ files were processed using the zUMIs pipeline [130] and the GRCh38 (v46) assembly of the human genome (GENCODE). Cell by gene count matrices were analysed using the statistical software R (v4.4.1), the integrated development environment RStudio (v2024.04.2+764) and the Seurat package (v5.3.0) [131, 132]. In parallel, cell metadata (patient of origin, sorting day and associated sorting index data) was manually collated and loaded in the metadata slot of the Seurat object.

2.11.2 Data Analysis

High quality cells were selected based on standard scRNAseq Quality Control parameters [133], that is, an adequate number of genes detected (>200) per cell and a low fraction of reads mapping to the mitochondrial genome (<15%), which is generally indicative of dying/stressed cells Fig. 2.7.

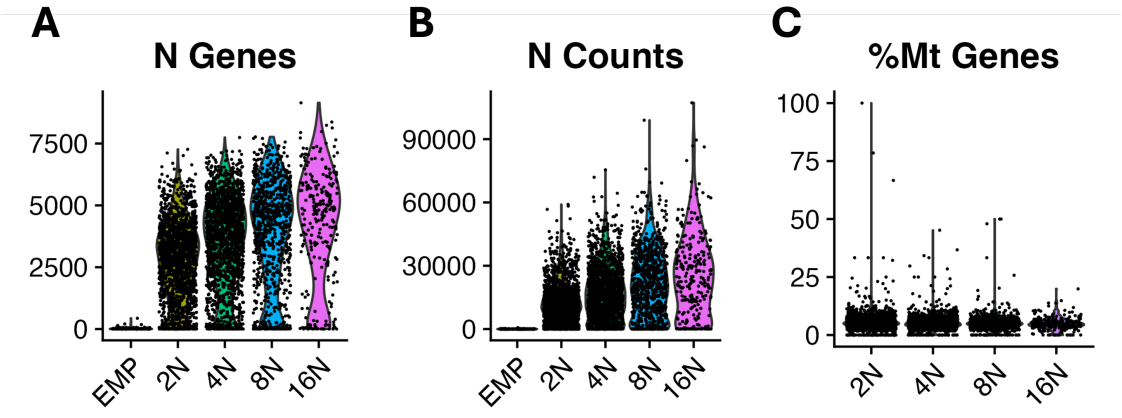


Figure 2.7: scRNAseq quality control metrics. **A**, number of genes detected per cell. **B**, number of read counts per cell. **C**, percentage of reads assigned to mitochondrial genes. **A-C**, cells are grouped by ploidy as determined by flow cytometry. Each dot represents a single cell. EMP = Empty well.

Gene expression counts were normalised using the Single Cell Transform algorithm [134] while eliminating potential confounding factors (fraction of reads mapping to the mitochondrial genome, S phase score and G2M phase score). Principal component analysis (PCA) was performed using the normalised counts matrix and inter-patient variability was corrected using Harmony [135]. The first 30 dimensions of the harmonised PCA matrix were used to compute a non-linear dimensionality reduction embedding using uniform manifold approximation and projection (UMAP) [136]. The K-nearest neighbour graph was calculated on the based on the first 30 dimensions of the harmonise PCA which was used to estimate the cell neighbourhoods (clusters) using Leiden's algorithm (resolution = 0.3) [133]. All functions utilised for processing are integrated in the Seurat v5 package. Clusters were manually annotated based on the expression of common marker genes (Section 4.2.1 , Fig. 4.6 A, B).

2.11.3 Cell Cycle Analysis

Cell cycle phase prediction was performed using the transfer learning approach Tricycle [137] on the log-normalised gene expression matrix with the default parameters. To correct for the confounding effects between ploidy and cell cycle phase, cells predicted to be in G2M phase were re-assigned the immediately lower ploidy class. To study gene expression changes across the cell cycle, cells were sorted based on their Tricycle-predicted cell cycle position and divided in quantiles.

2.11.4 Pathway Analysis

Global pathway gene expression was calculated using Seurat's AddModule-Score function and lists of genes obtained from published gene signatures[104, 138–140] and a manually curated list of target genes directly downstream of p53 (Appendix Table A.17). Differential pathway activity between diploid and polyploid classes was estimated as the coefficient for Ploidy on the generalised linear regression model $Pathway\ Score \sim Ploidy$ and the significance was obtained

from the associated p value after correcting for multiple comparisons using the False discovery rate (FDR) method.

2.11.5 Trajectory Analysis

The MK differentiation trajectory was estimated using Monocle3 [141] with optimised parameters (minimal branch length = 25) to avoid over-branching. Cells were divided in four pseudotime quantile groups and the pseudobulk gene expression for each quantile was estimated using DESeq2 [142].

2.12 Single Cell Whole Genome Sequencing Analysis

Illumina binary base call (BCL) files were loaded into a High Performance Computing server and demultiplexed into FASTQ files using bcl2fastq conversion software (v2.20.0.422, Illumina). FASTQ files were aligned to the GRCm38 (mm10) assembly of the mouse genome using a Burrows-Wheeler Aligner (v0.7.18) implemented in the BWA-MEM algorithm [143]. BAM files containing the aligned reads were coordinate-sorted using SAMtools [144] (v1.17) and duplicated reads were marked using the MarkDuplicates function from picard-tools (v3.2.0) [145].

Processed BAM files were analysed using the statistical software R (v4.4.1), the integrated development environment RStudio (v2024.04.2+764) and the package AneuFinder (v1.35.0) [146]. Unique reads were grouped in regions (bins) of 500 kilobases and counted. Regions of poor mappability (blacklist regions) were identified using a diploid control sample and defined as the regions with counts that deviate >1 standard deviation from the median counts of the control sample. Sex chromosomes were also excluded from the analysis. High quality cells were selected based on sufficient average number of reads per bin (>100) and low spikiness (<0.5), to accounts for local fluctuations in coverage derived from low-quality mapping. Copy Number Variation (CNV) calls were estimated using the AneuFinder-implemented algorithm edivisive including correction for GC content. The aneuploidy score was estimated using the function karyotypeMeasures from AneuFinder.

2.13 Cancer Cell Line Encyclopedia Analysis

Datasets containing the normalised mRNA gene expression values, WGD status, mutation status and characteristics for all cell lines in from the Cancer Cell Line Encyclopedia were obtained from the DepMap database [147]. Cells were called p53 wild-type when the number of p53 damaging mutations was equal to 0, and p53 mutant otherwise. Gene expression changes with ploidy were estimated as the coefficient for the WGD component of the following generalised linear regression model:

$$Expresion_{Gene\ i} \sim WGD + Lineage$$

Where WGD reflects the whole genome duplication status (Diploid or Polyploid) and Lineage the tissue of origin of each cell line. P values associated to the WGD component were corrected for multiple testing using the Family Discovery Rate method.

2.14 Statistical Analysis

All of the statistical analyses were performed using the the statistical software R (v4.4.1) and the base packages. For all comparisons, the Shapiro–Wilk normality test was performed to determine if the data was normally distributed. When the data was normally distributed parametric tests (i.e., t-test) were used. For non-normally distributed data non-parametric tests (i.e., Wilcoxon rank sum test) were performed. The p value = 0.05 was used as the significance threshold for all analyses. All p values are reported using the following notation: $ns = p > 0.5, * = p < 0.05, ** = p < 0.01, *** = p < 0.001, **** = p < 0.0001$.

3

Impact of Whole Genome Duplication on Megakaryocyte Genome Integrity

Contents

3.1 Introduction 48
3.1.1 Genomic Integrity in Scheduled Polyploidy 49
3.1.2 DNA Damage in Megakaryocytes 50
3.1.3 Chapter Aims 51
3.2 Results 52
3.2.1 Megakaryocytes Accumulate DNA Damage 52
3.2.2 Primary Polyploid Megakaryocytes Are Genetically Unstable 57
3.2.3 Copy Number Alterations on Primary Megakaryocytes . 59
3.3 Discussion 63

3.1 Introduction

Proliferation after whole genome duplication (WGD) is associated with catastrophic effects to DNA integrity, and inappropriate access to polyploidy can drive cancer progression. To prevent this, scheduled polyploidy often arises as a terminal differentiation event and is linked to cell cycle arrest. However, the consequences of WGD for the integrity of the megakaryocyte (MK) genome has not been previously interrogated.

3.1.1 Genomic Integrity in Scheduled Polyploidy

During homeostasis, renewal of the hepatic parenchyma is mostly sustained by diploid hepatocytes [148]. However, upon partial hepatectomy, both diploid and polyploid hepatocytes participate in liver regeneration. As detailed earlier, this process involves a combination of ploidy-increasing cell cycles and ploidy-reducing mitoses, a model that is commonly referred to as the "ploidy conveyor" [65]. Hepatocyte ploidy reversal occurs via multipolar mitoses whereby supernumerary centrosomes on polyploid hepatocytes form multipolar spindles that separate the genetic material into three or more daughter cells of lower ploidy. Imbalanced segregation of chromosomes during multipolar mitoses is frequent, and leads to chromosomal instability [109], yet the degree of aneuploidy on the regenerating liver is a matter of debate.

Original studies using fluorescence *in situ* hybridization (FISH) suggested that up to 60% of adult mouse hepatocytes were aneuploid [149]. However, follow-up work using single cell whole genome sequencing reported that only 5% human and mouse hepatocytes had detectable copy number variation (CNV) events [150]. Importantly, aneuploidy is mitigated on diploid livers from E2f7/E2f8-deficient mice demonstrating that, albeit at a small scale, WGD is a source of genetic variation in hepatocytes [151].

The scarcity of copy number aberrations observed on polyploid hepatocytes contrasts markedly with *in vitro* studies where multipolar mitoses give rise to highly aneuploid -often inviable- cells [109]. Crucially, seminal work comparing mitotic polyploid hepatocytes in mouse regenerating livers and primary cultures demonstrated that tissue architecture can enhance the correction of merotelic microtubule-kinetochore attachments, facilitating chromosome segregation fidelity on polyploid livers [152].

Interestingly, non-mitotic polyploid cells can also accumulate copy number alterations. Trophoblast Giant Cells (TGC) can acquire up to 1000 genome copies via recursive endocycling, therefore avoiding potentially error-prone mitotic progression. Nevertheless, whole genome sequencing revealed presence of

recurrent under- and over-represented genomic regions on polyploid murine TGCs, which are thought to arise from selective DNA replication during TGC endocycles [153, 154]. Perhaps most importantly, over-represented DNA regions were enriched in functionally relevant genes for mammalian placentation, indicating that TGC can harness genetic instability to enhance their biological functions [154].

Lastly, polyploid cells such as hepatocytes can accumulate other types of DNA damage in addition to aneuploidy events [155]. Strikingly, while diploid cells respond to genotoxic stress with apoptosis, polyploid cells appear more resistant to DNA damage accumulation. Mouse whole body γ-irradiation causes a strong activation of the apoptotic marker caspase-3 in the intestine and spleen whereas polyploid hepatocytes suppress apoptosis-inducing p53 target genes [156]. In polyploid TGC, suppression of apoptosis has also been described [52]. The mechanism behind this process is unclear, although appears to be liked to p21, which is highly expressed in non-proliferating polyploid cells and can block DNA damage-dependent apoptosis via Chk1 inhibition [52, 157].

3.1.2 DNA Damage in Megakaryocytes

Multiple megakaryopoietic factors have been liked to DNA damage repair [158]. GATA binding factor 1 (GATA1), an essential transcription factor of the erythroid/MK lineage, can induce the expression of the nucleotide excision repair pathway gene ERCC1 (excision repair cross-complementing 1) [159]. The essential megakaryopoietic transcription factor RUNX1 can facilitate DNA repair by recruiting FANCD2 -one of the key molecules in the Fanconi Anemia pathway- to the DNA damage site [160]. Lastly, the key physiological regulator of megakaryopoiesis thrombopoietin (TPO) can also play a role in the repair of DNA double-strand breaks. After binding to its receptor MPL, TPO can increase DNA-PK-dependent non homologous end joining repair efficiency. This process was demonstrated to be essential for the proper maintenance of the genomic integrity of haematopoietic stem cells (HSCs) which also express MPL [161, 162].

Importantly, the role of these megakaryopoietic factors on DNA damage repair have been demonstrated on HSC and MK progenitors and little is known about DNA damage repair dynamics on polyploid MKs.

DNA double-strand breaks have been detected in a subset of *in vitro*–derived MKs [163]. However, it remains unclear whether such DNA damage also occurs during primary megakaryopoiesis, and whether WGD contributes to this process. Notably, the karyotypic integrity of polyploid MKs has never been directly assessed. Genomic profiling of cell-free DNA (cfDNA) within platelets described recurrent copy number alterations that were absent from plasma cfDNA, raising the possibility that these reflect genomic changes originating from the parent MK [164]. Nevertheless, recent evidence indicates that platelet cfDNA is not exclusively derived from MKs [165], suggesting that DNA patterns observed in platelet cfDNA may not provide a definitive readout of MK biology.

3.1.3 Chapter Aims

Increasing evidence demonstrates that programmed WGD may compromise the genomic integrity of proliferating polyploid somatic cells. Yet, key questions on the impact of WGD on actively cycling highly polyploid MKs remain unanswered. Do 'healthy' MKs accumulate DNA damage, even in steady-state physiology? Is WGD itself linked to such damage? Are MKs genetically stable? To explore these questions, this chapter will address the following aims:

1. To study DNA damage across MK ploidy spectrum.
2. To evaluate DNA damage levels in primary unperturbed MKs.
3. To assess the genomic integrity of primary MKs.

3.2 Results

3.2.1 Megakaryocytes Accumulate DNA Damage

To begin exploring whether polyploidy has detrimental effects on the genome integrity of MKs, I first fluorescently labelled the erythroleukaemia cancer cell line HEL for the DNA double strain break marker γH2AX. HEL cells are hypotriploid but can spontaneously undergo one or more polyploidization rounds in culture. To accurately separate the different ploidy classes while simultaneously analysing nuclear γH2AX levels I utilised a flow cytometer equipped with a high-speed fluorescence imaging module [166]. Importantly, incorporation of imaging parameters on the gating strategy permitted faithful separation of truly polyploid cells from cell doublets (Fig. 3.1A). To validate this approach for the detection of DNA damage, HEL cells were exposed to X-ray irradiation to induce DNA double strand breaks and the formation of γH2AX foci was followed over time (0.5h and 4h after irradiation). There was significant upregulation of γH2AX levels 0.5h after irradiation and partial resolution of the DNA damage sites after 4h (Fig. 3.1B-D), demonstrating that this approach can be use to detect DNA damage formation and repair.

Next, the DNA content marker DRAQ5 was used in combination with γH2AX staining to determine if WGD has any effects on DNA damage accumulation. As expected, ploidy levels determined by flow cytometry correlated with the cell nuclear area estimated from the imaging module (Fig. 3.2A,C). More importantly, γH2AX mean fluorescence intensity increased significantly after each WGD round, indicating that polyploidization negatively impacts DNA integrity (Fig. 3.2B,D).

To validate these results in a more physiological system I analysed γH2AX levels on MKs derived *in vitro* from a human inducible pluripotent stem cell (iPSC) line. Since iPSC differentiations do not produce pure MK cultures but a combination of un-differentiated progenitor and fully matured iPSC-derived MKs (iMKs) the MK cell marker CD41 was included on the staining protocol to successfully identify iMK cells (Fig. 3.3A). Moreover, the fluorescence microscope

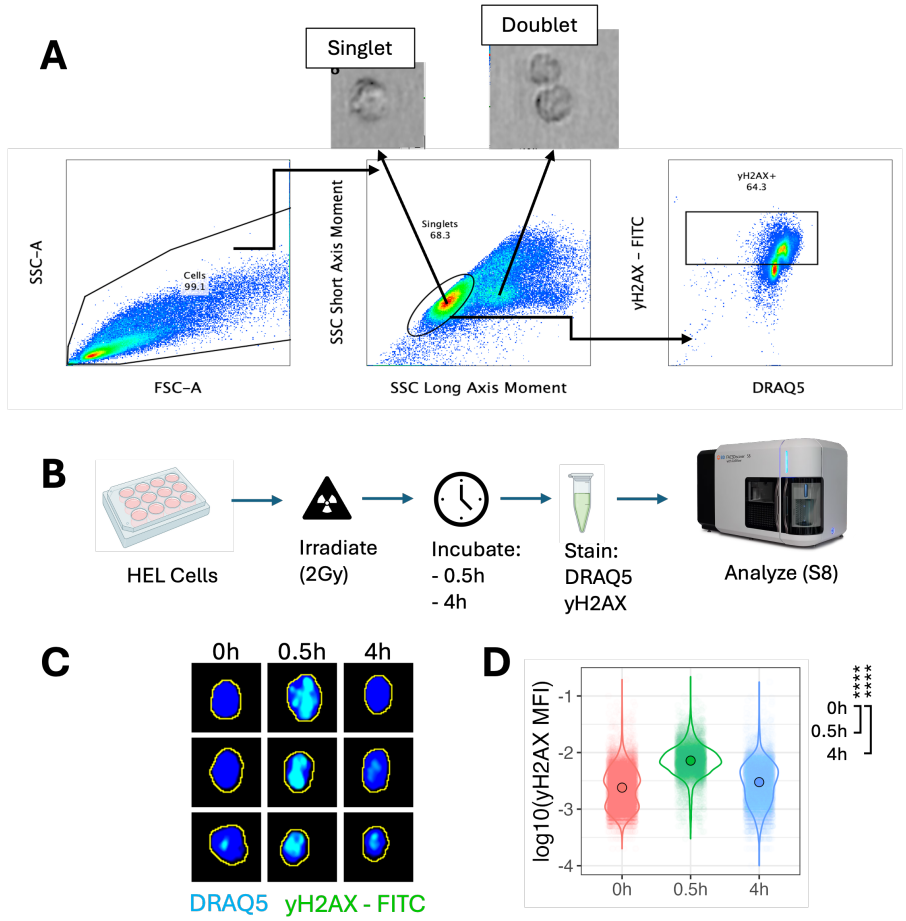


Figure 3.1: Validation of imaging flow cytometry for γH2AX detection. **A**, gating strategy for imaging flow cytometry. **B**, experimental design for DNA damage induction and analysis using imaging flow cytometry. **C**, representative images from three individual cells captured by the imaging module and showing DNA (DRAQ5, in blue) and DNA damage foci (γH2AX, in green, appearing as light blue on the image). The yellow line represents the computationally-defined nuclear border. **D**, quantification of the nuclear γH2AX mean fluorescence intensity from the images obtained. Data from n=1 experimental replicate. Significance obtained from Wilcoxon rank sum test. $ns = p > 0.5, * = p < 0.05, ** = p < 0.01, *** = p < 0.001, **** = p < 0.0001$

Leica DMi8 was used to increase the resolution of the γH2AX sites. This approach also permitted the analysis of z-stack series, ensuring that all regions of the diploid and polyploid nuclei were captured.

Analysis of unperturbed iMKs showed significantly increased γH2AX levels on CD41+ iMKs when compared with CD41- non-MK cells (Fig. 3.3C). Importantly, γH2AX levels were significantly elevated even when accounting for the potential differences in nuclear size (N^o γH2AX Foci/Nuclear Area). To validate if DNA

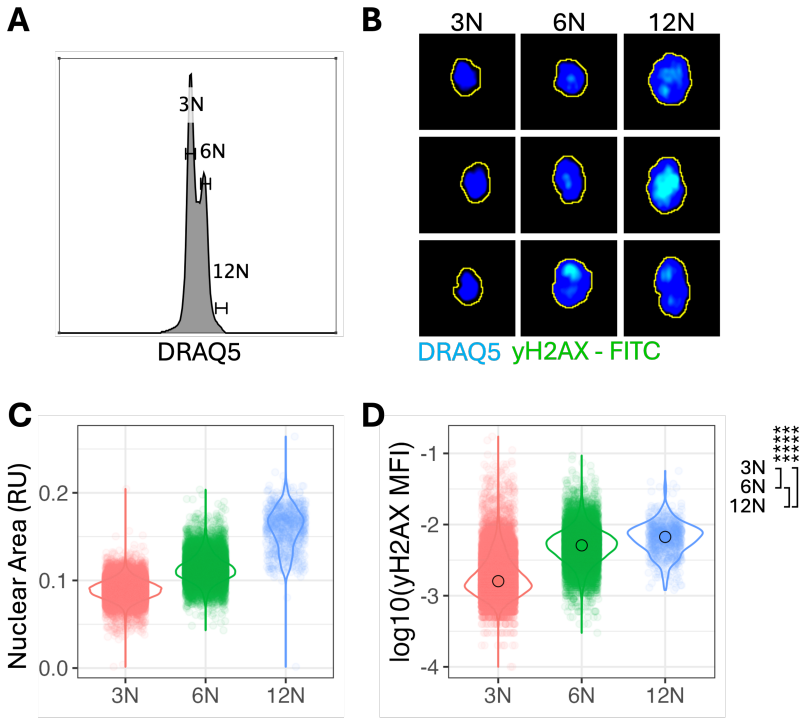


Figure 3.2: γH2AX detection on HEL cells by ploidy. **A**, gating strategy to separate ploidy populations. **B**, representative images from three separated cells captured by the imaging module and showing DNA (DRAQ5, in blue) and DNA damage foci (γH2AX, in green). The yellow line represents the computationally-defined nuclear border. **C**, quantification of nuclear area of different ploidy groups. **D**, quantification of the γH2AX nuclear mean fluorescence intensity of different ploidy groups. Data from n=1 experimental replicate. Significance obtained from Wilcoxon rank sum test. $ns = p > 0.5, * = p < 0.05, ** = p < 0.01, *** = p < 0.001, **** = p < 0.0001$

damage also increased with iMK ploidy, CD41+ cells were selected and stratified by increasing nuclear area on four groups (Fig. 3.3B). Interestingly, γH2AX density was significantly elevated on iMKs from the largest area group compared with the smaller iMKs analysed, indicating that DNA damage is accumulated following WGD (Fig. 3.3D).

It is important to note that the DNA damage accumulation observed on CD41+ iMKS when compared to CD41- non-MK cells (shown in Fig. 3.3C) could not solely be explained by differences in ploidy, since the vast majority of the MKs produced from iPSC cells are diploid (Fig. 3.3B). It is therefore possible that iMKs (diploid and polyploid) present altered DNA damage repair dynamics compared to non-iMKs. To test this hypothesis, I exposed CD41+/- iPSC-derived cells to

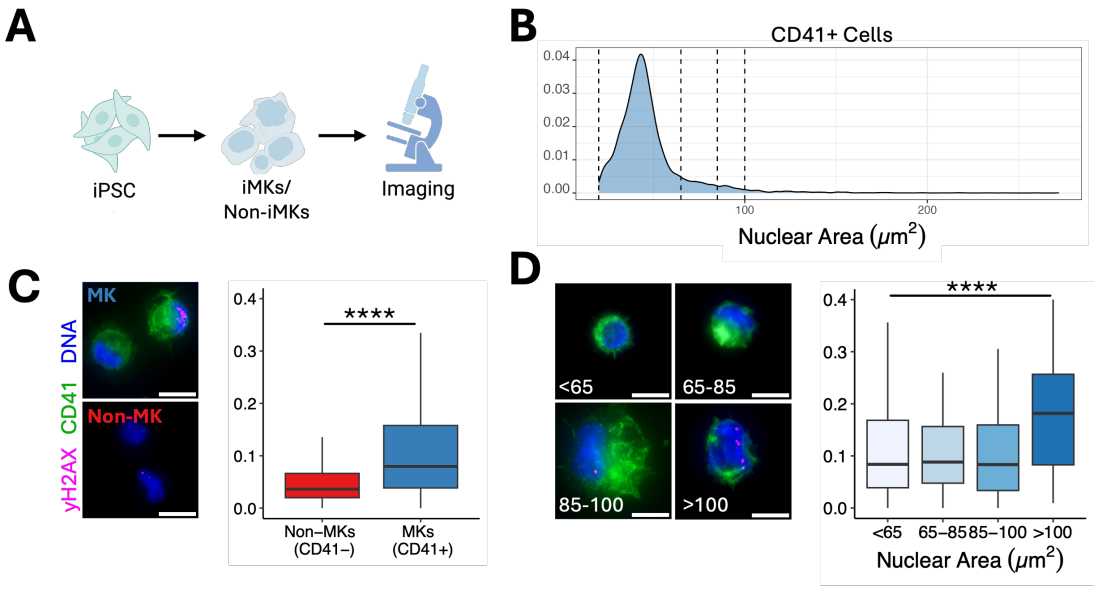


Figure 3.3: Analysis of γH2AX on iMKs. **A**, experimental approach to study DNA damage on iMKs. **B**, Nuclear area distribution of CD41+ iMKs. The dashed lines represent the intervals utilised for ploidy analysis on panel D. **C**-left, representative immunofluorescence images showing DNA (Hoechst, in blue), DNA damage foci (γH2AX, in magenta) and CD41 (in green). **C**-right, quantification of γH2AX foci in iMKs and non-iMK cells. Significance obtained from Wilcoxon rank sum test. **D**-left, representative images of CD41+ iMKs based on nuclear area. **D**-right, quantification of γH2AX foci in iMKs by nuclear area. Significance obtained from Wilcoxon rank sum test. Panels **B-D** show combined data from n=2 experimental replicates. Panels **C,D**; scale bar = 15μm. $ns = p > 0.5, * = p < 0.05, ** = p < 0.01, *** = p < 0.001, **** = p < 0.0001$.

low dosage (2 Gy) x-ray irradiation and followed the accumulation of γH2AX foci over time (Fig. 3.4A). In both cell groups (CD41 positive and negative cells) γH2AX foci peaked 0.5h post exposure with no significant differences between conditions (Fig. 3.4B,C). Strikingly, CD41+ iMKs showed delayed resolution of DNA damage sites over time, and γH2AX foci density was significantly higher for all time points evaluated after 0.5h (Fig. 3.4B,C). These result suggest that MKs have defective DNA damage repair capabilities.

To evaluate if DNA damage repair is also altered with ploidy, CD41+ iMKs were subdivided based on their nuclear area into diploid (<65μm^2) and polyploid (>65μm^2). As expected, before irradiation polyploid iMKs showed significantly higher γH2AX levels compared to diploid iMKs (Fig. 3.4D). Interestingly, DNA damage clearance dynamics were not significantly different between diploid

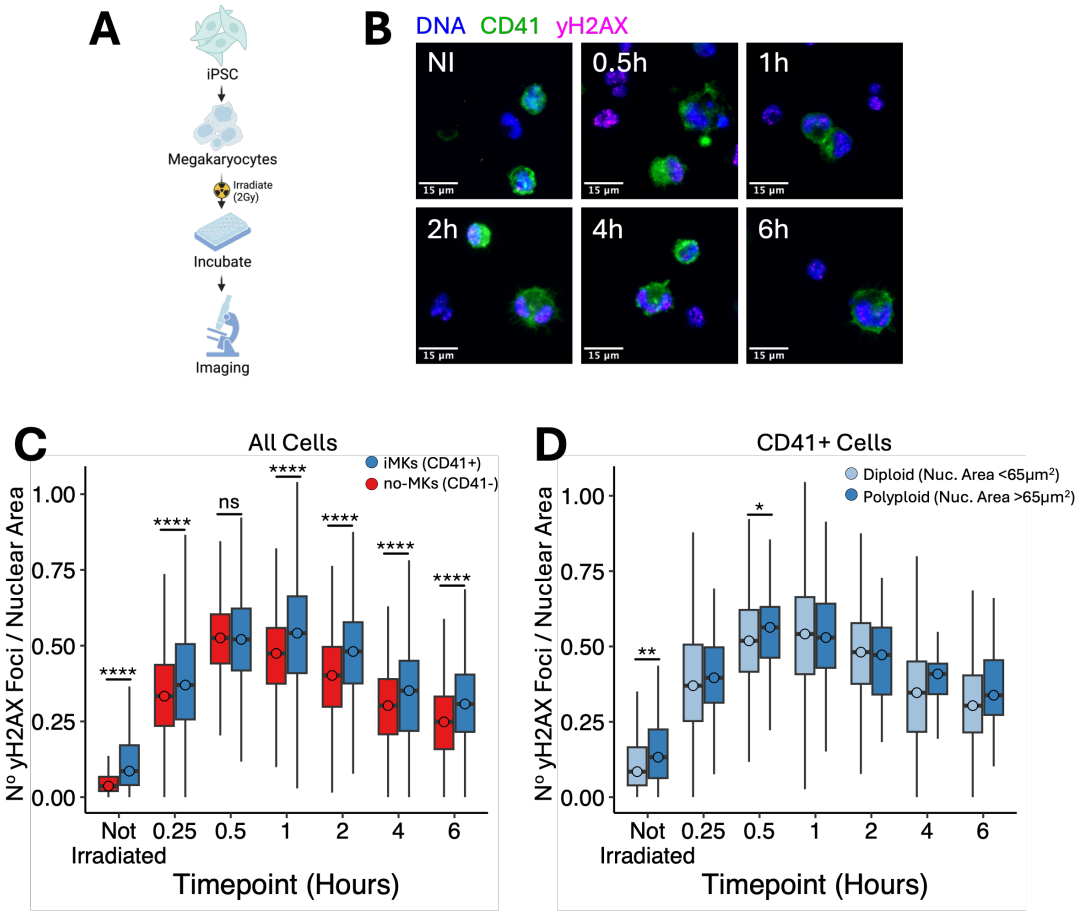


Figure 3.4: Study of DNA damage repair dynamics on iMKs. **A**, experimental approach to study DNA damage repair dynamics on iMKs. **B**, representative immunofluorescence images showing DNA (Hoechst, in blue), DNA damage foci (γH2AX, in magenta) and CD41 (in green). NI = Not Irradiated, scale bar = 15µm. **C**, γH2AX quantification results on iMKs (CD41+) and no-iMK (CD41-) for all time points. **D**, γH2AX quantification results on diploid (nuclear area <65µm^2) and polyploid (nuclear area >65µm^2) iMKs for all time points. Panels **B-D** show combined data from n=2 experimental replicates. Panel **B-C**, significance obtained from Wilcoxon rank sum test; $ns = p > 0.5, * = p < 0.05, ** = p < 0.01, *** = p < 0.001, **** = p < 0.0001$.

and polyploid iMKs, suggesting that defects on DNA damage repair are not enhanced by WGD.

Taken together, these results suggest that WGD increases the DNA damage burden in MKs. Importantly, MKs show intrinsic DNA repair deficiencies which might exacerbate the detrimental effects of WGD on MK genomic integrity.

3.2.2 Primary Polyploid Megakaryocytes Are Genetically Unstable

Following my previous observations *in vitro*, I set out to validate these results *in vivo*. The study of primary MKs presents several challenges. First, polyploid MKs are large and fragile, and do not survive cryopreservation methods, which impedes their study from human bone marrow samples. Moreover, histological examination of bone marrow sections is restricted to a single two-dimensional slice of the polyploid nucleus, missing the vast majority of structural and functional information. To bypass these limitations, I implemented a recently published method for fast and direct isolation of primary MKs from murine bone marrow samples [122].

Isolated mouse MKs were stained for γH2AX, CD41 and Hoechst, and imaged using the confocal microscope Zeiss LSM 880 over multiple z-stacks to capture the entire cell volume. MK-depleted bone marrow cells from the same mouse were used as isogenic diploid controls for the analysis (Fig. 3.5A). Imaging analysis revealed a significant increase of γH2AX foci on large polyploid MKs when compared to diploid bone marrow cells. Indeed, while over 80% of the bone marrow cells did not have a single DNA double strand break site, most of the MKs imaged contained at least 1 γH2AX foci in their nucleus (>60%, Fig. 3.5B, D). Interestingly, γH2AX levels did not significantly correlate with MK nuclear area (Fig. 3.5C).

Detailed inspection of the confocal images revealed an unexpected finding. A large proportion of the MKs analysed contained micronuclei inside their cytoplasm (Fig. 3.6A). Importantly, 3D reconstruction confirmed that the micronuclei where indeed independent DNA structures, completely separated form the main poly-lobulated MK nucleus (Fig. 3.6B). MKs can transiently engulf bone marrow cells -particularly neutrophils- inside their cytoplasm in a process termed emperipolesis [167]. Of note, the micronuclei area was significantly smaller than the average nuclear area of a diploid bone marrow cell, confirming that the DNA bodies observed inside the MKs were micronuclei an not emperipoletic cells (Fig. 3.6C). A

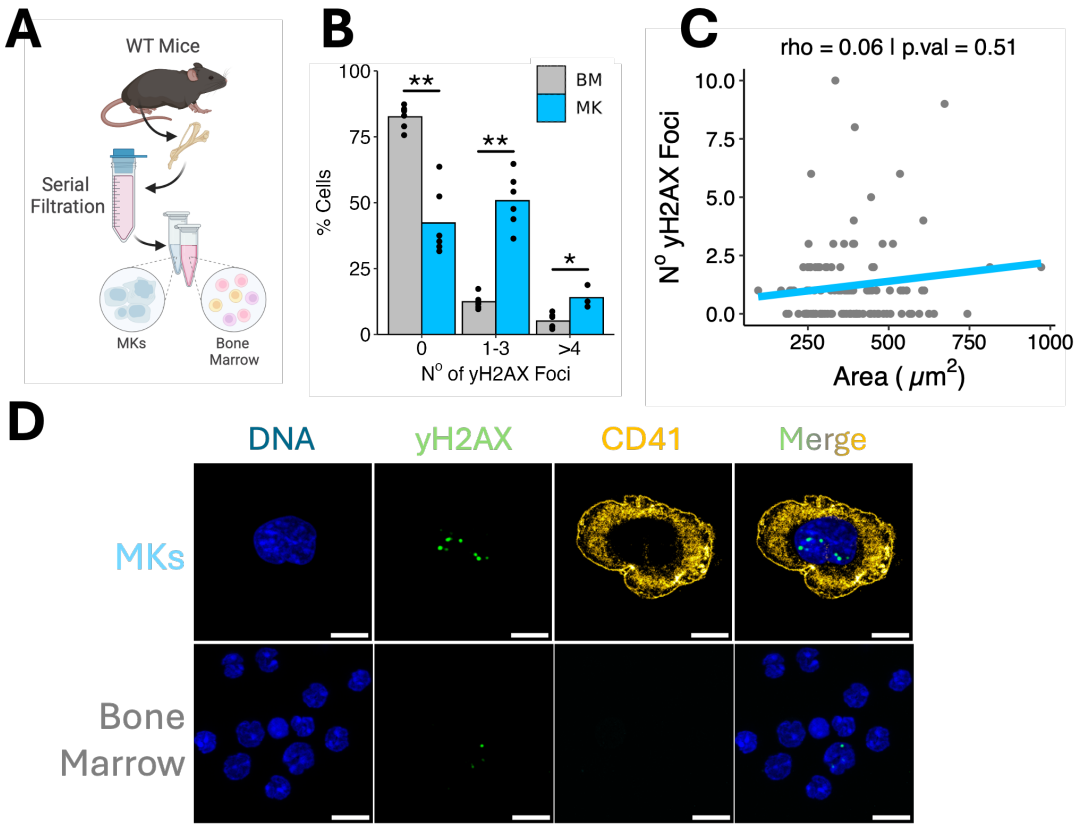


Figure 3.5: Primary mouse MKs accumulate DNA damage. **A**, experimental approach to isolate primary MKs from mouse bone marrow samples. **B**, quantification of γH2AX foci on MKs and diploid bone marrow cells. Each dots represents a mouse. Significance obtained from t-test. **C**, Spearman's rank correlation between γH2AX foci number and nuclear area on mouse MKs. Each dot represents an MK. **D**, representative confocal immunofluorescence images showing DNA (Hoechst, in blue), DNA damage foci (γH2AX, in green) and CD41 (in yellow). Scale bar = 15µm. Panels **B,C** show combined data from n=6 mice and three experimental replicates. $ns = p > 0.5, * = p < 0.05, ** = p < 0.01, *** = p < 0.001, **** = p < 0.0001$.

single MK could contain up to 10 micronuclei although most of the MKs analysed presented only one (Fig. 3.6E). Crucially, when stratified by nuclear area, the fraction of MKs containing at least one micronuclei significantly increased with ploidy, indicating that micronuclei formation was more frequent after each WGD round (Fig. 3.6D). Interestingly, approximately 30% of the micronuclei showed pan-nuclear γH2AX staining, and a single MK could contain both γH2AX+ and γH2AX- micronuclei within their cytoplasm (Fig. 3.7).

In summary, I have confirmed that primary MKs accumulate DNA damage during their healthy, unperturbed, steady-state physiology. Moreover, polyploid

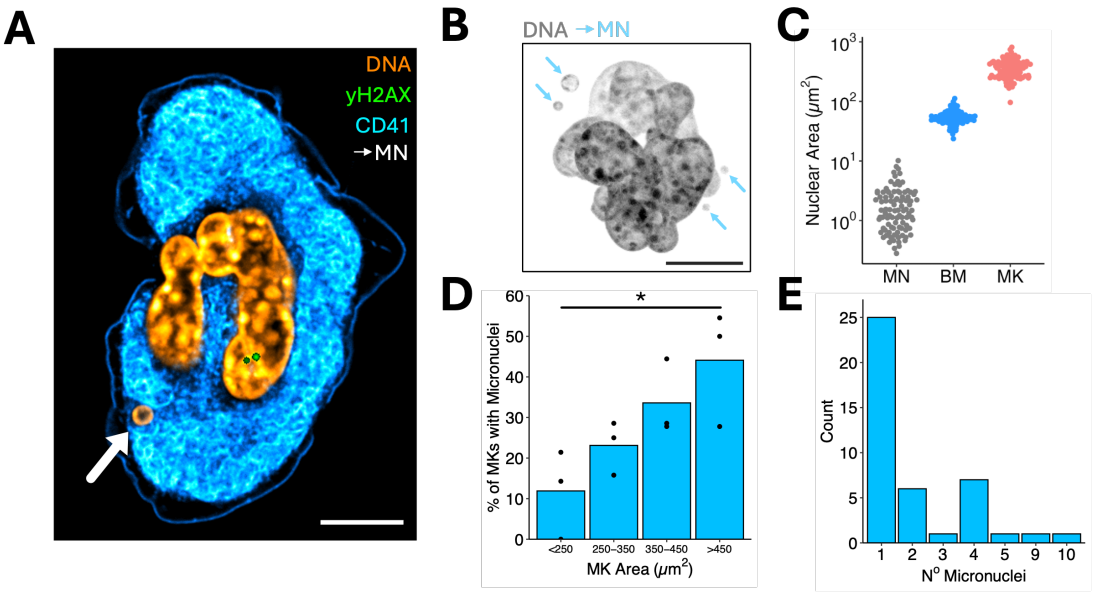


Figure 3.6: Evidence of micronuclei formation in primary mouse MKs. **A**, representative confocal immunofluorescence image showing DNA (Hoechst, in orange), DNA damage foci (γH2AX, in green) and CD41 (in cyan). The white arrow points at a micronuclear structure in the cytoplasm. Scale bar = 10μm. **B**, representative 3D reconstruction of a single primary mouse MK nucleus. Blue arrows indicate the micronuclei. Scale bar = 10μm. **C**, quantification of micronuclei, bone marrow and MK nuclear area. Each dot represents a cell. **D**, quantification of the proportion of MKs containing > 1 micronuclei as a function of their nuclear area. Each dot represents an experimental replicate. Significance obtained from T-test. **E**, histogram of the number of MKs based on the number of micronuclei they contain. Panels **C-E** show combined data from three experimental replicates and n=6 total mice. MN = micronuclei, BM = bone marrow, MK = megakaryocyte. $ns = p > 0.5, * = p < 0.05, ** = p < 0.01, *** = p < 0.001, **** = p < 0.0001$.

MKs show high levels of micronuclei, which are classic markers of chromosomal instability, and indicate that polyploid MKs are genetically unstable.

3.2.3 Copy Number Alterations on Primary Megakaryocytes

The high micronuclei frequency in MKs suggests that they might accumulate numerical and structural chromosomal abnormalities. To study the karyotype stability of MKs I implemented a previously published single cell whole genome sequencing method (scWGS) that had been utilised to reveal CNV profiles from polyploid cells [129] (Fig. 3.8A, Methods). For this analysis, nuclei from primary mouse MKs and matching MK-depleted diploid bone marrow cells were isolated and sorted into 384 well plates. DNA traces of scWGS libraries

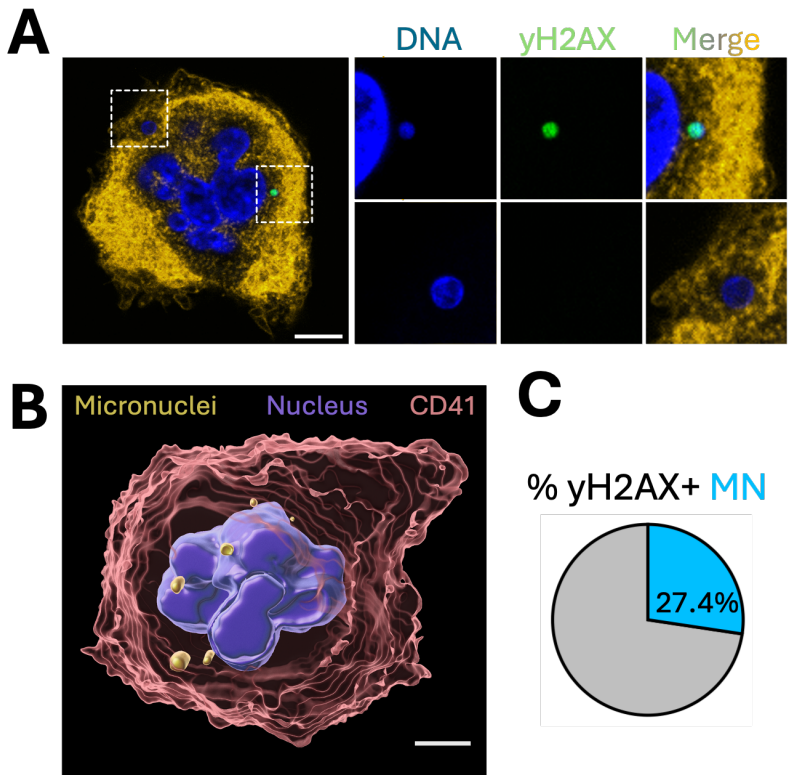


Figure 3.7: MK micronuclei are a source of DNA damage. **A**-left, representative confocal immunofluorescence image of a mouse MK stained for DNA (Hoechst, blue), CD41 (yellow) and DNA double strand breaks (γH2AX, green). Scale bar = 10µm. **A**-right, zoom-in of γH2AX+ (top row) and γH2AX- (bottom row) micronuclei detected within the body of an MK. **B**, 3D Render of MK shown in panel A highlighting the presence of multiple micronuclei. MK main nuclear body is depicted in blue and micronuclei in yellow, red colour shows CD41 cell surface expression (the CD41+ membrane demarcation system staining has been removed for clarity). Scale bar = 10µm. **C**, pie-chart showing the percentage of γH2AX positive micronuclei. Combined data from three experimental replicates and n=6 total mice.

were visually inspected (Fig. 3.8B) before performing low-coverage sequencing (~ 0.05X per cell). Interestingly, the distribution of the tagmented DNA fragment size changed with MK ploidy (Fig. 3.8B). After sequencing, high quality scWGS libraries were selected based on low spikiness (which reflects even coverage density of the mapped genome) and high average number of reads per binned region (Fig. 3.8C, Methods).

Selected high quality libraries were analysed for genomic CNVs. As hypothesized, MKs display significantly increased aneuploidy values (Fig. 3.9C). Genome wide analysis of CNV profiles showed both whole chromosome and structural

numerical alterations on MKs whereas no significant CNV were observed in MK-depleted diploid bone marrow cells (Fig. 3.9A, B). Interestingly, CNV events did not show any clonal patterns in MKs and where more commonly due to deletions, suggesting that they originate from random chromosome mis-segregation and loss events (Fig. 3.9B).

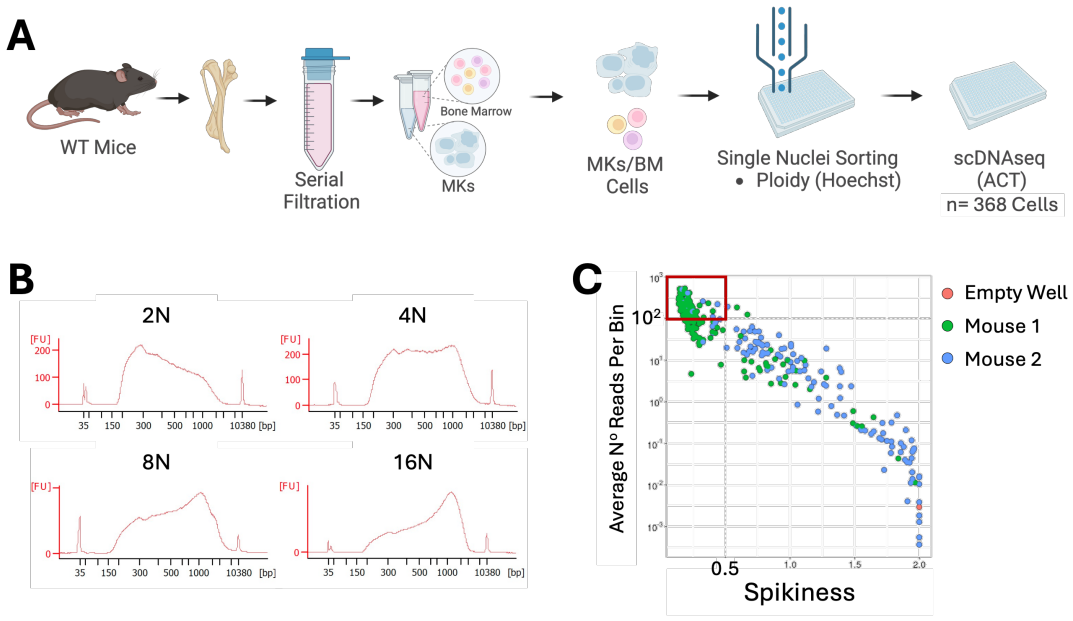


Figure 3.8: Preparation and quality control of single cell whole genome sequencing libraries. **A**, schematic showing the protocol used to isolate single nuclei for Single Cell Whole Genome Sequencing (scWGS) of MKs and MK-depleted bone marrow cells from healthy, adult mice. **B**, representative DNA fragment size analysis of pooled scWGS libraries for mMKs of increasing ploidy levels. **C**, scatter plot showing the quality control values utilised for selecting high-quality cells. Each dot represents a single cell. The red box highlights the high quality cells selected for analysis. Combined data from n=2 mice and one experimental replicate.

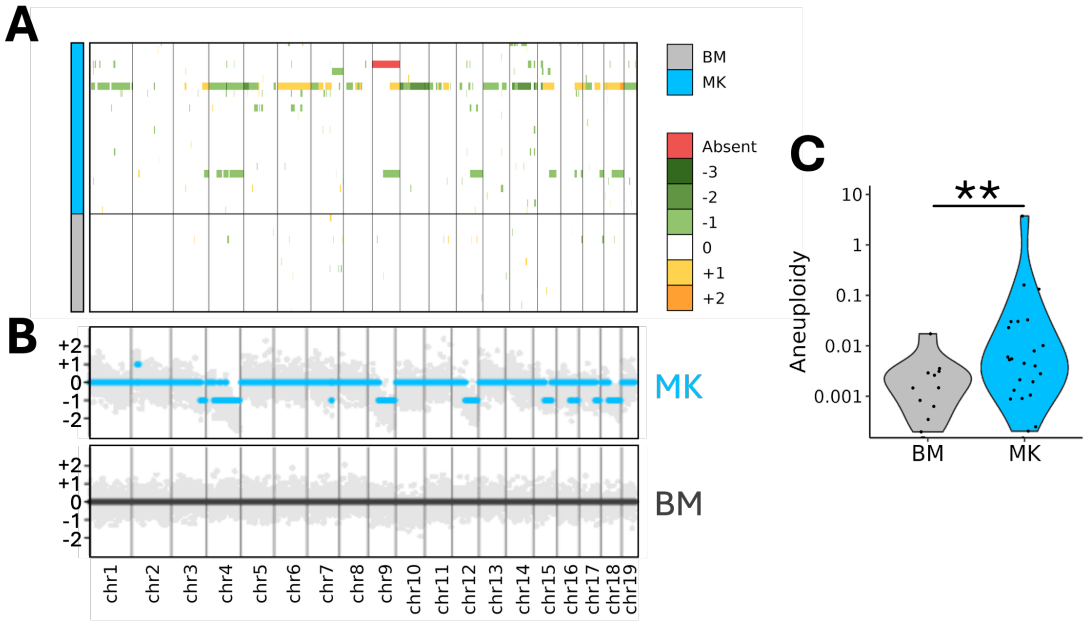


Figure 3.9: MKs are aneuploid. **A**, genome-wide heatmap of CNVs detected in MK-depleted bone marrow cells and MKs. Each row represents a single cell. Data combined from n=2 mice. **B**, representative CNV profiles from a single MK and non-MK bone marrow cell. **C**, aneuploidy scores for each cell. Significance obtained from Wilcoxon Rank Sum Test, $ns = p > 0.5, * = p < 0.05, ** = p < 0.01, *** = p < 0.001, **** = p < 0.0001$.

3.3 Discussion

The data presented on this chapter suggests that WGD elicits profound genome instability and DNA damage in healthy, MKs. To the best of my knowledge, this is the first example of such extensive DNA damage in an otherwise healthy mammalian cell in steady-state physiology. Analysis of cell lines and iMKs indicated that MKs accumulate DNA damage after the first round of WGD. The study of primary MKs directly isolated from healthy mouse bone marrow tissues showed no significant correlation between MK nuclear area and the the number of DNA damage sites observed. Of note, the protocol utilised to isolate murine MKs relies on serial filtration, and retains only large polyploid MKs while diploid cells (including less mature MKs) are pooled in the bone marrow fraction. Thus, γH2AX differences between low ploidy and high ploidy primary MKs are not captured on this analysis. Importantly, polyploid mouse MKs showed significantly higher γH2AX levels compared to diploid cells in the bone marrow, indicating that WGD is indeed detrimental for MK genomic integrity.

Analysis of iPSC-derived cells revealed that iMKs -diploid or polyploid- have significantly higher DNA damage levels compared to CD41- cells. Crucially, study of DNA damage repair dynamics showed impaired clearance of DNA double strand breaks upon x-ray exposure, indicating that MKs might be physiologically more vulnerable to DNA damage. These observations are in line with common toxicological profiles of DNA Damage response targeting agents which commonly present with thrombocytopenia [168]. Background DNA damage levels might have a role in MK biology, recent reports have suggested that inducing low levels of DNA damage can enhance platelet production in mouse models, although the mechanism behind this phenomenon and whether is relevant to human thrombopoiesis remains to be clarified [169].

Analysis of primary mouse MKs revealed that approximately 30% of polyploid MKs contain one or more micronuclei. Importantly, micronuclei frequency correlated with MK nuclear area, suggesting that micronuclei accumulate after

each round of WGD. To the best of my knowledge, this is the first time that micronuclei have been reported on primary MKs. In WGD+ cells, micronuclei formation is normally attributed to the presence of extra centrosomes during polyploid mitoses, which promote chromosome mis-segregation [109]. This mechanism might be relevant for endocycling tetraploid MKs, which undergo chromosome segregation and transition to the 8N status by abortive cytokinesis. However, higher ploidy MKs exit the cell cycle at the metaphase-anaphase transition, with no obvious chromosome separation [80]. Thus, given that micronuclei frequency increased with ploidy, other mechanisms might contribute to micronuclei formation in higher ploidy MKs.

Recent studies have demonstrated that formation of chromatin bridges during cytokinesis can compromise the centromere-kinetochore function of the bridging chromosome [170]. Importantly, these structures do not micronucleate immediately after bridge resolution, but instead persist as defective chromosomes that are inefficiently captured by the spindle machinery, and frequently separate from the main nuclear body during future mitoses [170]. During 2N–4N and 4N–8N transitions in MKs, DNA bridges often form between separating chromosomes [81]. These structures persist through interphase and connect the multiple MK nuclear lobules [81]. Therefore, it is possible that chromatin bridges during early endomitotic cycles generate defective chromosomes, which could later give rise to micronuclei during further MK polyploidization rounds. Lastly, unresolved DNA double strand breaks can produce acentric chromosome fragments that are prone to micronucleation [171]. Hence, MK's impaired DNA damage repair capabilities might indirectly contribute to micronuclei formation.

Micronuclei can undergo defective and asynchronous DNA replication, resulting in DNA damage and often pulverization of their chromosome content [172]. Concordantly, approximately 30% of the micronuclei imaged within the MKs show pan-nuclear γH2AX staining. Of note, micronuclei can be re-incorporated into the main nuclear body where they can sustain long-lived DNA damage [173]. Thus, persistent γH2AX levels observed on polyploid MKs might

-at least partially- come from re-incorporation of γH2AX+ micronuclei into the MK polyploid nucleus. Importantly, the presence of rupture-prone micronuclei frequently triggers the DNA sensing pathway cGAS-STING. Recent reports have shown that *in vitro*-derived MKs possess an active cGAS sting pathway [163]. Whether this pathway is activated in micronuclei+ polyploid MKs is not known. I will endeavour to describe the impact of WGD on the transcriptional landscape of MKs in the following chapter.

scWGS analysis revealed extensive copy number aberration patterns on primary MKs from healthy mice, providing the first direct demonstration that MKs are karyotypically unstable. CNV derived from polyploid mitoses is a source of genetic diversity in hepatocytes, and can serve as an adaptation mechanism to ensure liver regeneration in response to chronic liver disease [174]. Given that platelet production is essential for life, karyotypically unstable endomitoses might help MKs adapt to challenging environments. Although we did not observe any CNV patterns by scWGS during steady state thrombopoiesis, future analyses will help us understand if MK clonal selection can arise under selective pressures such as during inflammation.

Lastly, shattered chromosome fragments in the micronuclei can reassemble via non-homologous end joining into a highly unstructured chromosome with extensive rearrangements in a process called chromothripsis [175], a genetic lesion commonly observed in cancer genomes. Future work will elucidate if chromotripsis is a common phenomenon in polyploid MKs.

Chapter Summary Findings

1. Polyploid MKs accumulate DNA double strand breaks.
2. MKs show defective DNA damage repair capacity.
3. Polyploid MKs show sustained chromosome loss and micronuclei formation which increases with ploidy.
4. MKs are aneuploid.

4

Interrogation of the Megakaryocyte Cell Cycle And Tetraploid Checkpoint

Contents

4.1 Introduction 67
4.1.1 Intrinsic Ploidy Control in Somatic Cells 67
4.1.2 Ploidy Is a Hallmark of Adult But Bot Embryonic Megakaryocytes 69
4.1.3 Inherited Thrombocytopenias Associated With Germline ANKRD26 Mutations 70
4.1.4 Chapter Aims 72
4.2 Results 74
4.2.1 Single Cell RNAseq Allows Accurate Study of The Cell Cycle of Polyploid Cells 74
4.2.2 p53 Remains Functional During Megakaryocyte Polyploidization 81
4.2.3 ANKRD26 is Downregulated During Megakaryocyte Maturation 82
4.2.4 Whole Genome Duplication Tolerance on ANKRD26-Related Thrombocytopenia 84
4.2.5 Whole Genome Duplication Tolerance During Megakaryocyte Ontogenesis 90
4.2.6 Understanding of Ploidy Differences Across Megakaryocyte Ontogeny 90
4.3 Discussion 93

4.1 Introduction

Whole genome duplication (WGD) threatens the genetic integrity of proliferating cells, and is normally kept in check by ploidy-restraining pathways. These mechanisms are essential to safeguard somatic cells against malignant transformation.

4.1.1 Intrinsic Ploidy Control in Somatic Cells

Hippo Pathway Control

WGD can activate the Hippo pathway, which blocks cell proliferation via YAP inhibition and p53 activation (Fig. 4.1A)[117]. Evidence that the Hippo pathway controls ploidy has been provided by studies of hepatocytes, using genetically engineered murine models with enforced YAP expression. This mitigates hippo signalling upon WGD, leading to hepatocyte hyper-proliferation and hyper-polyploidization [117]. Dysregulation of the Hippo pathway and control of hepatocyte cell cycling has also been linked to cancer progression [176]. Notably, knocking out p53 in these mice leads to a further increase in ploidy, suggesting that Hippo is not the only pathway that exerts p53-dependent ploidy control in hepatocytes [176].

In contrast, genetic deactivation of the hippo pathway has no effect on cardiomyocyte ploidy, suggesting that somatic cells utilise different mechanisms to permit and regulate programmed polyploidy [177].

In trophoblast giant cells (TGCs), polyploidization is associated with centrosome accumulation [178] and hippo activation, which leads to cytoplasmic accumulation of YAP in its inactive form [179]. However, despite activating Hippo, TGCs are able to endocycle continuously and achieve nearly 1000 genomic copies in murine models. Interestingly, TGCs markedly reduce p53 protein levels during differentiation which is thought to permit cell cycle progression even with extreme polyploid levels [180].

Lastly, functional studies have demonstrated that MKs (MKs) also possess an active hippo pathway. One study demonstrated that MKs can circumvent the Hippo tetraploid checkpoint by uncoupling RhoA signalling from Hippo-p53 activation, enabling continuous cell cycle progression after WGD [181].

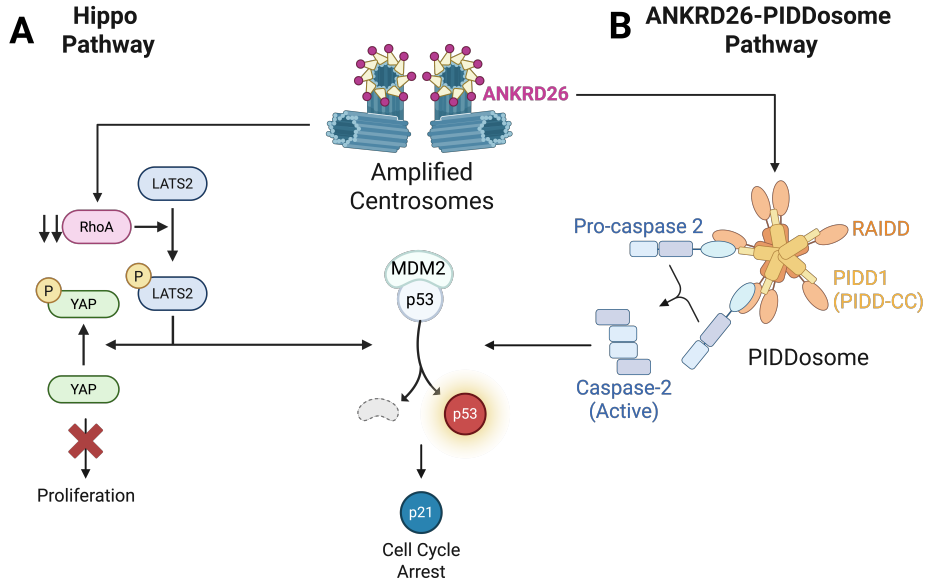


Figure 4.1: Pathways for centrosome amplification control. **A**, centrosome amplification leads to microtubule-dependent decrease in active RhoA. Reduced RhoA activity promotes the activation of LATS2 kinase, which phosphorylates and inactivates YAP, as well as stabilizes p53 through direct inhibition of MDM2. **B**, ANKRD26 located at the distal appendages of the mother centriole recruits and induces PIDD1 auto-processing. PIDD1 C-terminal fragment PIDD-CC binds the adapter protein RAIDD to form the PIDDosome. Binding of RAIDD in the PIDDosome to pro-caspase-2 promotes its dimerisation and auto-cleavage to form caspase-2. The active caspase-2 proteolytically inactivates MDM2, thus inducing a p53 response. Adapted from [117, 182]. Created in https://BioRender.com.

Centrosome Amplification And The ANKRD26-PIDDosome Complex

Centrosome amplification following WGD induces the formation of the PIDDosome, a multiprotein complex responsible for p53 stabilisation through Caspase-2 activation and MDM2 degradation (Fig. 4.1B) [118]. In the liver, seminal studies have demonstrated that amplified centrosomes act as a signalling hub to control hepatocyte polyploidization through PIDDosome-p53 activation [118]. During development and liver regeneration, cell cycle progression of polyploid cells is achieved via transcriptional modulation of PIDDosome components

(PIDD1, RAIDD and CASP2), a process that is controlled by balanced expression of E2F family members [183].

Centrosome-induced PIDDosome formation requires the recruitment of PIDD1 to the centriole distal appendages by the ankyrin repeat domain-containing protein 26 (ANKRD26, Fig. 4.1B) [115, 119]. Liver-specific genetic ablation of either the centrioles, or of ANKRD26 in mouse models leads to uncontrolled liver polyploidization [184]. Perhaps more importantly, ANKRD26 knockout mice phenocopy the increased hepatocyte polyploidy observed in mice lacking p53 suggesting that the ANKRD26-PIDDosome pathway is the main signalling axis for p53 activation in response to WGD [184].

In mice, postnatal heart development correlates with an increase in cardiomyocyte ploidy which is controlled by PIDDosome components [185]. Murine models lacking individual PIDDosome elements exhibit an increased nuclear and cellular ploidy status in cardiomyocytes [185]. Interestingly, while the PIDDosome restricts polyploid cardiomyocyte cycling through p21 expression, this process is independent of p53. The mechanism for p53-independent induction of p21 expression is not clear, but it is suggested that Caspase-2 -which is activated upon PIDDosome formation- can enhance p21 activity by stabilising its mRNA translation [185].

Centrosome amplification has been documented in polyploid MKs, where their activity as microtubule-organizing centres is indispensable for platelet biogenesis [186]. Despite carrying supernumerary centrosomes, MKs appear capable of cell cycle progression without restraint. However, the mechanisms that MKs utilise to avoid the activation of the PIDDosome pathway remain unexplored.

4.1.2 Ploidy Is a Hallmark of Adult But Bot Embryonic Megakaryocytes

Similar to hepatocytes and cardiomyocytes, post-natal megakaryopoiesis is characterised by the expression of a transcriptional program that promotes polyploidization [5]. This program is intrinsically regulated. *In vitro* production

of MKs from embryonic HSCs produces mature but largely diploid MKs, in contrast to MKs derived from adult HSCs which are mostly polyploid [187]. The mechanism underlying these ontogenic differences in ploidy is incompletely understood and likely multifactorial.

The switch from mitosis to endomitosis is thought to be controlled by RUNX1, particularly via the transcriptional modulation of the non-muscle myosin protein MYH10, which permits cytokinesis failure during early WGD events [85]. However, comparison between embryonic/fetal and adult MKs showed no differences in MYH10 mRNA expression, suggesting that failure to undergo endomitosis is not the mechanism behind this ontogenic switch in ploidy [9]. Compared to their embryonic counterparts, adult MKs express higher levels of cell cycle-related genes including E2F transcription factor target genes and DNA replication factors, indicating that ploidy differences might be related to differences in cell cycle controls [9].

More recently, it was demonstrated that *in vitro* treatment with the CDK8 and CDK19 inhibitor cortistatin A could induce polyploidization of cord blood-derived MKs [188]. Gene expression analysis revealed that cortistatin A induced an adult MK expression program in cord blood-derived MKs, including RUNX1 targets and cell cycle-related genes [188], indicating that post-natal MK polyploidization may be governed by RUNX1.

Of note, RUNX1 is also expressed during cardiomyocyte development and sustained cardiac-specific overexpression of Runx1 in mouse models leads to cardiomyocyte hyper-polyploidization, indicating that the polyploidization program controlled by RUNX1 is not exclusive to MKs [189].

4.1.3 Inherited Thrombocytopenias Associated With Germline ANKRD26 Mutations

Inherited thrombocytopenias comprise a heterogeneous group of disorders characterized by a reduced platelet count, and understanding their causative gene defects shed some light into the regulatory mechanisms that govern

megakaryopoiesis and platelet production. Among them, ANKRD26-related thrombocytopenia (ANKRD26-RT) is a rare autosomal-dominant form, reported in approximately 10% of all inherited thrombocytopenia cases, mostly of Italian origin [190]. Although patients with ANKRD26-RT generate functionally competent platelets, they are produced in insufficient numbers, and patients present with mild to severe thrombocytopenia, and bone marrow histology characterized by small, hypo-polyploid MKs [191].

Initial genetic studies of 20 independent families identified six mutations in the 5′ untranslated region (UTR) of ANKRD26, all fully penetrant for the disease [192]. Subsequent investigations in larger cohorts confirmed these findings [193]. Most ANKRD26-RT pathogenic variants lie within a 22-nucleotide stretch of the ANKRD26 5′ UTR region (Fig. 4.2) [190]. Only two exceptions have been described: a missense mutation in exon 1 [194], and a complex structural variant resulting in an ANKRD26–WAC fusion transcript [195].

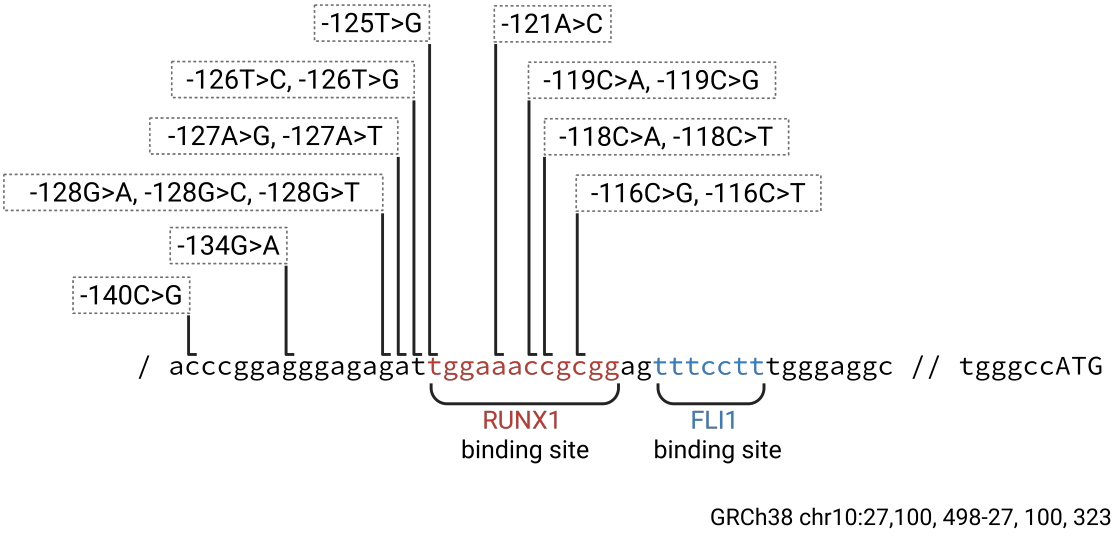


Figure 4.2: Common somatic mutations associated with ANKTD26-RT. Adapted from [190, 196]. Created in https://BioRender.com.

Functional studies in MK model systems demonstrated that ANKRD26-RT causing mutations drive aberrant ANKRD26 overexpression during megakaryopoiesis [192]. Mechanistically, they disrupt the binding of the transcription

factors RUNX1 and FLI1 to the ANKRD26 5′ UTR. In healthy individuals, RUNX1 and FLI1 silence ANKRD26 expression during late megakaryopoiesis, and the transcript expression is lowest in mature MKs and platelets [197]. In patients with ANKRD26-RT, this repression is lost, resulting in constitutive overexpression of functional ANKRD26 throughout MK differentiation [197].

ANKRD26 encodes for a 192-kDa protein containing an N-terminal ankyrin domain that mediates protein–protein interactions, and anchors the ANKRD26 to the plasma membrane [198, 199]. During megakaryopoiesis, ANKRD26 is thought to interact with type I cytokine receptors, including the thrombopoietin (TPO) receptor (MPL), thereby enhancing their signalling. Persistent expression of ANKRD26 results in increased TPO/MPL signalling through MAPK/ERK1/2, which is strongly hyper-activated in patients with ANKRD26-RT [197]. Since inhibition of MAPK/ERK1/2 activity is normally required for pro-platelet formation, sustained activation of MAPK/ERK1/2 in patients with AKNRD26-RT blocks platelet production, which may contribute to the thrombocytopenia phenotype [197].

Beyond thrombocytopenia, ANKRD26-RT is associated with a markedly elevated risk of myeloid neoplasms, estimated at 20- to 30-fold higher than in the general population. The mechanisms underlying this predisposition remain unclear, although recent reports suggest that pathological ANKRD26 overexpression might also enhance cytokine type I signalling by blocking the internalization of its receptors, inducing a pathological proliferation of haematopoietic progenitors [200].

4.1.4 Chapter Aims

Several fundamental aspects of MK biology remain unresolved. Centrosome signalling through the ANKRD26–PIDDosome pathway is a well-established regulator of WGD in hepatocytes and cardiomyocytes. Yet, whether this pathway functions during megakaryopoiesis, and whether it contributes to the developmental transition from fetal to adult megakaryopoiesis, remains

unknown. Importantly, despite the clear clinical impact of ANKRD26 mutations, the rarity of ANKRD26-RT and the limited availability of patient samples mean that the contribution of the ANKRD26–PIDDosome pathway to the disease pathogenesis has never been explored.

Furthermore, I have previously shown that polyploidy in MKs leads to pronounced genomic instability and defects in DNA repair. Yet, it remains unresolved whether WGD drives unique transcriptional reprogramming in MKs or merely results in proportional scaling of cellular functions. To address these unresolved questions, I investigated the following aims, as described in this chapter:

1. To investigate how transcriptional programs in adult MKs change with ploidy at single cell resolution.

2. To determine the integrity of the ANKRD26-PIDDosome-p53 pathway in healthy and ANKRD26-RT MKs.

3. To assess whether developmental differences in ploidy between fetal (cord blood-derived) and adult MKs are determined by ANKRD26.

4.2 Results

4.2.1 Single Cell RNAseq Allows Accurate Study of The Cell Cycle of Polyploid Cells

Studying cell cycle dynamics in MKs is technically challenging. Their rarity, fragility, and large size make them difficult to isolate, and current *in vitro* differentiation protocols fail to generate pure MK cultures. In addition, when analysed by flow cytometry for DNA content, cells in G2-M phase of the cell cycle will 'masquerade' as cells of the higher ploidy class, which impedes accurate annotation, and isolation of pure MKs from specific ploidy groups.

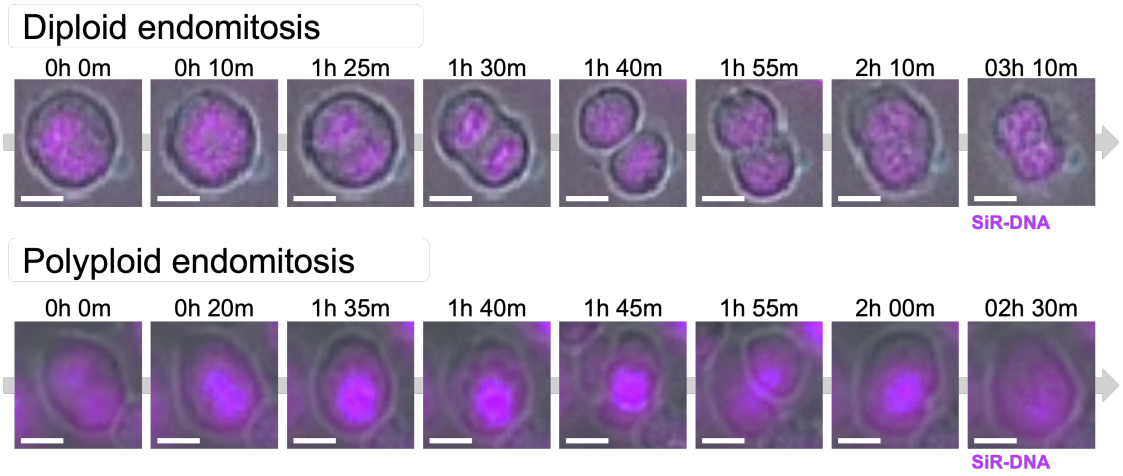


Figure 4.3: In vitro derived MKs can complete endomitosis. Live cell imaging snapshot series of *in vitro* differentiated human MKs from adult HSPCs. DNA is labelled with the cell-permeable non-toxic DNA dye SiR-DNA (pink). Top, diploid endomitosis. Bottom, tetraploid endomitosis. Scale bar = 10μm

To overcome these limitations, I employed single cell RNA sequencing (scRNAseq), using a plate-based method (Smart-seq3 protocol [126]), this was necessary as mature MKs are too large in size to be captured by droplet-based methodologies. I differentiated human MKs from adult donor–derived CD34+ stem/progenitor cells using an optimized differentiation protocol (Methods 2.5.2), enabling me to generate MKs that underwent successive rounds of endomitosis *in vitro*, as confirmed by live-cell imaging (Fig. 4.3).

Cultured MKs were analysed at four differentiation time-points (Days 4, 7, 10 and 12) to recapitulate the entire MK differentiation trajectory. Prior sorting, cells were stained with the early and late MK differentiation markers CD41 and CD42 respectively, as well as the cell-permeable DNA content marker Hoechst. Cells were single cell sorted based on their affiliation with the MK lineage (CD41+) and their DNA content (Hoechst), to accurately capture ploidy status and ensure sufficient representation of the rarer high polyploid MKs in the dataset (Fig. 4.4).

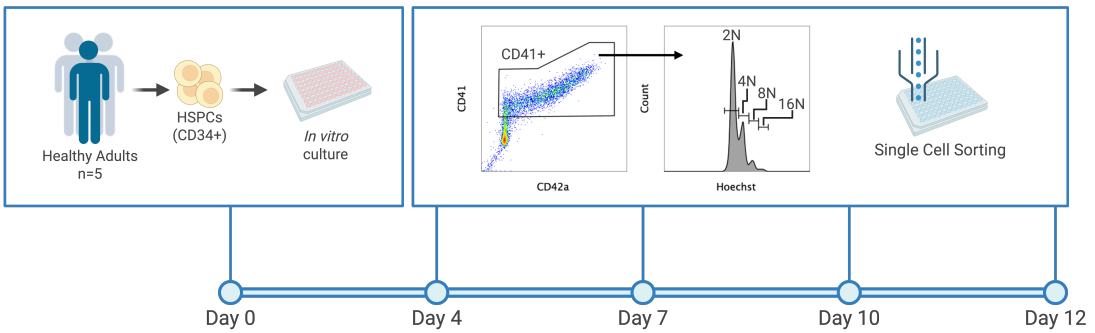


Figure 4.4: Experimental layout for *in vitro* study of the polyploid MK cell cycle by scRNAseq. Created in https://BioRender.com.

After applying essential QC steps (Methods 2.10.2), 2346 cells from 5 donors were included in the analyses. Correlating index flow cytometry data with scRNAseq results permitted the classification of the individual cells into distinct ploidy classes. Using a transfer learning approach [137] I accurately discerned the cell cycle position of each ploidy group (Fig. 4.5).

Characteristics of In Vitro Differentiated Megakaryocytes

Non-linear dimensionality reduction and clustering analysis revealed three populations: MK progenitors (MkPs), identified by the co-expression of MK-affiliated (CD41) and HSPC-affiliated (CD34) cell surface antigens, cycling MKs and non-cycling MKs, together representing the complete MK differentiation trajectory (Fig. 4.6A-E). As expected, MkPs were more frequent at day 4 of the differentiation and fully matured non-cycling MKs appeared at days 10 and 12 of the differentiation process (Fig. 4.6C).

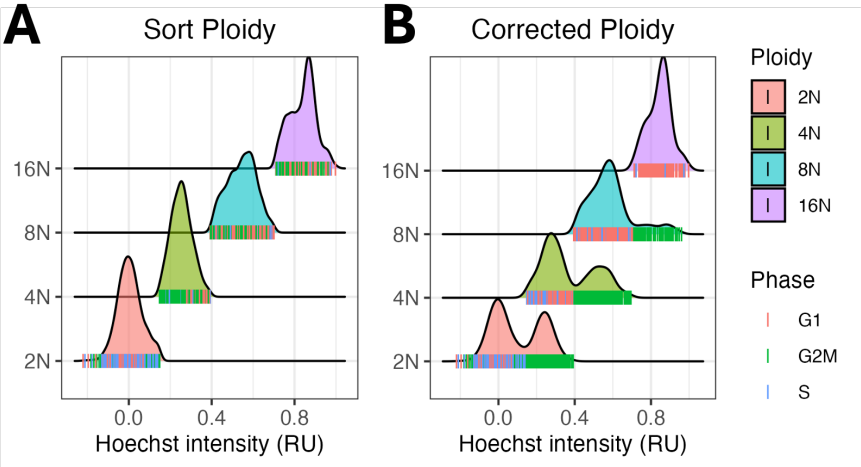


Figure 4.5: Cell cycle correction for polyploid cells. **A**, cell classification in ploidy groups as determined by flow cytometry gating on Hoechst intensity. **B**, cell classification in ploidy groups after ploidy-reassignment based on computationally-predicted cell cycle position. Each vertical line represents a single cell.

Non-cycling MKs were larger than their cycling counterparts, as indicated by flow cytometry Side Scatter Area (SSC-A), and exhibited the strongest expression of haemostasis-associated genes such as von Willebrand Factor (VWF), platelet factor 4 (PF4), and platelet glycoprotein IIIa (ITGB3/CD61) —hallmarks of fully differentiated, platelet-producing MKs (Fig. 4.6B, F). Notably, these mature MKs also displayed elevated levels of the cyclin-dependent kinase inhibitor p21 (CDKN1A), consistent with recent reports that G1 arrest is necessary for platelet formation [186] (Fig. 4.6G). Although more common among highly polyploid cells, mature G1-arrested MKs were detected across all ploidy states, including diploid MKs, suggesting that CDKN1A expression is not a consequence of WGD (Fig. 4.6D). Conversely, 4N and 8N MKs were also actively progressing through the cell cycle, even after undergoing one and two rounds of WGD (4N and 8N, Fig. 4.7A).

Recent work has shown that malignant polyploid cells can exhibit disrupted temporal patterns in cell cycle gene expression [201]. To investigate whether MKs display a similar behaviour, cycling MKs were arranged along their inferred cell cycle trajectory, and gene expression dynamics were compared across different ploidy levels. Overall, canonical cell cycle regulators showed consistent expression across ploidy classes, suggesting that WGD does not disrupt the expression

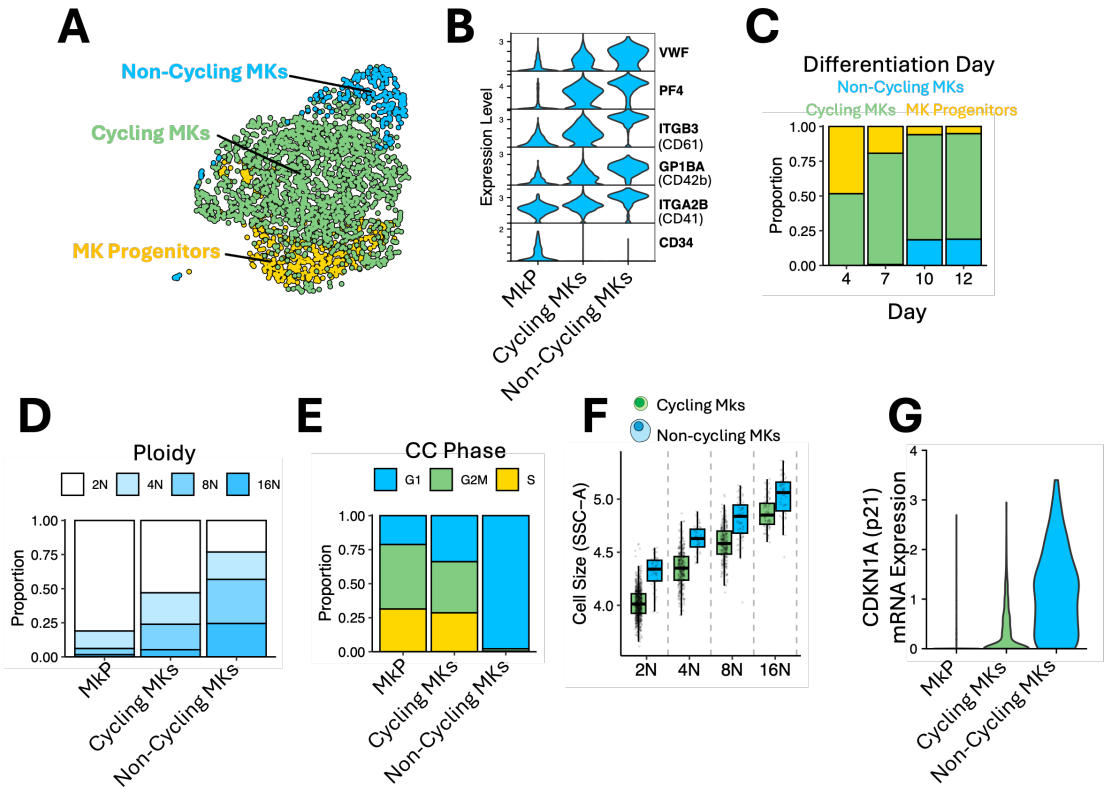


Figure 4.6: Single Cell characterization of *in vitro* differentiated MKs. **A**, Uniform Manifold Approximation and Projection (UMAP) and clustering results. Each dot represents a single cell. **B**, mRNA expression of HSPC progenitor (CD34) and MK/platelet (CD41, 42, 61, PF4 and VWF) markers. **C**, proportion of each cell type identified per differentiation day. **D** fraction of cells of each ploidy class per cell group. **E**, proportion of cells on each cell cycle phase per cell group. **F**, cell size assigned by side scatter (SSC-A) from index flow cytometry data acquired during cell sorting, for cycling and non-cycling MKs of each ploidy class. **G**, mRNA expression of the cyclin-dependent kinase inhibitor CDKN1A (p21).

of cell cycle regulators (Fig. 4.7B). Pseudotime analysis, however, revealed a gradual lengthening of the G1 phase with each additional round of WGD (Fig. 4.7B). Importantly, this G1 prolongation was not associated with increased expression of the p53-dependent inhibitor p21 (CDKN1A), and the expression of p53 target genes showed only modest induction at terminal maturation (16N), indicating that the extended G1 phase observed is not driven by p53-mediated cell cycle arrest (Fig. 4.7C).

To validate whether G1 extension occurs independently of p53 activity, I transduced the p53-mutant megakaryoblastic cell line UT7 with a viral vector

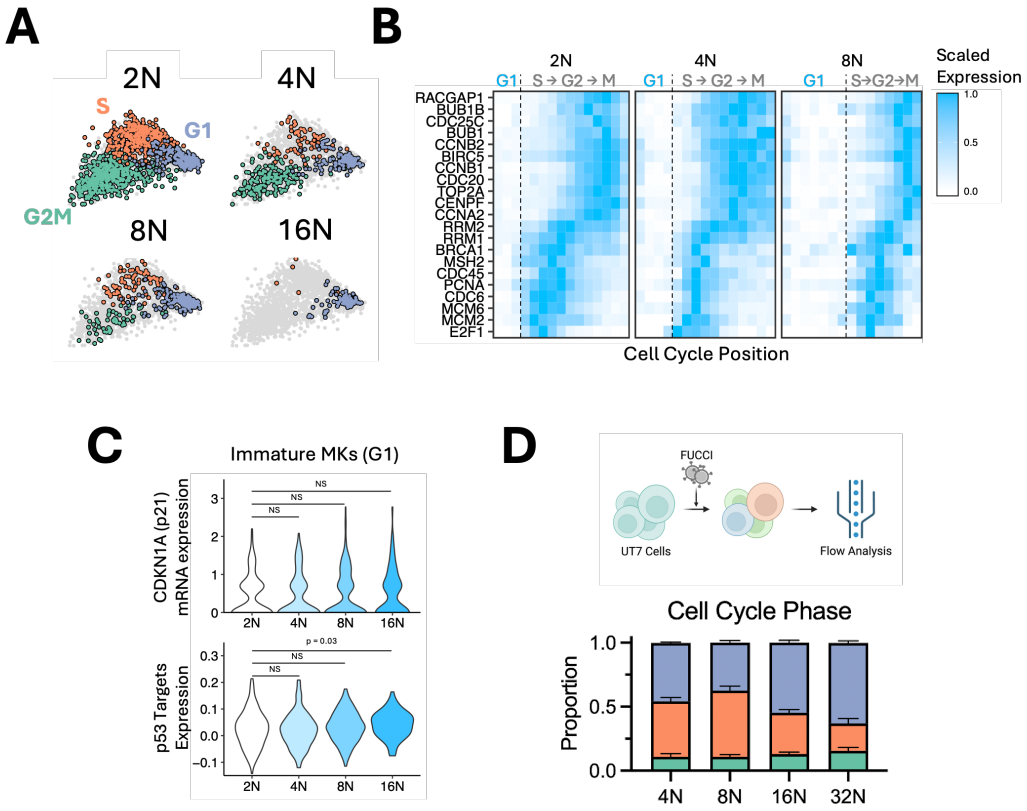


Figure 4.7: Properties of cycling MKs. **A**, Tricycle cell cycle embedding showing the cell cycle position of all cycling MKs in the data set (gray) and cycling MKs by ploidy (coloured cells). Each dot represents a single cell. **B**, scaled expression of cell cycle components across the tricycle cell cycle trajectory for cycling MKs of 2N, 4N and 8N ploidies. **C**, expression of p53-triggered cell cycle arrest protein CDKN1A (p21) and p53 targets in cycling MKs (G1 phase) by ploidy class). **D**, quantification of cell cycle phase distribution across ploidy in the p53 mutant MK cell line UT7 based on the expression of the FUCCI reporter.

encoding the cell cycle reporter FUCCI (Fluorescent Ubiquitination-based Cell Cycle Indicator) [120]. Proper correlation of the FUCCI signal with cell cycle position was confirmed using a combination of chemical inhibitors and cell culture regimens that arrest cells at defined stages of the cycle (Fig. 4.8).

UT7 cells are mostly tetraploid but, similar to other MK-like cell lines, they can spontaneously undergo further WGD events *in vitro*. Flow analysis of the FUCCI-expressing UT7 cells stained with the DNA content marker Hoechst showed that MKs progress through the cell cycle after WGD, with a progressively higher proportion of cells in G1 even in the absence of functional p53 (Fig. 4.7D).

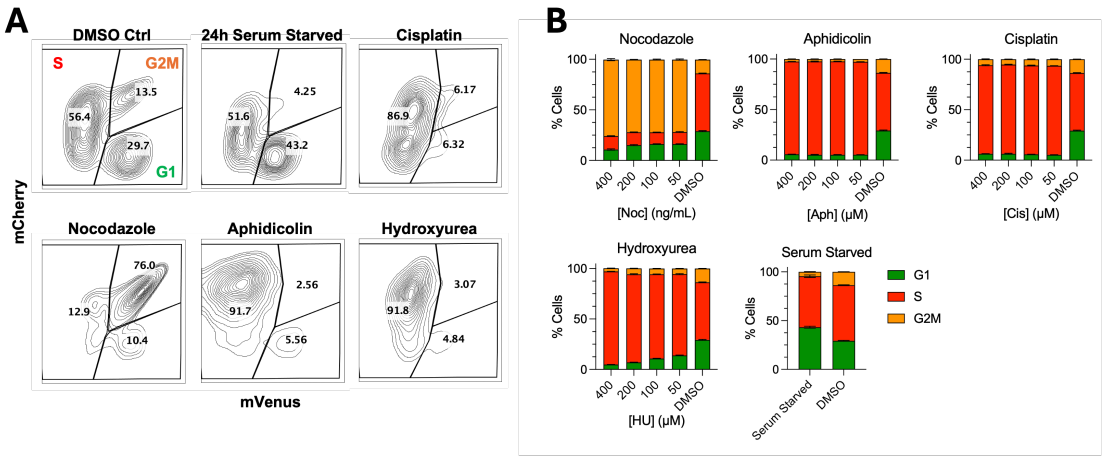


Figure 4.8: Functional validation of the FUCCI system on UT7 cells. **A**, representative flow cytometry plots of mVenus vs mCherry intensity for each condition. **B**, quantification of dose-dependent cell cycle changes for each treatment and cell culture regimen.

Taken together, these results indicate that MK can progress normally through the cell cycle regardless of their ploidy. This process is only interrupted for terminal maturation, which can occur at any ploidy stage (including 2N), where MKs undergo p53-mediated G1 arrest.

Transcriptional Changes During Polyploidization

Cell cycle progression after WGD requires unique adaptations [108] and gene expression does not necessarily scale up equally with ploidy [106]. In line with this, although the total mRNA counts increased with the number of WGD events, it did not scale linearly, indicating that doubling of the nuclear genomic content does not lead to 2-fold higher gene expression in MKs (Fig. 4.9).

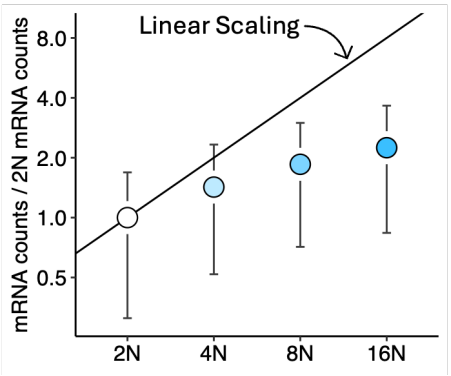


Figure 4.9: Fold change in mRNA abundance (mRNA counts) for every ploidy class compared to diploid MKs.

To evaluate the impact of polyploidy on MK phenotypes I compared the expression of several curated gene signatures between diploid (2N) and polyploid (4N+) MKs. Importantly, to avoid confounding factors originating from relative differences in

cell cycle and cell maturation across ploidy classes, I focussed this analysis on cycling MKs in G1 phase. As expected, polyploid MKs (4N+) showed statistically increased expression of genes related to coagulation, in line with polyploidization and MK maturation being highly intertwined processes (Fig. 4.10 A, B). Strikingly, polyploid (4N+) MKs showed a significant increase in type II interferon (IFNγ) inflammatory pathways and non-canonical NF-κB pathway target genes relative to diploid MKs, while the expression of Type I interferon (IFNα) and senescence markers did not significantly change with ploidy (Fig. 4.10 A, B).

NF-κB and interferon activation are common pathways downstream cGAS-STING activation, suggesting that polyploid MKs contain an active cGAS-STING pathway that responds to chromosomal instability (CIN)-derived cytosolic DNA and micronuclei formation following WGD. Importantly, cGAS-STING activation in MKs seems to operate through the Non Canonical NF-κB pathway, which promotes type II over type I interferon signalling and avoids the induction of senescence in response to micronuclei formation (Fig. 4.10C)[104, 202].

While expression of genes associated with MK maturation and nuclear envelope components increased with ploidy, likely to meet the requirements of increased cell size, genes associated with multiple DNA damage repair pathways decreased after each WGD event (Fig. 4.10 A, B). These observations suggest that large, polyploid MKs inadequately scale their DNA repair machinery, potentially explaining the slower clearance of yH2AX foci, previously described (Chapter 3, Fig. 3.4).

In summary, MKs continue efficient progression through the cell cycle even after multiple rounds of WGD and the acquisition of significant genomic instability until terminal maturation, when they undergo p53-mediated G1 arrest. Moreover, this requires unique transcriptional adaptations, including rewiring of STING signalling in response to CIN.

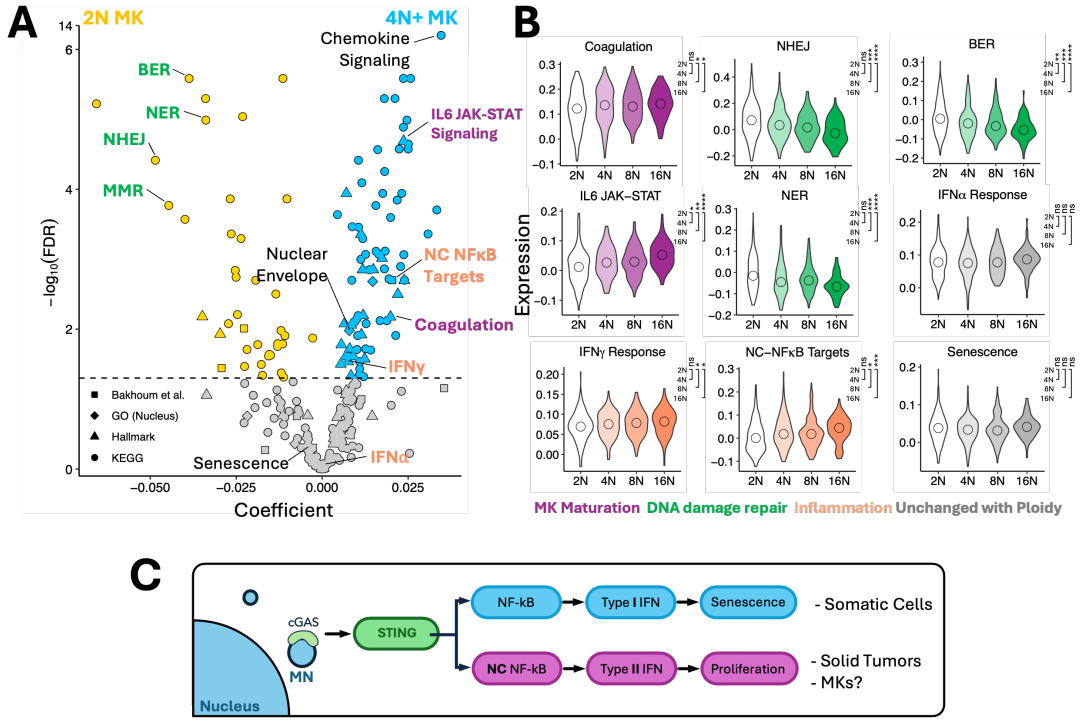


Figure 4.10: Transcriptional changes of MKs across ploidy. **A**, Volcano plot showing differentially expressed genes/pathways in polyploid (4N+) versus diploid (2N) cycling MKs (G1 phase). **B**, mRNA expression score of MK maturation, DNA damage repair and Inflammation in MKs by ploidy class. Central point represents median expression for each group. **C**, schematic showing alternative activation pathways downstream of STING-cGAS signalling. Adapted from [104, 202]. MN: micronuclei; IFN: interferon; NC NF-κB: non-canonical Nuclear factor kappa-light-chain-enhancer of activated B cells; BER: Base Excision Repair; NER: Nucleotide Excision Repair; NHEJ: Non-Homologous End Joining; MMR: Mismatch Repair. Significance obtained from T test. *p <0.05; **p <0.01; ***p <0.001; ****p <0.0001.

4.2.2 p53 Remains Functional During Megakaryocyte Polyploidization

Cell cycle progression after WGD in cells with functional p53 requires bypassing the Hippo and the PIDDosome checkpoints. However, the ability of MKs to cycle unrestrained by ploidy suggests that they are transcriptionally adapted to tolerate WGD.

Since both the PIDDosome and Hippo pathways act through p53 activation [115, 117], I first asked whether MKs completely suppress the p53 pathway. To test this, I assessed whether genotoxic stress could induce p53-dependent cell cycle arrest in cycling MKs by measuring Ethynyl-2'-deoxyuridine (EdU) incorporation

(as a marker of S-phase progression) following irradiation (5 Gy). Although this is correlative evidence of p53 pathway activation, X-ray irradiation of human Induced Pluripotent Stem Cells (iPSC)-derived human MKs indeed induced cell cycle arrest, whereas the p53 loss-of-function mutant MK line UT7 showed only minimal reduction in EdU incorporation (Fig. 4.11A).

To further examine whether p53 constrains MK polyploidization, I compared MK ploidy profiles from primary and *in vitro* derived MKs from global p53 knockout and wild-type mice. Strikingly, p53 deficiency did not alter MK frequency or ploidy distribution, demonstrating that, although p53 is functionally active in MKs, it does not limit polyploidization under steady-state conditions (Fig. 4.11B-C, Appendix Fig. A.1).

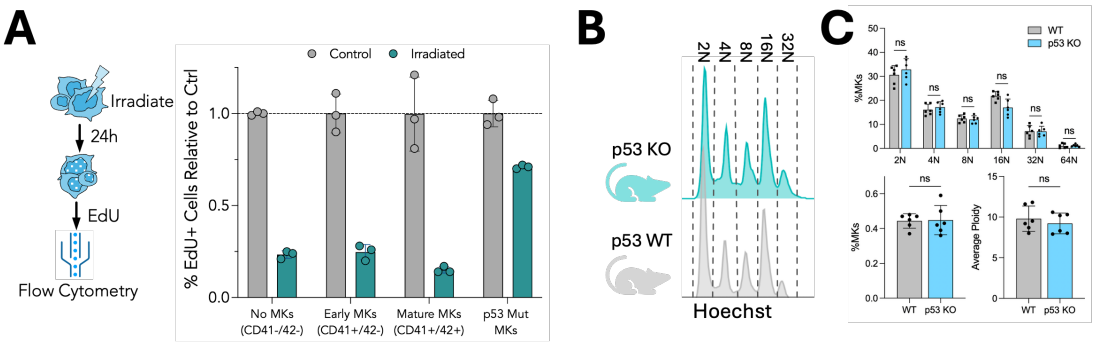


Figure 4.11: p53 is functional in MKs. **A**, % cells showing EdU incorporation after irradiation (5 Gy), relative to non-irradiated control, as a marker of new DNA synthesis occurring during proliferation. Chart shows % EdU positivity for non MKs (identified by the absence of CD41), early MKs (CD41+42-), mature MKs (CD41+42+) and the UT7 p53 mutant MK cell line. **B-C**, ploidy analysis by Hoechst staining of MKs from wild-type (WT) and p53 knockout (KO) mice, n = 6 mice per group. **B**, exemplar flow plots. **C**-top %MKs in each ploidy class for wild-type and p53 knockout mice. **C**-bottom left % of immunophenotypically defined MKs (CD41+/42+). **C**-bottom right average ploidy of primary MKs from p53 wild-type and knockout mice. Significance obtained from Wilcox Rank Sum test. *p <0.05; **p <0.01; ***p <0.001; ****p <0.0001. *p53 knockout mice were kindly shared by a collaborator, Stephan Contanstinescu (Louvain's de Duve Institute, Brussels)*

4.2.3 ANKRD26 is Downregulated During Megakaryocyte Maturation

Previous studies have investigated the Hippo-p53 pathway in MKs [181]. On the other hand, previous reports have suggested that the transcription factors

RUNX1 and ANKRD26 can downregulate the expression of ANKRD26 [197]. To validate this, I first explored my scRNAseq data, which demonstrated near-absent expression of ANKRD26 and PIDD1 –the central components of the PIDDosome pathway– in MK progenitors, and mature (cycling or non-cycling) MKs, suggesting active transcriptional repression of the genes (Fig. 4.12A).

Since the scRNAseq dataset was restricted to CD41+ MK-committed progenitors, I extended the analysis to earlier stages of the differentiation trajectory. Reverse transcription quantitative polymerase chain reaction (RT-qPCR) on purified human cells spanning the progression from haematopoietic stem cells (HSCs) to mature MKs confirmed a progressive downregulation of ANKRD26 expression during megakaryopoiesis (Fig. 4.12B). Importantly, western blot analysis of human *in vitro* differentiated MKs sampled at early (day 6) and late (day 12) time-points of differentiation confirmed complete suppression of the ANKRD26 protein in mature MKs (Fig. 4.12C).

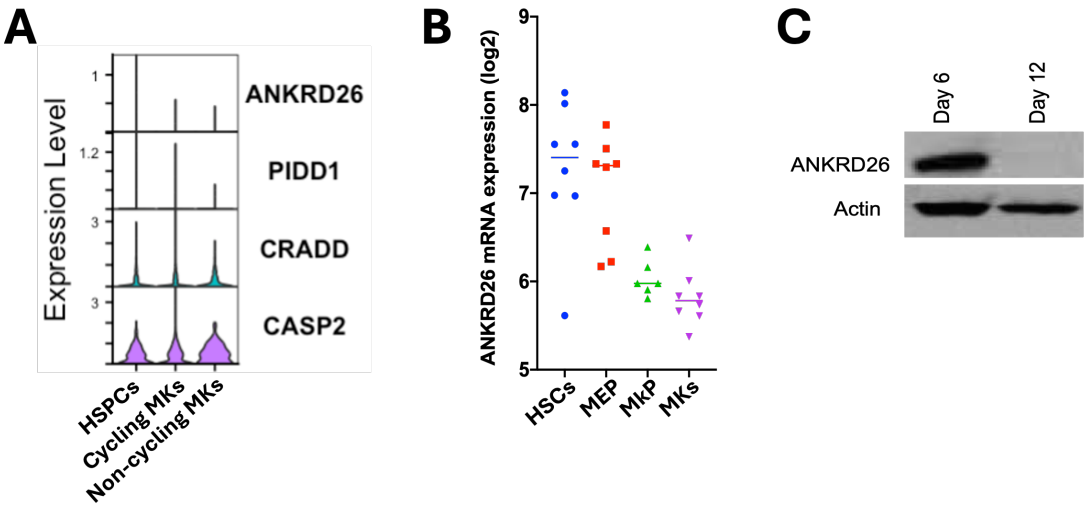


Figure 4.12: ANKRD26 is downregulated during megakaryopoiesis. **A**, expression of PIDDosome components in single cell RNA sequencing (scRNAseq) data. **B**, ANKRD26 mRNA expression (Log2) in hematopoietic stem/progenitor cells (HSPCs), MK-erythroid progenitors (MEP), MK progenitors (MkP) and mature MKs. **C**, ANKRD26 protein levels at day 6 and 12 of human *in vitro* MK differentiation, measured by western blot. *Data from panels B and C was generated and kindly shared by Dr. Nah-Young from the Alan Cantor Lab at the Dana-Farber Cancer Institute.*

Together, these findings indicate that ANKRD26 downregulation is an integral feature of the MK differentiation program, and raise the possibility that its suppression is required to prevent p53 activation in response to WGD.

4.2.4 Whole Genome Duplication Tolerance on ANKRD26-Related Thrombocytopenia

In ANKRD26-RT, mutations in the 5′ UTR regulatory region of ANKRD26 prevent RUNX1-mediated transcriptional suppression of ANKRD26. Given the hypothesis that ANKRD26 repression might be essential for MKs to bypass the PIDDosome checkpoint, I hypothesized that MKs from individuals with ANKRD26-RT would be prevented from reaching a polyploid state due to pathological PIDDosome activation and p53-mediated cell cycle arrest upon WGD.

Megakaryocytes From Patients With ANRKD26-Related Thrombocytopenia Activate p53 During Maturation

To test this hypothesis, I isolated CD34+/Lineage- haematopoietic stem/progenitor cells (HSPCs) from cryopreserved, bone marrow mononuclear cells of patients with ANKRD26-RT and healthy controls (n=2 patients per group), and induced MK differentiation *in vitro*. Unexpectedly, when isolating CD34+/Lineage- HSPCs by Fluorescence-Activated Cell Sorting (FACS), I noticed a ~5.4 fold expansion of the HSPC compartment in samples from patients with ANKRD26-RT compared to healthy controls (Fig. 4.13).

MKs generated from ANKRD26 mutant HSPCs were significantly smaller than those derived from healthy adult HSPCs, with a notable reduction in average ploidy (Fig. 4.14A-D). To test whether this phenotype resulted from the PIDDosome pathway triggering aberrant p53 activation after WGD, I performed immunofluorescent imaging of p53 nuclear translocation. This revealed a significant increase in p53 nuclear staining only in ANKRD26 mutant MKs, to a similar extent to that seen in MKs after 4hr of etoposide treatment. Importantly, no nuclear p53 signal was seen in healthy adult MKs (Fig. 4.15A, B).

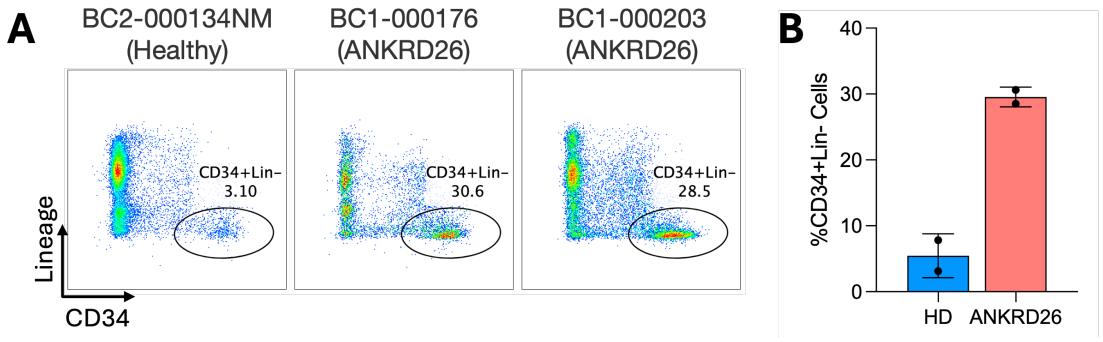


Figure 4.13: HSPCs are expanded in the bone marrow of patients with ANRKD26-RT. **A**, representative flow cytometry plots for one healthy control and the two patients with ANRKD26-RT analysed. **B** quantification of the fraction of HSPCs in the bone marrow of healthy controls and patients with ANRKD26-RT.

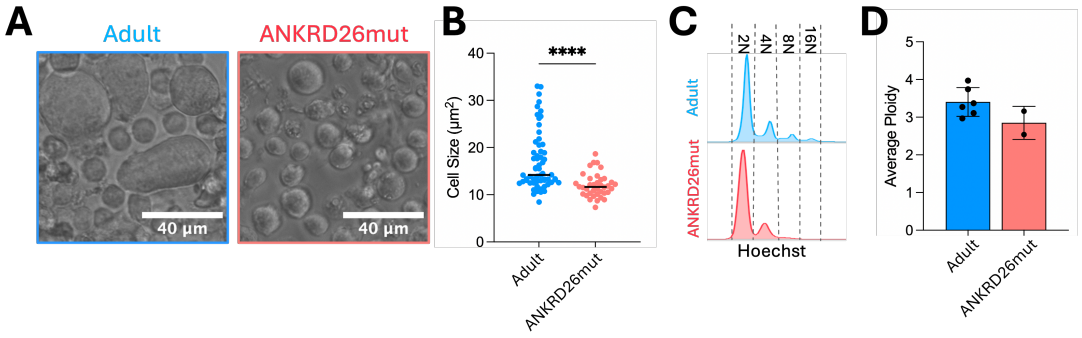


Figure 4.14: ANKRD26 mutant MKs are low polyploid. **A**, representative bright field images of *in vitro* differentiated MKs from healthy adult and patients with ANRKD26-RT. Scale bar = 40μm. **B**, cell size quantification of *in vitro* differentiated MKs. **C**, representative ploidy profiles determined by flow cytometry of CD41+/42+ MKs from healthy adults and patients with ANRKD26-RT. **D**, quantification of the average ploidy of *in vitro* differentiated MKs.

To confirm that p53 activation was directly linked to mutations in ANKRD26 and not other genomic variants carried by the patients, I utilised a human iPSC line that was genetically engineered to harbour a previously described ANKRD26 5'UTR mutation (c.-116C>T) and an isogenic control line. In line with my observations of ANKRD26-RT derived MKs, immunofluorescence analysis of iPSC-derived MKs showed higher nuclear accumulation of p53 in cells derived from ANKRD26 mutant iPSCs compared to isogenic controls, confirming that ANKRD26 mutations are directly linked to p53 activation in MKs (Fig. 4.15C, D).

Lastly, to verify that these results were not artifacts of the cell culture setting,

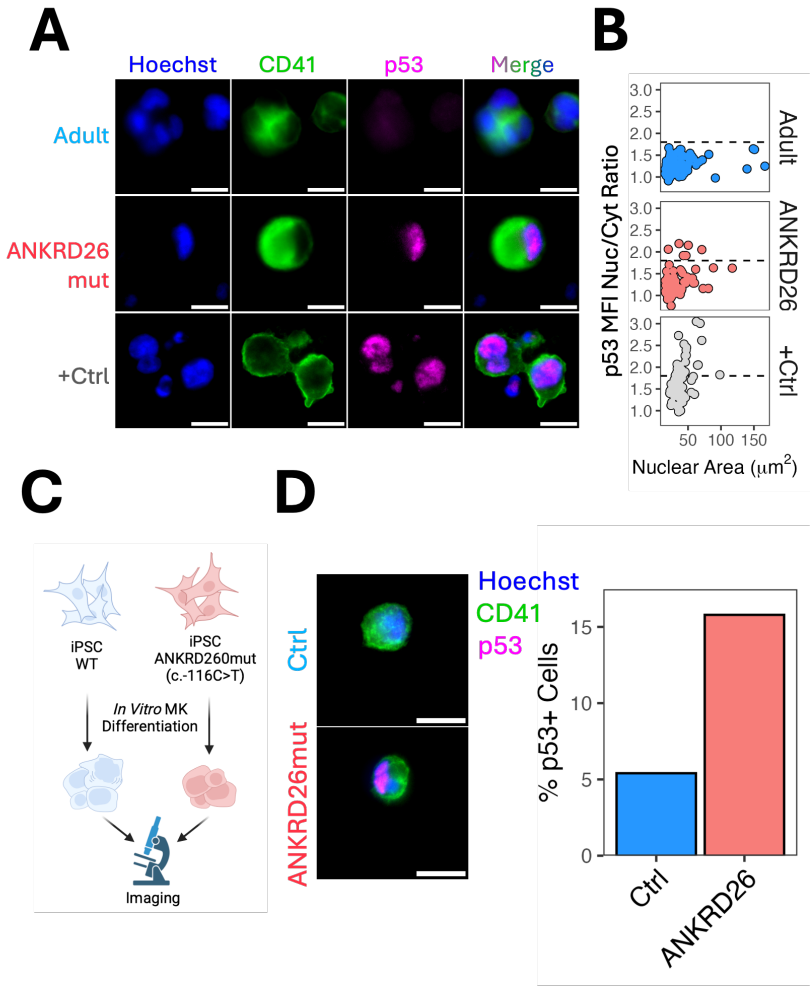


Figure 4.15: Mutations on ANKRD26 activate the p53 pathway. **A**, representative immunofluorescence images of MKs differentiated *in vitro* from healthy adult donors and patients with ANKRD26 mutations stained for p53 (magenta), CD41 (green) and DNA (Hoechst, blue). MKs treated with etoposide for 4h used as a positive control (+Ctrl). **B**, quantification of p53 nuclear translocation analysed by immunofluorescence imaging. **C** schematic showing experimental strategy for studying the effects of ANKRD26 mutation (c.-116C>T) on MK differentiation using human iPSCs. **D**-left, representative immunofluorescence images of MKs derived from wild-type (Ctrl) and ANKRD26 mutant iPSCs stained for p53 (magenta), CD41 (green) and DNA (Hoechst, blue). **D**-right, quantification of p53 nuclear translocation (n=1 experimental replicate). Significance obtained from t-test. ns p>0.05, *p <0.05, **p <0.01, ***p <0.001, ****p <0.0001. Panel C schematic created using BioRender.com.

immunohistochemistry staining for p53 was performed on bone marrow biopsy sections from patients with ANKRD26-RT and healthy controls (n=4 and n=3 respectively). This showed clearly increased nuclear p53 accumulation and reduced nuclear area in ANKRD26-RT MKs, compared to healthy controls (Fig.

4.16A-C). Strikingly, nuclear p53 intensity significantly correlated with nuclear size, indicating dependence of p53 activation with MK ploidy status (Fig. 4.15D). Of note, these effects were consistent across all ANKRD26 variants analysed.

Taken together, these results confirm that aberrant ANKRD26 expression triggers p53 activation in ANKRD26-RT MKs, blocking their polyploidization.

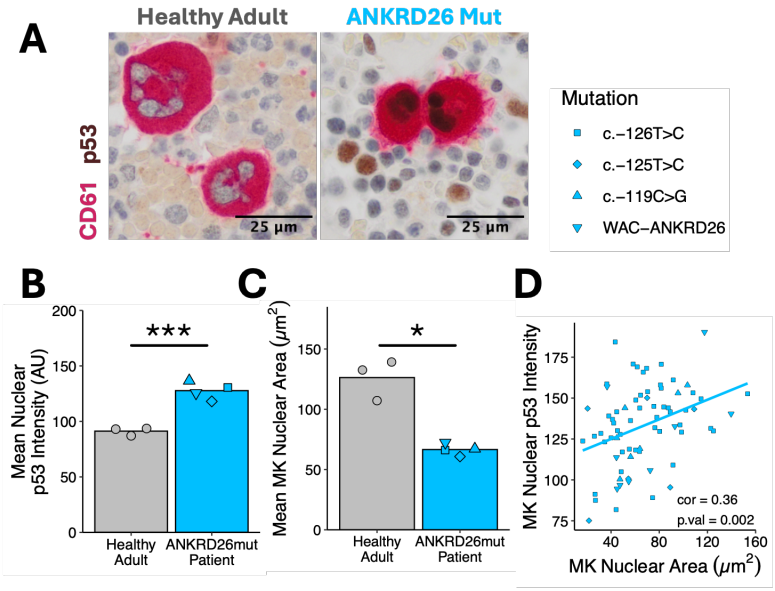


Figure 4.16: Mutations in ANKRD26 activate the p53 pathway. **A**, representative immunohistochemistry images of bone marrow biopsies from healthy adults and patients with ANRKD26-RT stained for CD61 (pink) and p53 (brown). **B**, **C**, quantification of MK average p53 nuclear intensity and nuclear area per patient (T-test). **D**, correlation between MK p53 nuclear intensity and MK nuclear area (Pearson correlation test). *p <0.05; **p <0.01; ***p <0.001; ****p <0.0001.

scRNAseq Analysis on In Vitro Derived Megakaryocytes From Patients With ANRKD26-RT

To further examine the impact of pathological ANKRD26 overexpression during megakaryopoiesis, I performed scRNAseq on *in vitro* differentiated MKs from HSPCs isolated from healthy adults and patients with ANKRD26-RT following the same methods described previously.

Gene expression analysis revealed similar cluster identities as described in healthy adult samples (Fig. 4.6A, Fig. 4.17A). Patients with ANRKD26-RT and healthy adult donor-derived samples showed comparable frequencies of MkPs,

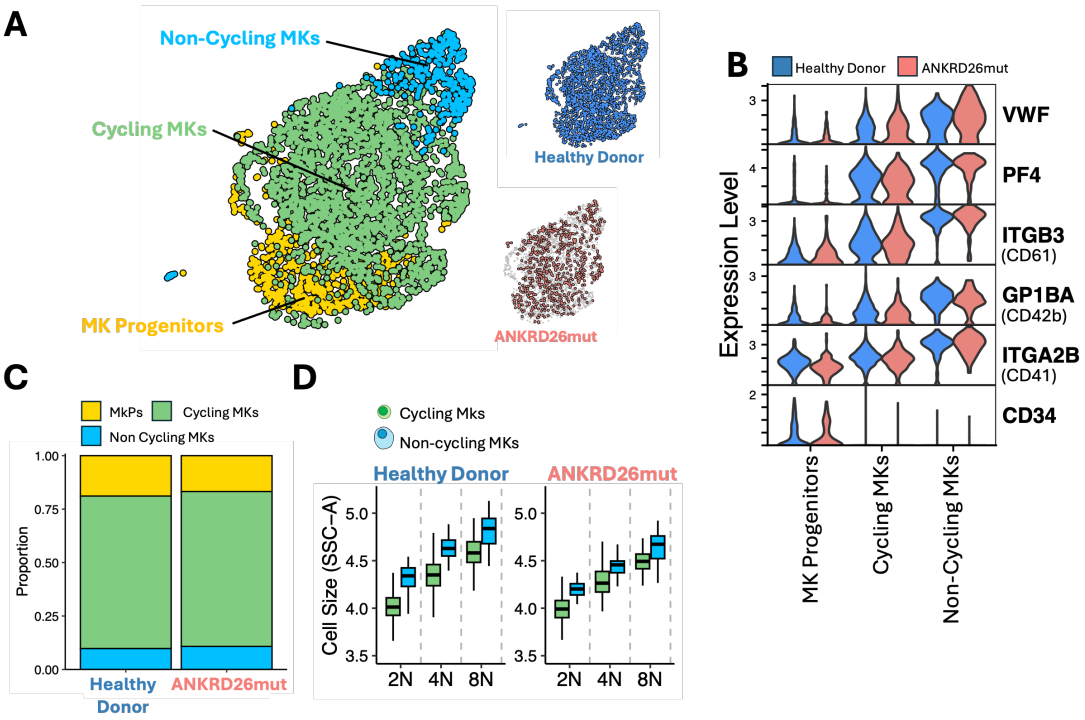


Figure 4.17: Mutations in ANKRD26 do not block MK lineage commitment. **A**, UMAP and clustering results. Each dot represents a single cell coloured by cell identity (left) or patient of origin (right). **B**, mRNA expression of HSPC (CD34) and MK/platelet (CD41, 42, 61, PF4 and VWF) markers. **C**, proportion of cell types identified in healthy controls and patients with ANRKD26-RT. **D**, cell size analysis (SSC-A) between cycling and non cycling cells for healthy donors and patients with ANRKD26-RT.

cycling and non-cycling mature MKs (4.17C). Notably, despite their lower ploidy, mature MKs from patients with ANKRD26-RT showed similar characteristics to healthy adult-derived MKs including increased cytoplasmatic cell size, and high expression of haemostasis-related genes (Fig. 4.17B, D). These results indicated that the low ploidy phenotype and low efficiency of platelet production is not due to a block in MK lineage commitment or differentiation *per se*, but a specifically a defect in polyploidization.

Next, I applied Monocle3 [141] to reconstruct the pseudo-temporal ordering of cells along the MK differentiation trajectory. This revealed persisting ANKRD26 expression throughout differentiation in the ANKRD26-RT samples, in contrast to adult megakaryopoiesis, where ANKRD26 expression was nearly absent from early lineage commitment (Fig. 4.18A). Importantly, while healthy adult MKs

exhibited a progressive increase in ploidy during maturation, the average ploidy of ANKRD26-RT-derived MKs failed to increase beyond 4N (Fig. 4.18A).

If dysregulated ANKRD26 expression causes PIDDosome activation, then the impact should only manifest after the first round of WGD. I leveraged the plate-based scRNAseq approach to study gene expression changes in across ploidy classes. Expression of p53 targets was not significantly different between diploid MKs from patients with ANRKD26-RT and healthy subjects. In contrast, WGD+ ANKRD26 mutant MKs of ploidy classes 4N and higher showed significantly increased expression of p53 targets compared to MKs derived from healthy adults (Fig. 4.18B), with induction of the p53-mediated, cell cycle inhibitor p21 (CDKN1A) only in ANKRD26 mutant MKs after the first round of WGD (Fig. 4.18B).

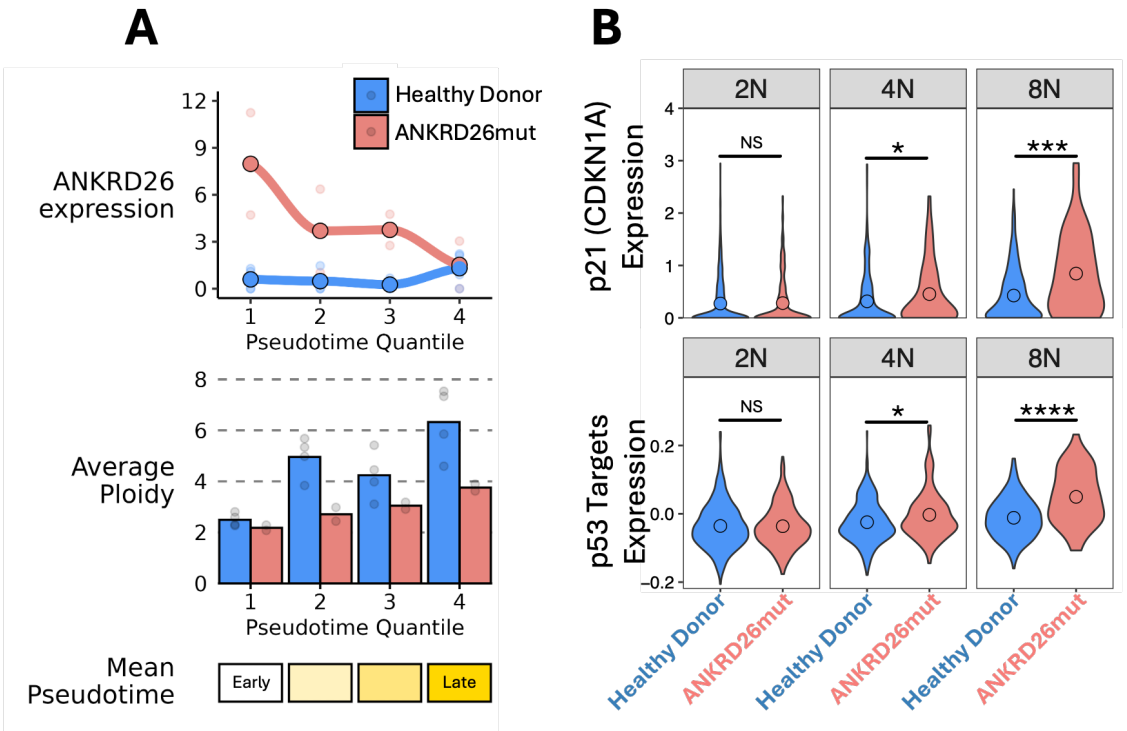


Figure 4.18: Sustained ANKRD26 expression triggers p53 on polyploid MKs. **A**, mRNA expression of ANKRD26 in pseudo-bulk MKs and average ploidy changes along the pseudotime differentiation trajectory from early to terminal late maturation. **B**, mRNA expression of p53 target genes in MKs of different ploidy classes. Statistics shown is for a Wilcoxon rank sum test. NS p >0.05; *p <0.05; **p <0.01; ***p <0.001; ****p <0.0001.

Taken together, these data confirmed that pathological ANKRD26 expression

in MKs de-represses the PIDDosome checkpoint, leading to WGD-dependent p53 activation and a block to polyploidization.

4.2.5 Whole Genome Duplication Tolerance During Megakaryocyte Ontogenesis

Polyploidization events in somatic cells typically occur shortly after birth. For instance, while foetal liver cells are diploid, almost 30% of hepatocytes are polyploid in human adults [46], a process that is facilitated by transient transcriptional regulation of PIDDosome components [183]. Given my previous observations that RUNX1-mediated transcriptional suppression of ANKRD26 is required for the production of polyploid MKs, I hypothesized that the reduced ploidy of embryonic MKs may also result from a limited capacity to tolerate WGD, a property that is only acquired postnatally through RUNX1-dependent ANKRD26 repression.

4.2.6 Understanding of Ploidy Differences Across Megakaryocyte Ontogeny

To test this hypothesis, an experimental strategy analogous to the one described previously was employed. CD34+/Lineage- HSPCs were isolated from cord blood and mobilised peripheral blood of healthy adults, flow-sorted, and cultured for 12 days to induce MK differentiation. Consistent with published observations [5], MKs derived from embryonic progenitors were significantly smaller and displayed reduced ploidy compared with those derived from adults (Fig. 4.19A-D). In contrast to prior findings in ANKRD26 mutant-MKs, p53 stabilisation and nuclear translocation was not significantly elevated (Fig. 4.19E, F), indicating that low ploidy in embryonic megakaryopoiesis does not involve p53 activation.

To further investigate the developmental differences in megakaryopoiesis, single cell sorting and whole transcriptome analysis of CD41+ MKs and progenitors differentiated *in vitro* from cord blood HSPCs (n = 3 donors) was performed using the previously described workflow. Their gene expression profiles were

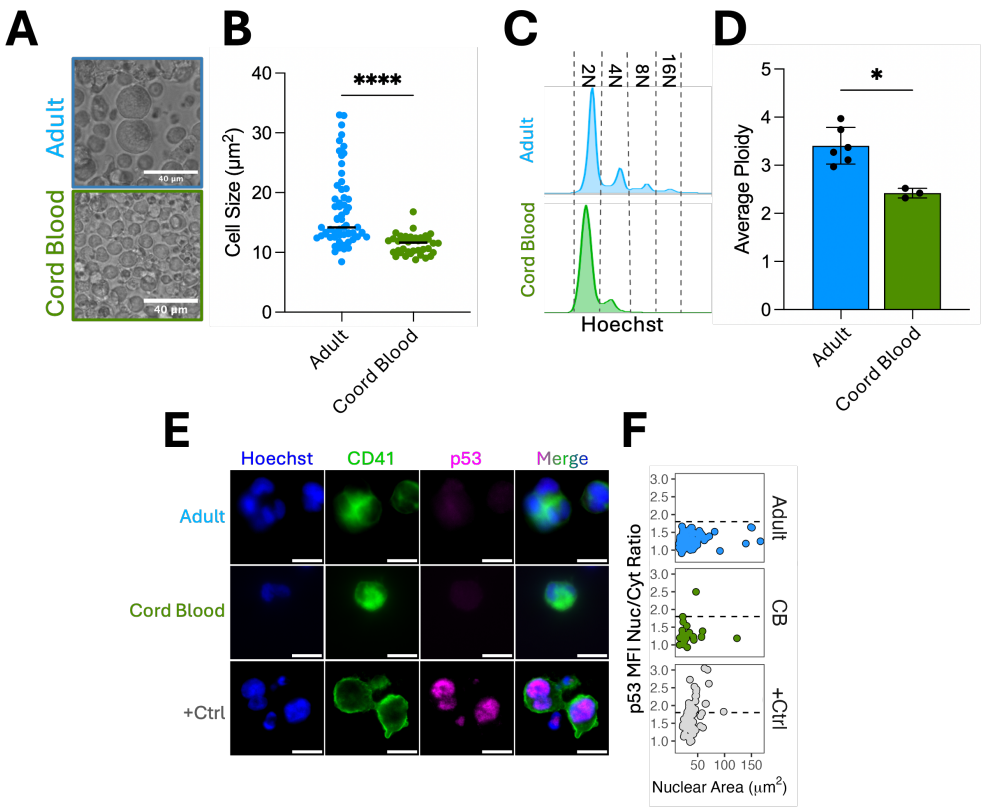


Figure 4.19: Unlike ANKRD26 mutant MKs, embryonic MKs do not activate p53. **A**, representative bright field images of *in vitro* differentiated MKs from healthy adults and cord blood samples. Scale bar = 40μm. **B** cell size quantification of *in vitro* differentiated MKs. **C** representative ploidy profiles determined by flow cytometry of CD41+/42+ MKs from healthy adults and cord blood samples. *D*, quantification of the average ploidy of *in vitro* differentiated MKs. **E** representative immunofluorescence images of MKs stained for p53 (magenta), CD41 (green) and DNA (Hoechst, blue). MKs treated with etoposide for 4h used as a positive control (+Ctrl). **F**, quantification of p53 nuclear translocation analysed by immunofluorescence imaging. Statistics shown is for a Wilcoxon rank sum test. NS p >0.05; *p <0.05; **p <0.01; ***p <0.001; ****p <0.0001

then compared with transcriptional data previously generated from adult MKs. Pseudotemporal trajectory analysis demonstrated a block in polyploidisation, with average ploidy in cord blood-derived MKs rarely exceeding 4N. However, ANKRD26 expression was consistently low throughout the differentiation trajectory, suggesting that the reduced polyploidisation observed in foetal MKs was not attributable to differences in the silencing of ANKRD26 (Fig. 4.20A).

Finally, p53 target gene expression -including p21 (CDKN1A)- remained unchanged across all ploidy classes. Collectively, these data indicate that WGD

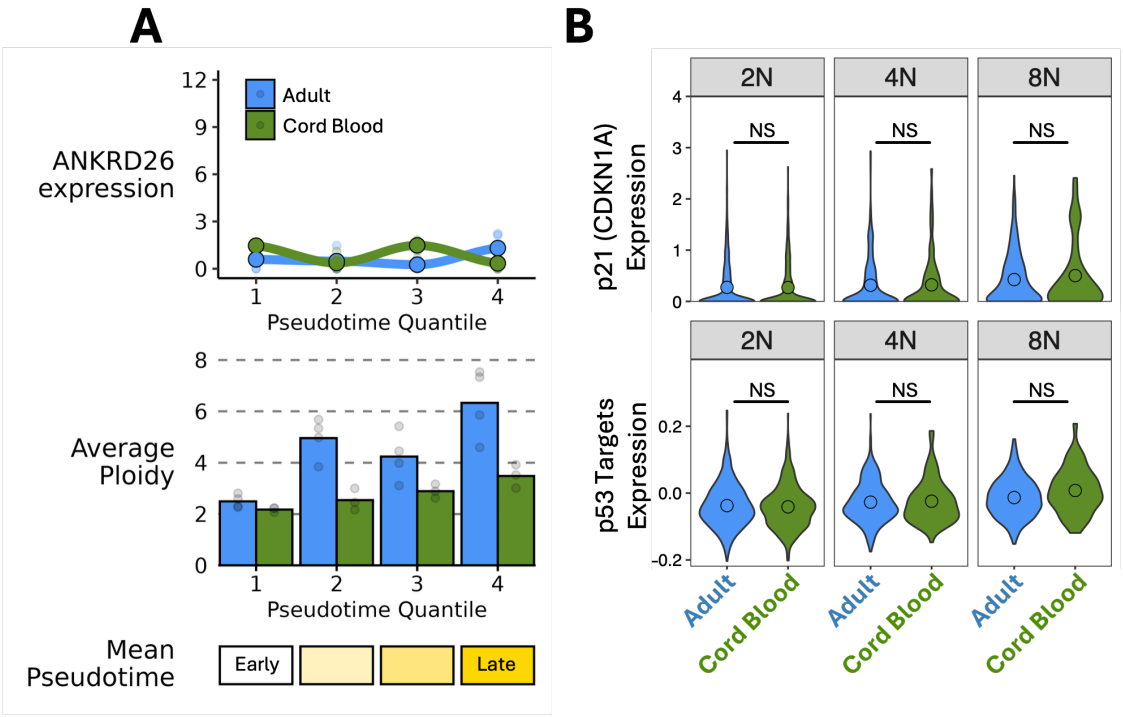


Figure 4.20: Embryonic MKs do not express ANKRD26 or activate p53 in response to WGD. **A**, mRNA expression of ANKRD26 in pseudo-bulk MKs and average ploidy changes along the pseudotime differentiation trajectory from early to terminal late maturation. **B**, mRNA expression of p53 target genes in MKs of different ploidy classes. Statistics shown is for a Wilcoxon rank sum test. NS p >0.05; *p <0.05; **p <0.01; ***p <0.001; ****p <0.0001.

in embryonic MKs does not result in transcriptional activation of p53-dependent pathways, and further work is required to discover why fetal MKs are of lower ploidy than adult MKs(Fig. 4.20B).

4.3 Discussion

Megakaryocytes adapt to tolerate Whole Genome Duplication using mechanisms that have previously only been observed in transformed cells

WGD in MKs is thought to contribute to the tremendous synthetic capacity required for the production of thousands of platelets per cell. The data presented here shows that while WGD results in a increase mRNA production, it does not scale linearly with ploidy.

Non-stoichiometric scaling of the cellular content after WGD can lead to DNA replication stress and alterations in the chromatin structure, which can be mitigated by pharmacological extension of the G1 phase [111, 114]. Importantly, G1 lengthening has recently been associated with WGD+ tumour cells which is thought to improve the fitness of the tetraploid status by promoting a balanced upregulation of the cell machinery [201]. Similarly, my analysis of cell cycle dynamics showed that MKs also extend their time on G1 phase before entering the cell cycle in a p53-independent manner, which might promote proper scaling of the cellular content.

However, while WGD was associated with increased expression of nuclear envelope and haemostasis-related genes, I observed a lack of scaling of multiple DNA damage repair pathways after each round of WGD, including Base Excision Repair, Nucleotide Excision Repair, Non-Homologous End Joining and Mismatch Repair. These observations suggest that MKs are unable to properly upregulate DNA damage repair machinery and provide a possible explanation for the sluggish DNA damage clearance observed previously on MKs after irradiation. Also, it suggests that scaling of transcriptional activity is selective - i.e. that only 'mission critical' gene expression pathways are scaled with ploidy, and DNA damage repair may be dispensible for MK function.

In line with this, WGD occurring during physiological MK maturation has profound consequences for genome integrity, leading to the accumulation of dsDNA breaks, CNA and micronuclei. In autoimmune disorders and cancer, the formation of micronuclei fuels cancer evolution, and their rupture triggers

epigenetic reprogramming and cGAS-STING signalling – creating a surveillance mechanism for genetic instability [203]. Crucially, genetically unstable tumour cells can rewire STING signalling through the non-canonical NF-κB pathway to promote cell survival while avoiding the deleterious effects of IFN Type I activation and triggering senescence [104]. Similarly, MKs activate Type II (but not Type I) interferon signalling and non-canonical NF-κB pathway target genes after WGD, without displaying a senescence phenotype, indicating that they might utilise a similar mechanism to tolerate micronuclei formation and genetic instability following WGD. Of note, recent reports have demonstrated that IL6 signalling is required for cell survival following mirconuclei rupture and cGAS-STING activation [204] and could explain why IL6 signalling promotes MK polyploidization.

ANKRD26 Downregulation is Required to Bypass the Tetraploid Checkpoint Activation

During steady-state megakaryopoiesis, p53 has no control over MK ploidy and previous studies have shown that only under emergency thrombopoiesis (i.e., after acute platelet depletion or TPO stimulation) p53 knockout MKs show a slight increase in ploidy [205]. Concordantly, I showed that MKs maintain active p53 surveillance but it does not restrain WGD as demonstrated using p53 knockout mouse models. These observations contrast markedly with previous studies on heart and liver tissues, where hepatocyte and cardiomyocyte ploidy are controlled by PIDDosome activation [183–185], and knocking out p53 results in a dramatic increase in polyploidization. Thus, MKs must undergo unique molecular adaptations to avoid tetraploid checkpoint activation and permit recursive WGD.

The first step in PIDDosome activation is recruitment of ANKRD26 to the distal appendages of the mother centriole [115, 119]. In line with previous studies [197], I showed that ANKRD26 is suppressed during MK differentiation. However, whether this is required for WGD tolerance has never been established. Using samples from patients with a rare genetic variant in the regulatory region of ANKRD26 that prevents its transcriptional silencing during megakaryopoiesis,

I examined the functional consequences of persistent ANKRD26 expression, gaining additional mechanistic insights into this phenomenon.

Single cell transcriptomic profiling of *in vitro* differentiated MKs from ANKRD26-RT and healthy donors HSPCs demonstrated that ANKRD26 overexpression does not result in a block of MK differentiation but rather in a WGD-dependent activation of the p53 response. In line with this, ANKRD26 mutant MKs show a dramatic reduction of ploidy and a significant p53 stabilisation and nuclear translocation both in bone marrow biopsies and *in vitro* cultures. These results confirmed that ANKRD26 de-repression results in the reactivation of the tetraploid checkpoint in MKs, causing hypo-ploidy, explaining the pathological mechanism behind ANKRD26-RT.

Interestingly, and contrary to previous observations in hepatocytes where PIDDosome modulation is required for postnatal polyploidization [183], multimodal single cell profiling demonstrated that low ploidy embryonic megakaryopoiesis is not determined by p53 activation following WGD. Given that ANKRD26 is transcriptionally suppressed in embryonic MKs, I hypothesize that low ploidy MKs results from an proficient mitotic machinery, unable to engage in endocytotic cycles.

Although requiring further validation studies, the results presented here suggest that pharmacological suppression of PIDDosome signalling, for example using Caspase-2 inhibitors [206], might present a pharmacological avenue to alleviate thrombocytopenia in patients with ANKRD26-RT.

Chapter Summary Findings

1. MKs utilise unique adaptations akin to those observed in malignant cells to tolerate WGD, including G1 lengthening and cGAS-STING signalling alteration.
2. ANKRD26 downregulation is essential for MKs to bypass the PIDDosome tetraploid checkpoint.
3. p53 activation in response to WGD is the pathological mechanism behind ANKRD26-RT.
4. Transcriptional control of the tetraploid checkpoint does not change during MK ontogeny.

5

Role of ANKRD26 on WGD tolerance in solid tumours

Contents

5.1 Introduction 98
5.1.1 Genetic Strategies That Favour Whole Genome Duplication in Cancer 98
5.1.2 Therapeutic Strategies for the WGD Status 99
5.1.3 Chapter Aims 100
5.2 Results 102
5.2.1 CCLE Analysis Reveals ANKRD26–PIDDosome Downregulation After Whole Genome Duplication 102
5.2.2 Unscheduled WGD Prevents ANKRD26 Protein Recruitment to The Centrosome in a p53-Dependent Manner . . 102
5.3 Discussion 106
5.4 Summary Findings 107

5.1 Introduction

Increasing the total gene dosage improves the fitness of aneuploid cells and facilitates rapid genome adaptation [62, 102, 207]. However, non-scheduled Whole Genome Duplication (WGD) is poorly tolerated in mammalian cells, which typically arrest through p53 activation [208]. Consequently, for solid tumours to exploit the malignant potential of WGD, they must evolve mechanisms to bypass p53-mediated checkpoints [102].

5.1.1 Genetic Strategies That Favour Whole Genome Duplication in Cancer

Broadly, three main routes enable polyploid cancer cells to regain proliferative capacity.

First, because ploidy-restricting pathways converge on p53 stabilisation, disruption of the p53/p21 axis is a common adaptive mechanism for tolerating tetraploidy. This was elegantly demonstrated in a mouse model of pancreatic cancer, where WGD occurred only after TP53 loss [209]. Consistently, WGD+ tumours are highly enriched for TP53 mutations, found in roughly 50% of cases [100]. The frequency of such mutations, however, varies across tumour types, and some cancers inactivate p53 signalling through alternative mechanisms, such as MDM2 amplification or CDKN2A loss [100].

Second, polyploid cells can restore proliferation by enhancing E2F-driven G1–S progression. This is often achieved through amplification of Cyclin D and E genes, a feature commonly observed in p53-proficient WGD+ tumours [100, 210, 211]. Interestingly, recent work showed that p53 signalling enables mitotic bypass and polyploidisation under replication stress induced by Cyclin E1 (CCNE1) overexpression, suggesting that, upon CCNE1 amplification, intact p53 may paradoxically be required for WGD to happen [212].

Lastly, inactivation of Hippo pathway, which functions as a tetraploid checkpoint control, provides a third route to restore proliferation. Indeed, Cancer Cell Line Encyclopedia data show that YAP overexpression or deletions of

the YAP inhibitors LATS1/2 -both of which result in Hippo signalling inhibition- are significantly enriched in polyploid lines relative to diploid counterparts [117]. In melanoma, for example, Hippo pathway inactivation is specifically required to drive tumour progression after WGD [213].

The contribution of the ANKRD26–PIDDosome pathway to polyploid tumours remains poorly defined. Its role has been studied mostly in the context of centrosome amplification, where PIDD1 downregulation has been shown to promote malignant transformation after DNA damage in a B cell tumour model, indicating a tumour-suppressive function [214]. Mutations in ANKRD26 that impair its interaction with PIDD1 and the activation of the PIDDosome have been described [115], however, they are rare in cancer and their association to WGD remain unclear.

5.1.2 Therapeutic Strategies for the WGD Status

Evolving to a tetraploid state during cancer progression is associated to therapy resistance and poor prognosis [207, 215]. Drug sensitivity profiling of diploid and tetraploid cells derived from the same p53 wild-type line revealed that polyploidy confers broad resistance to chemotherapeutic agents, including topoisomerase II inhibitors such as daunorubicin, doxorubicin, and etoposide [216]. Interestingly, p53 proficient polyploid cells were also significantly more resistant to Nutlin-3 treatment, a small molecule inhibitor of the p53 ubiquitin ligase MDM2 [216]. The mechanism behind these adaptations is unclear, although chromosome instability (CIN) subsequent to tetraploidization was accompanied by suppression of the p53 signalling, which could confer increase resistance to p53 activators [216].

Current proposed therapeutic strategies to target polyploid cells, capitalise on the unique vulnerabilities imposed by the tetraploid status, offering a therapeutic window to selectively eliminate WGD+ clones while sparing normal diploid cells [108, 217].

Polyploid cells show signs of DNA damage and replication stress [111], and higher DNA content in polyploid cells can render them more sensitive to ionizing

radiation [218]. Systematic analysis of polyploid compared with diploid cell lines revealed multiple genes whose loss was specifically lethal to polyploid cells [108]. As expected, these genes were mostly related to pathways crucial for the tolerance of a tetraploid genome, including DNA replication [108].

Proper positioning of extra chromosomes during mitosis is challenging, and significantly extends the mitotic time owing to the activation of the Spindle Assembly Checkpoint (SAC) [219]. This might also make polyploid cells more prone to the activation of the mitotic stopwatch pathway [220], a p53-dependent surveillance mechanism that selectively arrests cells after completing an abnormally long mitosis [221]. Thus, polyploid cells are more vulnerable to the loss of genes involved in chromosome positioning and mitotic spindle formation, and are more sensitive to anti-mitotic agents [108]. One example for this is KIF18A, a mitotic kinesin that regulates microtubule dynamics to ensure the adequate aliment of the chromosomes at the metaphase plate. While KIF18A is largely dispensable on diploid cells, KIF18A loss in cancer cells that exhibit whole genome doubling or chromosomal instability results in mitotic defects and eventual cell death [108, 222].

Lastly, polyploid cells rapidly become aneuploid, which leads to proteotoxic stress [116, 223]. As a result, WGD+ cell lines are more vulnerable to the loss of proteasome regulators and more sensitive than WGD- cells to the proteasome inhibitor MG132 [108].

5.1.3 Chapter Aims

The discovery of WGD-specific therapeutic targets starts by understanding the molecular adaptations that are required to proliferate after tetraploidy. Loss of p53 is a common mechanism to tolerate polyploid genomes, however, approximately 50% of the WGD+ tumours remain p53 proficient. Why some cancer cells can circumvent the p53-dependent checkpoint after WGD is a major open question [224].

Previous work presented in this thesis demonstrated that, in megakaryocytes (MKs), polyploidy inevitably provokes genome instability, DNA damage, and micro-nucleation. Despite these liabilities, MKs display unique adaptations that permit tolerance of WGD. Notably, they rewire STING-mediated immunosurveillance to bypass senescence —a strategy previously described only in malignant contexts- highlighting striking parallels between the adaptive programs of MKs and cancer cells.

Moreover, I have also demonstrated that transcriptional modulation of a single gene, ANKRD26, is both necessary and sufficient for MKs to evade tetraploidy-induced arrest under p53 surveillance. However, the integrity of the ANKRD26 – PIDDosome axis in WGD+ tumours with intact p53 remains largely unexplored. These observations led me to hypothesize that downregulation of the ANKRD26 – PIDDosome pathway may constitute a critical adaptation enabling p53-proficient tumours to tolerate genome doubling.

In this chapter, I present my initial preliminary results where I explored the role of the ANKRD26 – PIDDosome in WGD tolerance in p53 proficient malignant cells.

5.2 Results

5.2.1 CCLE Analysis Reveals ANKRD26–PIDDosome Downregulation After Whole Genome Duplication

To test whether downregulation of the ANKRD26–PIDDosome pathway allows cancer cells with functional p53 to tolerate WGD (WGD), I analysed the Cancer Cell Line Encyclopaedia (CCLE), which provides mutational and transcriptional profiles of over 1,000 cell lines [225].

Cell lines were stratified by p53 status into wild-type (p53 WT, n=453) and mutant (p53 Mut, n=730) groups. Within each group, I compared the transcriptional profiles of WGD– (diploid or near-diploid; n_{p53WT}=197, n_{p53Mut}=147) and WGD+ (tetraploid or higher; n_{p53WT}=256, n_{p53Mut}=583) cells (Fig. 5.1A).

In WGD+ p53 wild-type cells, but not in WGD+ p53 Mut cells, both PIDD1 —an essential PIDDosome component— and TP53 were significantly downregulated compared to WGD– cells, suggesting that suppressing this pathway enables proliferation after WGD in the presence of intact p53. Consistent with this, no significant downregulation of PIDD1 or TP53 was observed in the p53 Mut group (Fig. 5.1B, C). Notably, ANKRD26 expression was unchanged in both groups (Fig. 5.1, B).

5.2.2 Unscheduled WGD Prevents ANKRD26 Protein Recruitment to The Centrosome in a p53-Dependent Manner

To experimentally test whether PIDDosome suppression is required for proliferation of p53 wild-type tetraploid cells, I performed an *in vitro* evolution experiment (Fig. 5.2, A). The colorectal cancer line HCT116 (p53 wild-type) was transduced with either a TP53-targeting shRNA or a non-targeting control.

HCT116 wild-type and knockdown cells ($HCT116^{p53WT}$ and $HCT116^{p53KD}$) were treated with dihydrocytochalasin D (DCD) for 18h to induce tetraploidy via cytokinesis failure. Cells were then washed, seeded at low density, and cultured in DCD-free media for two weeks to generate single cell-derived colonies [121].

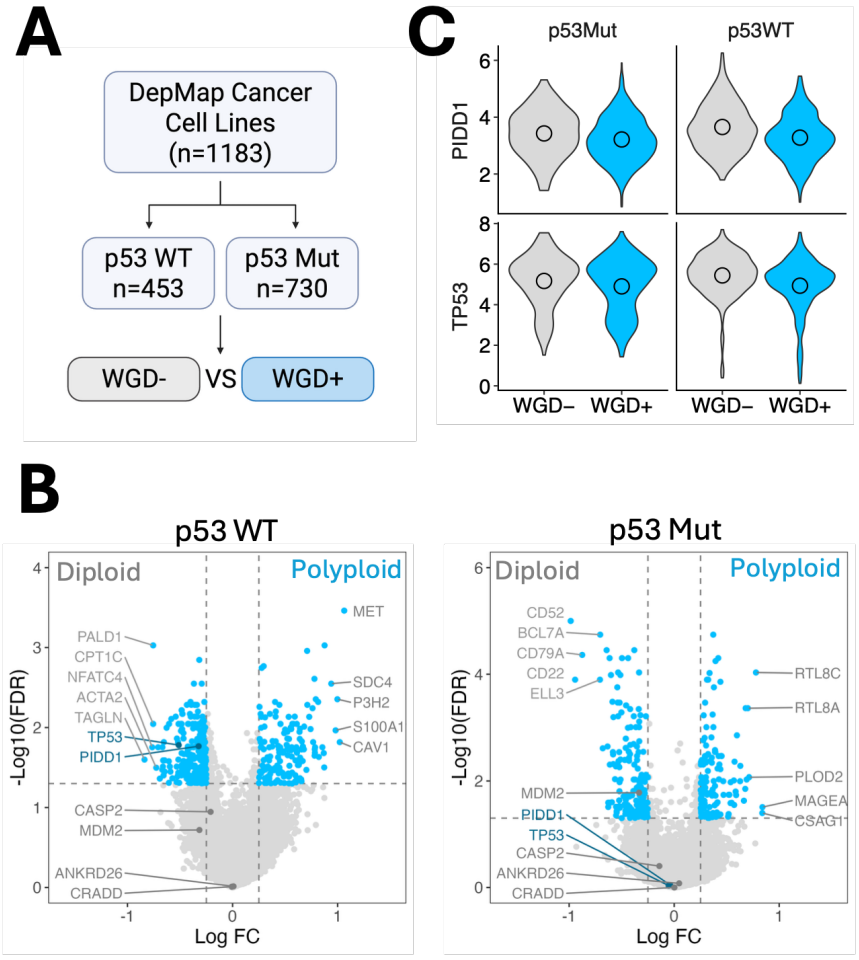


Figure 5.1: Cancer Cell Line Encyclopaedia analysis of diploid and polyploid cells. **A**, schematic depicting analysis of 1183 cancer cell lines in the CCLE database according to their p53 mutation (wild-type, WT vs. mutated (mut) and whole genome duplication (WGD+ vs WGD-) status. **B**, volcano plots showing log fold change in gene expression between diploid and polyploid cells split by p53 mutation status. TP53 and PIDD1 genes are highlighted in blue. **C**, violin plots showing the mRNA expression TP53 and PIDD1 on WGD+/- cell lines depending on their p53 status. The central point represents the median expression value for all cell lines on that group.

Isogenic clones were isolated and screened by flow cytometry, confirming the presence of stable diploid and tetraploid populations (Fig. 5.2A, B).

If PIDDosome suppression is required for tetraploid proliferation in p53 wild-type cells, then p53-proficient polyploid clones should selectively downregulate this pathway. Indeed, RT-qPCR revealed reduced ANKRD26 and PIDD1 expression in DCD-treated HCT116^{p53WT} clones compared to untreated cells, although this was observed regardless of whether clones were diploid or tetraploid

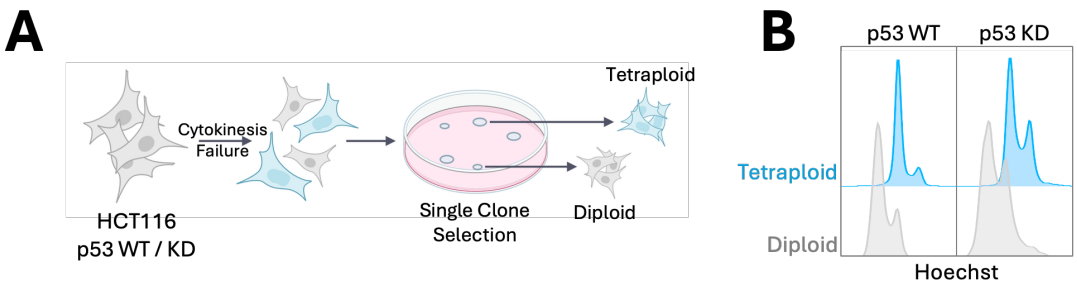


Figure 5.2: Experimental layout for *in vitro* evolution experiment. **A**, schematic showing the experimental strategy followed to isolate isogenic diploid and tetraploid clones. **B**, representative flow plots of a diploid and tetraploid clone from p53 wild-type and knockdown HCT116 cells after selection. Panel A created in https://BioRender.com.

(Fig. 5.3A, B). This suggests that either DCD treatment led to downregulation of these genes due to an alternative mechanism that did not involve WGD, or alternatively that the cells went through a transient WGD stage triggering coordinated downregulation of both genes, before reverting to diploid status. In contrast, expression remained unchanged in HCT116^{p53KD} clones, indicating that this transcriptional response is only required in cells with intact p53.

Activation of the PIDDosome pathway requires ANKRD26-dependent recruitment of PIDD1 to the centrosome. In diploid HCT116^{p53WT} clones, centrosomal ANKRD26 was detected in 65–80% of cells, whereas only 40% of tetraploid clones retained detectable ANKRD26 centrosomal signal (Fig. 5.4A, B). By contrast, HCT116^{p53KD} clones did not consistently show reduced ANKRD26 localisation (Fig. 5.4A, B).

Together, these results indicate that suppression of the ANKRD26 – PIDDosome – p53 pathway is a key mechanism by which cancer cells with functional p53 tolerate WGD, echoing the strategy used in physiological polyploidisation of MKs.

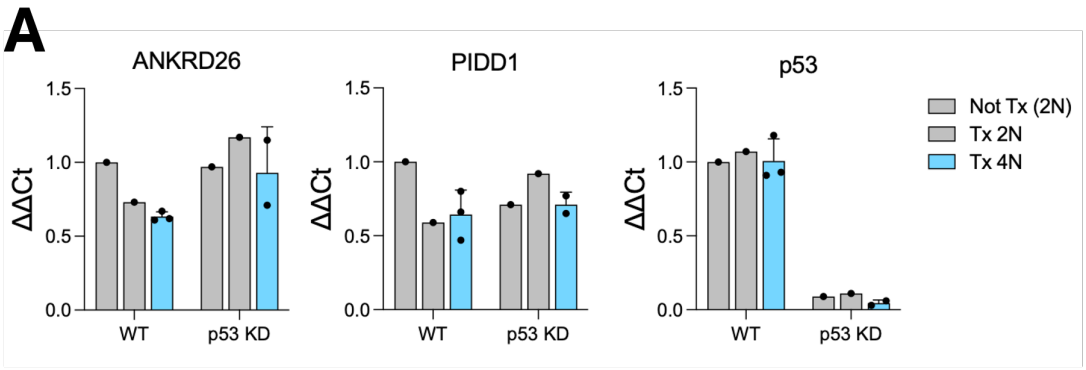


Figure 5.3: Dihydrocytochalasin D (DCD) treated p53 proficient cells downregulate PIDDosome components. **A**, mRNA expression measured by RT-qPCR (ΔΔCt method) of three essential components of the ANKRD26-PIDDosome-p53 signalling pathway on DCD treated and untreated HCT116 cells.

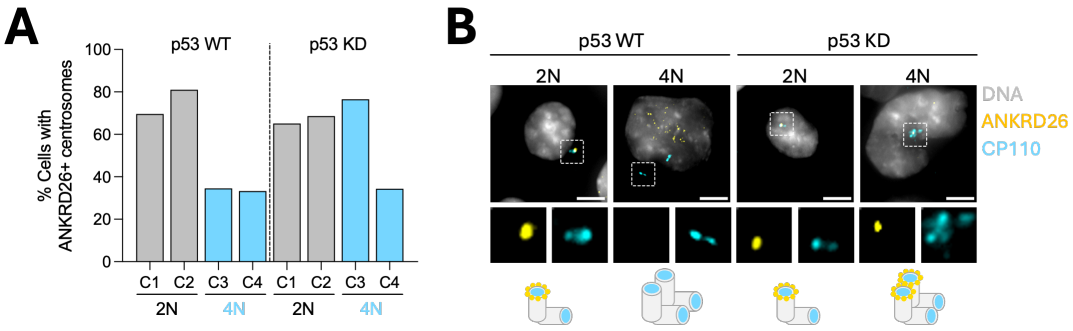


Figure 5.4: Tetraploid HCT116 cells loose ANKRD26 at their centrosomes in a p53-dependent manner. **A**, percentage of cells with ANKRD26 recruitment to nuclear centrosomes in 2N vs 4N clones, with and without p53 shRNA-mediated knockdown. n>30 cells analyzed per group. **B**, representative immunofluorescence images of diploid and tetraploid HCT116 cells stained for DNA (Hoechst, grey), the centrosome protein CP110 (blue) and the distal appendage protein ANKRD26 (yellow). Scale bar = 5μm.

5.3 Discussion

The findings presented here suggest that adaptations involving the ANKRD26 – PIDDosome pathway in MKs may also be co-opted by malignant tetraploid cells to sustain viability following WGD while maintaining functional p53. Analysis of the Cancer Cell Line Encyclopedia revealed that p53-proficient cancer cells markedly downregulate both PIDD1 and TP53 expression after WGD, consistent with an adaptive mechanism to attenuate p53 signalling. Interestingly, ANKRD26 expression remained largely unchanged across ploidy groups irrespective of TP53 status.

PIDD1 (p53-induced death domain protein 1) is the core component of the multiprotein complex PIDDosome, which was originally described as a member of the DNA damage response pathway [226]. Indeed, PIDD1 co-localises with histone H2AX phosphorylated at Ser139 at DNA damage sites during interphase and treatment with DNA-damaging agents such as camptothecin induces PIDD1 auto-proteolysis and PIDDosome formation resulting in CASP2 activation, MDM2 degradation and p53 stabilisation [227, 228]. Interestingly, PIDDosome formation in response to DNA damage is also dependent on PIDD1 recruitment to the distal appendages of the mother centriole by ANKRD26 [115]. Given that WGD provokes replication stress and DNA damage [45, 111], the observed selective downregulation of PIDD1 over other components of the tetraploid checkpoint pathway may provide survival advantages to p53-proficient tetraploid cells that extend beyond tolerating extra centrosomes.

Nevertheless, in an *in vitro* evolution system, ANKRD26 was found to be selectively lost from the centrosomes of proliferating tetraploid clones that retained supernumerary centrosomes. The mechanism underlying this loss of ANKRD26 remains unclear and is likely multifactorial. Recent work has demonstrated that WGD perturbs chromatin organization, enabling the transcriptional repression of tumour-suppressive elements to support the survival of polyploid cells [114]. It

is therefore plausible that tetraploid clones downregulate ANKRD26 expression through transcriptional reprogramming as a means of adaptation.

Future studies will be required to determine the physiological relevance of ANKRD26 loss *in vivo* for the tolerance of centrosome amplification, with or without accompanying WGD. Importantly, the results presented in this chapter are preliminary and not exempt of limitations that will require future validation. These will be discussed in Chapter 6.

5.4 Summary Findings

Chapter Summary Findings

1. p53-proficient cancer cells utilise similar pathways to MKs in order to tolerate WGD, involving silencing of the ANKRD26-PIDDosome tetraploid checkpoint, therefore avoiding p53 activation.

6
Conclusions And Future Work

Contents

6.1 Outcomes And Broad Implications of This Research 109
6.1.1 Genome Doubling Shapes Megakaryocyte Biology . . . 109
6.1.2 ANKRD26 Plays a Key Role in WGD Tolerance 110
6.2 Limitations of This Work 112
6.3 Future Work 114
6.3.1 Other Forms of DNA Damage on MKs 114
6.3.2 What is the Role of ANKRD26 Dysregulation in the Predisposition to Acute Myeloid Leukaemia? 114
6.3.3 Can we Harness ANKRD26 as a Therapeutic Target for p53 Proficient WGD+ Cells? 116
6.4 Conclusion 117

6.1 Outcomes And Broad Implications of This Research

6.1.1 Genome Doubling Shapes Megakaryocyte Biology

Megakaryocyte (MK) maturation is characterised by a procession of endomitotic cycles and continuous accumulation of genomic copies. Multiples lines of evidence, mostly from the setting of cancer, demonstrate that polyploid cells that continue to proliferate are genetically unstable and accumulate DNA damage, structural and numerical chromosomal aberrations [102, 103, 110, 111, 207, 229]. In this work, I have demonstrated that MKs are not indifferent to these liabilities and that polyploidization results in DNA damage accumulation, chromosomal instability and micro-nucleation.

The extensive chromosomal instability (CIN) observed in MKs is highly unusual for somatic healthy cells. The study of liver regeneration shows that proliferating hepatocytes largely preserve their genomic integrity, partially aided by mechanical forces of intact tissue architecture [150, 152]. Only trophoblast giant cells, which also engage in multiple polyploidization rounds, suffer similar levels of instability, where over- and under-replicated regions selectively select for the expression of functionally relevant genes [154]. Nevertheless, and to the best of my knowledge, MKs are the only 'healthy' cell in the human adult body that shows extensive rearrangements of their genome makeup, a phenotype otherwise restricted to malignant cells.

The profound impact of WGD on MKs prompted me to studying the transcriptional consequences of polyploidy on MK biology. In other studies, analysis of MKs at single cell level has recently demonstrated functionally diverse MK subtypes (i.e., niche-supporting, platelet-producing or immunological regulators). However, scRNAseq captures single snapshots of cell state - and whether these represent stable functionally distinct cellular subsets, or MKs 'caught' undergoing specific cell functions, is not known. Integration of DNA content measurements with MK scRNAseq profiles has revealed variation in

ploidy distribution across these transcriptionally-defined subsets, with immune MKs predominantly maintaining a diploid state [41]. However, the direct impact of ploidy itself on MK identity and function remains uncharacterised.

In my DPhil research, I revealed that MKs undergo specific adaptations in response to each round of WGD.

Firstly, after WGD MKs extend their time in G1, a process that in cancer cells occurs independently of p53 function and is thought to enable proper scaling of the cell cycle machinery, in preparation for a mitosis with supernumerary chromosomes [111, 114, 201]. My pathway analysis also revealed significant activation of inflammatory signalling pathways in high ploidy MKs, also reminiscent of previously reported transcriptional profiles of CIN-high cancer cells in response to cGAS-STING activation [104]. Importantly, the transcriptional analysis suggested that polyploid MKs selectively activate the Non-canonical KF-κB pathway, avoiding the deleterious effects of type I interferon signalling and senescence. This adaptative mechanism has been recently described in chromosomally unstable tumours, and it is required to bypass the immunosurveillance control of cGAS-STING [104, 202, 204]. Importantly, this is the first time that this pathway is described in healthy somatic cells.

Finally, MK polyploidization was also accompanied by a previously unappreciated broad downregulation of DNA repair genes, correlating with the functional data I reported showing that MKs are slow to clear yH2AX breaks and repair dsDNA breaks. This may explain why thrombocytopenia is a common side effect of treatment with DNA damage repair inhibitors [168].

6.1.2 ANKRD26 Plays a Key Role in WGD Tolerance

Through both functional *in vitro* studies and analysis of MKs *ex vivo* from genetic mouse models I showed that while MKs retain some aspects of p53 function, p53 is not activated in response to WGD, unlike other diploid and polyploid somatic cells [183, 208]. In this work, in line with previous reports [197], I showed that the key initiator of the tetraploid checkpoint response, ANKRD26,

is selectively downregulated during megakaryopoiesis. My data is the first to study the role of ANKRD26 on MK polyploidization, and to confirm that this protein enables MKs to operate in 'p53 stealth mode' to tolerate WGD.

By studying a rare form of inherited thrombocytopenia where somatic mutations in the 5'-UTR region of ANKRD26 prevent its transcriptional downregulation, I demonstrated that ANKRD26 transcriptional repression is necessary to avoid the detection of centrosome amplification upon WGD in MKs, which otherwise results in PIDDosome formation and p53 activation.

Previous work on samples from patients with ANKRD26-related thrombocytopenia (ANKRD26-RT) suggested that the low platelet production might result from an over-activation of Type I cytokine signalling receptors, facilitated by ANKRD26 [197, 200]. Although not mutually exclusive with my findings, the results presented in this thesis suggest that an important pathobiological consequence of persistent ANKRD26 expression is that it re-instates the tetraploid checkpoint. Thus, while ANKRD26 overexpression does not impede MK maturation *per se*, it prevents them from achieving high polyploid levels, from where MKs produce platelets more efficiently [23]. This mechanism explains the clinical manifestations of ANKRD26-RT - as these patients typically present with mild, often undetected, thrombocytopenias [190]. In other words, ANKRD26 overexpression in ANKRD26-RT does not result in a complete block in platelet production but simply makes platelet production inefficient, due to the lack of high ploidy MKs.

The work in this thesis shows for the first time remarkable parallelism between MK and cancer cell biology. Both cell systems operate unique adaptations to tolerate whole genome duplication (WGD). Mining the Cancer Cell Line Encyclopaedia and using an *in vitro* evolution experiment I showed that, similar to MKs, downregulation of components of the ANKRD26–PIDDosome axis commonly accompanies polyploidization in p53-proficient tumour cells, suggesting a shared strategy to tolerate centrosome amplification following WGD in cells that do not acquire inactivating p53 mutations.

All these observations raise important questions: Firstly, why do MKs so rarely transform? Despite their genetic instability, megakaryoblastic leukaemias represent < 1% of acute myeloid leukaemias in adults [230]. There are some possible explanations for this. First, mature MKs do not complete mitosis [80]. Therefore even if they lose tumour suppressor genes and acquire a malignant phenotype, MKs might only be able to increase their cell size, but not their number, ultimately entering apoptosis as genomic lesions accumulate beyond a tolerable threshold. Second, WGD may paradoxically buffer the cells against malignant evolution by providing extra "healthy" alleles that mitigate the impact of deleterious mutations [231]. In line with this, liver carcinomas frequently arise from diploid hepatocytes and increasing the average ploidy of the liver has a protective effect on liver malignant transformation [232]. A second question relates to the fate of MK micronuclei. Micronuclei are prone to rupture, leading to cytosolic DNA and GAS-STING activation. Potentially, this might lead to inflammation-primed MKs, and also be a source of DNA fragments detectable in circulating blood platelets.

6.2 Limitations of This Work

There are several limitations to this work, including:

(1) Although I have comprehensively interrogated the genomic and transcriptomic features of MKs in this work, I have not explored how DNA methylation, accessibility and chromosome confirmation alters with ploidy. Secondly, while the accumulation of DNA damage in MKs was demonstrated across multiple systems (cell lines, induced Pluripotent Stem Cell (iPSC)-derived MKs and primary mouse MKs), impaired DNA damage–repair capacity was functionally shown in iPSC-derived MKs. Whether impairment of DNA damage–repair is a generalized phenomenon in MKs *in vivo* remains unresolved. Future studies could assay DNA damage-repair kinetics in MKs from irradiated mice to define physiological relevance. In addition, downregulation of DNA damage-repair pathways has been shown at the transcript level as technical constraints — specifically, an

inability to obtain sufficient numbers of polyploid MKs — means that accurate quantification of protein levels are difficult. An alternative approach would be to infer functional DNA damage-repair defects from DNA mutational signatures [233, 234]. This could involve reanalysing single-cell DNA-sequencing data from primary mouse MKs or applying SComatic, a method for detecting somatic mutations from single-cell RNAseq datasets [235].

(2) A further limitation is that the single cell transcriptional characterisation of MKs derived from patients with ANKRD26-RT was limited to two patients, largely owing to the rarity of the disease and the scarcity of samples available. This limited the statistical power of some of the results. Nonetheless, the mechanistic observations described are in line with the reported role of ANKRD26 in centrosome amplification control [115, 119], and p53 activation was also confirmed by immunohistochemistry analysis of bone marrow biopsies from a larger ANKRD26-RT cohort (n=4).

(3) My analyses of tumour cell lines assumed that WGD+ cells uniformly harbour supernumerary centrosomes. This is assumption is not always true. Diploid cell lines can also exhibit elevated centrosome numbers [236], and WGD+ cancer cells may also not amplify their centrosomes. Unfortunately, there is no *bona fide* transcriptional signature that can identify centrosome amplification [237]. Therefore cell line work validation like the one provided remains essential.

(4) Finally, the role of ANKRD26 in WGD tolerance in cell lines requires further testing. Although my results show that ANKRD26 is selectively lost from the centrosomes of proliferating cells after WGD in a p53-dependent manner, I have not directly demonstrated that this is required for WGD tolerance, and this observation could be secondary to the true permissive mechanism. Re-introducing ANKRD26 into p53-proficient, evolved tetraploid clones will be a necessary validation for this project. Moreover, current *in vitro* data are limited to a single colorectal cancer line (HCT116). Broader validation in additional systems (e.g., RPE1) will clarify generality across tissues and utilising different modes

of WGD induction (endoreplication, mitotic slippage, cytokinesis failure) will determine their influences on ANKRD26 loss and WGD tolerance.

6.3 Future Work

6.3.1 Other Forms of DNA Damage on MKs

In this thesis I have uncovered several genotoxic processes in MKs including dsDNA breaks, chromosome miss-segregation (micro-nucleation) and chromosome copy number variations. DNA confined to micronuclei can undergo chromothripsis, whereby chromosomes are pulverized and rearranged into a highly unstructured sequence [172, 175]. Imaging analysis revealed pan-nuclear DNA damage staining (γH2AX) in approximately 30% of the MKs micronuclei, indicating frequent DNA damage. Testing whether chromothripsis is a routine feature of megakaryopoiesis will require isolating and sequencing MK micronuclei using recently developed purification strategies of MKs and single-micronucleus isolation methods [122, 238, 239].

Extrachromosomal DNA (ecDNA) are circular DNA fragments of varied sizes (from 100 kilobases to several megabases) located within the cell nucleus. They are frequently found in cancer cells where they harbour and amplify specific oncogenes, drug-resistance and immunomodulatory genes, conferring malignant cells a fitness advantage [240]. ecDNAs are frequently generated from circularization of DNA fragments originating from DNA double strand breaks or chromosome bridges [240, 241]. Given that megakarycoytes present both forms of genomic stress, it is possible that MKs also form ecDNA during their maturation. To tackle this question ecDNA sequencing techniques such as Circle-Seq [242] may be applied to single-cell sorted MKs.

6.3.2 What is the Role of ANKRD26 Dysregulation in the Predisposition to Acute Myeloid Leukaemia?

Unfortunately, patients with ANKRD26-RT have a 20-30 fold increase in developing myeloid neoplasms. The mechanism for this remains poorly defined.

Large, polyploid MKs contribute to the regulation of the haematopoietic stem cell (HSC) niche by promoting quiescence and limiting HSC proliferation [38, 39]. In mouse models, selective genetic ablation of polyploid MKs results in marked HSCs expansion [23, 38, 39]. Consistent with this, when isolating CD34+/Lineage- haematopoietic stem/progenitor cells (HSPCs) by Fluorescence-Activated Cell Sorting I noticed a ~5.4 fold expansion of the HSPC compartment in patients with ANKRD26-RT relative to healthy controls (Section 4.2.4, Fig. 4.13). This observation aligns with recent reports describing an expanded CD34+ HSPC population in the bone marrow biopsies of patients with ANKRD26-RT with no evidence of blood malignancies [243]. It is therefore possible that the alteration to MK ploidy in patients with ANKRD26-RT not only impairs platelet production, but also results in HSC-niche dysregulation.

Niche-induced quiescence prevents HSCs from undergoing frequent and potentially error-prone DNA replication and mitosis, preserving their genetic integrity and protecting from malignant transformation [244]. Disruption of MK-mediated quiescence in ANKRD26–RT could therefore contribute to the elevated neoplasia risk.

Testing this hypothesis will require the use of multicellular systems such as mouse models. To this date only a zebra fish model of ANKRD26-RT has been reported in the literature [245], and mouse models are restricted to global Ankrd26 knockouts [184, 246]. More recently, the group of Alan Cantor, at the Dana-Farber Cancer Institute, and an essential collaborator for this project, developed a haematopoietic cell-specific, cre-inducible *Ankrd26* over-expression mouse line that recapitulates dysmegakaryopoiesis and thrombocytopenia characteristic of ANKRD26–RT (data not shown). This mouse model will permit dissection of the role of the MK-niche disruption in malignant progression in patients with ANKRD26-RT.

An alternative hypothesis is that p53 activation in MKs enhances inflammation in the bone marrow micro-environment, creating a selective pressure for the evolution and expansion of p53-mutant clones.

6.3.3 Can we Harness ANKRD26 as a Therapeutic Target for p53 Proficient WGD+ Cells?

Therapeutic activation of p53 has focused on the inhibition of the E3 ubiquitin ligase MDM2 [247]. The first such inhibitors were the Nutlins, cis-imidazolines that elicit p53 activation in p53 wild-type cancer cells [248]. Interestingly, thrombocytopenia is a common side effect of Nutlins [247] and *in vivo* administration of the MDM2 inhibitor RG7112 reduces MK ploidy [249] in murine models, suggesting that cycling polyploid cells such as MKs might be specifically sensitive to MDM2 inhibition. Indeed, the third-generation MDM2 inhibitor idasanutlin showed encouraging benefits in a phase I clinical trial in patients with polycythaemia vera [250], a p53-proficient myeloid malignancy characterised by the pathological expansion of polyploid MKs and platelets. However, haematological and low-grade gastrointestinal toxicity led to frequent discontinuation of the drug in a subsequent phase II trial [251], underscoring the need for more selective strategies.

Manipulating ANKRD26 expression would be an interesting therapeutic strategy for WGD+ cancers, since its overexpression in patients with ANKRD26-RT is non toxic for diploid cells, and targets polyploid MKs in a highly selective manner. The use of lipid nanoparticles (LNPs) *in vivo* is a promising strategy to deliver biologically active compounds such as mRNA molecules to specific tissues *in vivo* [252], and can be adapted to selectively target certain cell types to induce over-expression of clinically relevant molecules [253]. It would be interesting to test if LNPs loaded with ANKRD26 can be used to transiently express ANKRD26 in MKs from myeloproliferative neoplasms potentially blocking the pathological MK polyploidization in this disease.

More broadly, although additional validation is required, the results presented in this thesis suggest that re-introduction of ANKRD26 might selectively target proliferating, p53-proficient tumour cells that have undergone WGD or centrosome amplification. Given that approximately 50% of WGD+ tumours retain p53 functionality, it will be important to test if ANKRD26-mRNA loaded LNPs can be used to stop the proliferation of malignant cells after WGD.

6.4 Conclusion

In summary, in this work I have shown that WGD reshapes the biology of MKs in unanticipated ways. Polyploid MKs are genetically unstable, partially owing to chromosome mis-segregation and micronucleation but also due to a impaired scaling of the DNA damage repair machinery after WGD. These unusual levels of genetic instability are tolerated by polyploid MKs by utilising pathways only previously ascribed to malignant cells, highlighting an unexpected convergence between MK and cancer cell biology. By studying a rare inherited thrombocytopenia, I revealed that downregulation of ANKRD26 is essential to avoid activation of the PIDDosome-p53 pathway upon WGD in megakaryopoiesis, uncovering new unusual aspects of MK biology and revealing the mechanism behind the pathobiology of ANKRD26-related thrombocytopenia. Expanding these observations to tumour biology, I demonstrated that p53-proficient cancer cells promote the downregulation of elements of the ANKRD26-PIDDosome pathway upon WGD, revealing a potential mechanism for cancer cell adaptation and survival. Together, these findings illustrate how investigating the exceptional biology of rare cell types such as MKs can broaden our understanding of human physiology and disease.

7 Publications

Contents

7.1 Published Articles 119
7.2 Manuscripts in Preparation 120

7.1 Published Articles

- Brierley, C. K., Yip, B. H., Orlando, G., Wen, J., Wen, S., Goyal, H., Levine, M., Jakobsdottir, G. M., Tapinos, A., Cornish, A. J., **Rodriguez-Romera, A.**, et al. (2025). Chromothripsis-associated chromosome 21 amplification orchestrates transformation to blast-phase MPN through targetable overexpression of DYRK1A. *Nature Genetics*.

- Asquith, N. L., Carminita, E., Camacho, V., **Rodriguez-Romera, A.**, et al. (2024). The bone marrow is the primary site of thrombopoiesis. Blood.

- Li, R., Colombo, M., Wang, G., **Rodriguez-Romera, A.**, et al. (2024). A proinflammatory stem cell niche drives myelofibrosis through a targetable galectin-1 axis. *Science Translational Medicine*.

- Olijnik, A. **Rodriguez-Romera, A.**, Wong, Z. C., Shen, Y., Reyat, J. S., Jooss, N. J., Rayes, J., Psaila, B., & Khan, A. O. (2024). Generating human bone marrow organoids for disease modeling and drug discovery. *Nature Protocols*.

- **Rodriguez-Romera, A.**, & Psaila, B. (2024). Turn It Off! Genetic Switch System Suggests Targeting of Mutant JAK2 Reverses Myeloproliferative Neoplasms. *The Hematologist*.

- Khan, A. O., **Rodriguez-Romera, A.**, Reyat, J. S., Olijnik, A. A., Colombo, M., et al. (2023). Human Bone Marrow Organoids for Disease Modeling, Discovery, and Validation of Therapeutic Targets in Hematologic Malignancies. *Cancer Discovery*.

- Li, L., Kim, J. H., Lu, W., Williams, D. M., Cope, J. K. L., Rampal, R. K., Koche, R. P., Xian, L., Luo, L. Z., Vasiljevic, M., Matson, R. D., Zhao, Z. J., Rogers, O., Stubbs, C. M., Reddy K., **Rodriguez-Romera, A.**, et al. (2022) HMGA1 chromatin regulators induce transcriptional networks involved in GATA2 and proliferation during MPN progression. *Blood*

- Sims, M. C., Mayer, L., Collins, J. H., Bariana, T. K., Megy, K., Lavenu-Bombled, C., Seyres, D., Kollipara, L., Burden, F. S., Greene, D., Lee, D., **Rodriguez-Romera, A.**, et al. (2020). Novel manifestations of immune dysregulation and granule defects in gray platelet syndrome. *Blood*.

7.2 Manuscripts in Preparation

- **Rodriguez-Romera, A.**, Shin N., Li R., et al. Megakaryocytes acquire profound genetic instability and tolerate whole genome duplication using a physiological mechanism hijacked by p53-intact cancers. *In Preparation*.

Appendices

A

Supplementary Information

Contents

A.1 Supplementary Figures 123
A.2 Supplementary Tables 124

A.1 Supplementary Figures

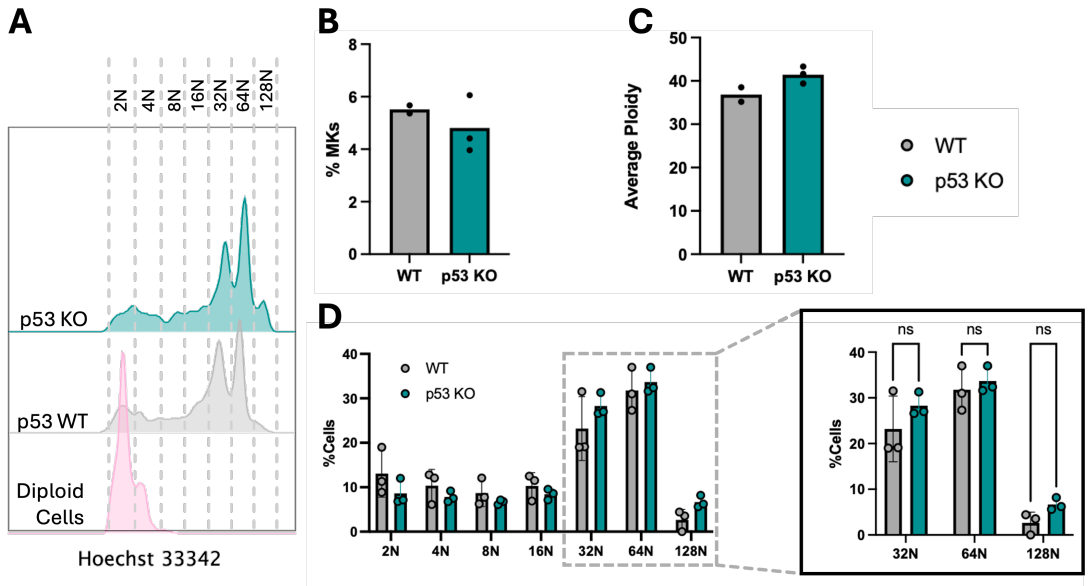


Figure A.1: p53 does not affect ploidy of *in vitro* differentiated megakaryocytes. **A**, exemplar flow plots of *in vitro* differentiated MKs from wild-type (WT) and p53 knockout (KO) murine progenitor cells. **B**, % of immunophenotypically defined MKs (CD41+/42+). **C**, average ploidy of primary MKs. **D**, % of MKs for each ploidy group n = 3 mice per group. Significance obtained from Wilcox Rank Sum test. *p <0.05; **p <0.01; ***p <0.001; ****p <0.0001. *p53 knockout mice were kindly shared by a collaborator, Stephan Contanstinescu (Louvain's de Duve Institute, Brussels)*

A.2 Supplementary Tables

Guide Name	Antisense Sequence (5′-3′)	Cat ID
Guide 1	TAAACTAACCCTTAACTGC	V3SVHS09_9347563
Guide 2	GACCCAAAACCCAAAATGG	V3SVHS09_8623444
Guide 3	AGAAACTACCAACCCACCG	V3SVHS09_10470487

Table A.1: Details of human TP53 targeting shRNA guides.

Reagent	Supplier	Catalogue	Concentration
StemPan SFEM II	StemCell Tech	09655	–
Penicillin/Streptomycin	Gibco	15140-163	100 U/mL
L-Glutamine	Gibco	25030024	2 mM
hSCF	Peprotech	300-07	1 ng/mL
hTPO	Peprotech	300-18	50 ng/mL
hIL6	Peprotech	200-06	10 ng/mL
hIL9	Peprotech	200-09	20 ng/mL
LDL	StemCell Tech	02698	40 μg/mL

Table A.2: Details of reagents utilised for human megakaryocyte differentiation.

Reagent	Supplier	Catalogue
StemFlex	STEMCELL Technologies	A3349401
RevitaCell	Life Technologies	A2644501
APEL2	STEMCELL Technologies	05275
hBMP-4	Peprotech	120-05-100uG
hVGEF-A	Peprotech	100-20-100uG
hFGF-2	Peprotech	100-18B-100uG
hFLT3-Ligand	Peprotech	300-19-100uG
hSCF	Peprotech	300-07-100uG
hTPO	Peprotech	300-18-100uG
hIL-3	Peprotech	200-03-100uG
hIL-6	Peprotech	200-06-100uG
Chemically Defined Lipids	ThermoFisher Scientific	11905021

Table A.3: Reagents used for iPSC-derived MK differentiation.

Target	Target Sp	Conjugate	Supplier	Catalogue	Dilution
CD41	Mouse	AF700	BioLegend	133926	1:50
CD42a	Mouse	FITC	Emfret	M051-1	1:50
CD41a	Human	PE-Cy7	BioLegend	303718	1:100
CD42b	Human	AF647	BioLegend	303923	1:100
CD34	Human	APC-eF780	BioLegend	303704	1:150
γH2AX (pS139)	Human/Mouse	AF488	BD Biosciences	560445	1:100
Lineage	Human	FITC	BioLegend	348801	1:50
DAPI	-	-	Life Tech	D3571	1:50,000
Hoechst 33342	-	-	Life Tech	H3570	1:1000
PI	-	-	Merck	P4864-10ML	1:200

Table A.4: Details of flow cytometry reagents.

Guide Name	Sequence
i7	5′-CAAGCAGAAGACGGCATACGAGAT**XXXXXXXX**GTCTCGTGGGCTCGG-3′
i5	5′-AATGATACGGCGACCACCGAGATCTACAC**XXXXXXXX**TCGTCGGCAGCGTC-3′

Table A.5: i7 and i5 primer sequences. XXXXXXXX denotes the 8 base pair dual barcode sequences in the primers.

Reagent	Concentration	Supplier	Catalogue
PEG 8000	0.05	Sigma-Aldrich	P1458-25ML
Triton X-100	0.001	Sigma-Aldrich	T8787-50ML
RNAse Inhibitor	0.5 U/µL	TakaraBio	#2313A
OligodT30VN	0.5 µM	IDT	-
dNTPs	0.5 mM/ea	ThermoFisher	R0182
Nuclease Free Water	-	ThermoFisher	AM9935

Table A.6: Lysis Buffer reagents used for SmartSeq-3 protocol.

Reagent	Concentration	Supplier	Catalogue
Tris-HCl pH 8.3	25 mM	Sigma-Aldrich	T6791-100G
NaCl	30 mM	Invitrogen	AM9760G
$MgCl_2$	2.5 mM	Invitrogen	AM9530G
GTP	1 mM	ThermoFisher	R1461
DTT	8 mM	ThermoFisher	707265ML
RNase Inhibitor	0.5 U/µL	TakaraBio	#2313A
TSO	2 µM	IDT	-
Max H-min RT enzyme	2 U/µL	ThermoFisher	EP0751
Nuclease Free Water	-	ThermoFisher	AM9935

Table A.7: Retro-transcription reagents used for SmartSeq-3 protocol.

Reagent	Concentration	Supplier	Catalogue
Kapa HiFi HotStart buffer (5X)	1X	Roche	KK2502
dNTPs	0.3 mM/ea	ThermoFisher	R0182
$MgCl_2$	0.5 mM	Invitrogen	AM9530G
Fwd Primer	0.5 µM	IDT	-
Rev Primer	0.1 µM	IDT	-
Polymerase	0.02 U/µl	Roche	KK2502
Nuclease Free Water	-	ThermoFisher	AM9935

Table A.8: cDNA PCR reagents used for SmartSeq-3 protocol.

Reagent	Concentration	Supplier	Catalogue
Tris-HCl pH 7.5	10 mM	ThermoFisher	15567027
$MgCl_2$	5 mM	Invitrogen	AM9530G
Dimethylformamide	0.05	Merck	D4551-250ML
ATM Solution (Tn5)	0.2 µL/rx	Illumina	FC-131-1096
Nuclease Free Water	-	ThermoFisher	AM9935

Table A.9: Tagmentation reagents used for SmartSeq-3 protocol.

Reagent	Concentration	Supplier	Catalogue
Phusion HF buffer (5X)	1X	ThermoFisher	F530L
dNTPs	0.3 mM/ea	ThermoFisher	R0182
Phusion HF	0.01 U/µL	ThermoFisher	F530L
Tween-20	0.00025	Merck	P9416-50ML
i7/i5 Primer Mix	0.05 µM/ea	IDT	-
Nuclease Free Water	-	ThermoFisher	AM9935

Table A.10: Library Indexing reagents used for SmartSeq-3 protocol.

Target	Target Sp	Supplier	Catalogue	Dilution
CD41	Human/Mouse	Abcam	ab134131	1:400
γH2AX	Human/Mouse	Merck	05-636	1:400
p53	Human	Cell Signaling	#2527	1:400
ANKRD26	Human	GeneTex	GTX128255	1:500
CP110	Human	Proteintech	12780-1-AP	1:500

Table A.11: Reagents used for immunostaining experiments.

Host	Reactivity	Conjugate	Dilution	Supplier	Catalogue
Goat	Mouse	AF488	1:500	Invitrogen	A-11001
Goat	Rabbit	AF488	1:500	Invitrogen	A-11034
Goat	Mouse	AF647	1:500	Invitrogen	A-21235
Donkey	Rabbit	AF647	1:500	Invitrogen	A-31573
Goat	Rabbit	AF647	1:500	Invitrogen	A-21244

Table A.12: Secondary antibodies used for immunostaining experiments.

Reagent	Concentration	Supplier	Catalogue
Tris-HCl pH 7.5	10 mM	ThermoFisher	15567027
NaCl	10mM	Invitrogen	AM9760G
MgCl2	3mM	Invitrogen	AM9530G
Tween-20	0.1%	Merck	P9416-50ML
IPEGAL CA-630	0.1%	Merck	I8896-50ML
Digitonin	0.01%	Promega	G9441
BSA	1%	Miltenyi	130-091-376
Nuclease Free Water	-	ThermoFisher	AM9935

Table A.13: Nuclei isolation buffer reagents for scDNAseq.

Reagent	Concentration	Supplier	Catalogue
Tris-HCl pH 7.5	10 mM	ThermoFisher	15567027
NaCl	10mM	Invitrogen	AM9760G
MgCl2	3mM	Invitrogen	AM9530G
Tween-20	0.1%	Merck	P9416-50ML
BSA	1%	Miltenyi	130-091-376
Nuclease Free Water	-	ThermoFisher	AM9935

Table A.14: Nuclei wash buffer reagents for scDNAseq.

Reagent	Concentration	Supplier	Catalogue
Tris-HCl pH 8.3	30 mM	Sigma-Aldrich	T6791-100G
Triton X-100	0.5%	Sigma-Aldrich	T8787-50ML
Tween-20	5%	Merck	P9416-50ML
Protease	0.136 AU/mL	Qiagen	19157
Nuclease Free Water	-	ThermoFisher	AM9935

Table A.15: Nuclei lysis buffer reagents for scDNAseq.

Reagent	Concentration	Supplier	Catalogue
K HiFi HotStart buffer (5X)	1X	Roche	KK2502
dNTPs	0.3 mM/ea	Sigma-Aldrich	T8787-50ML
$MgCl_2$	0.5 mM	Invitrogen	AM9530G
Primers	1.11 μM	IDT	-
Polymerase	0.02 U/μL	Qiagen	19157
Nuclease Free Water	-	ThermoFisher	AM9935

Table A.16: PCR reagents for scDNAseq.

Gene Set Name	Genes
p53 Targets	CDKN1A, SFN, RPRM, GADD45A, GADD45B, GADD45G, GTSE1, ZNF385A, FAS, PIDD1, BAX, SIVA1, EI24, SHISA5, PERP, ZMAT3, SIAH1, AIFM2, IGFBP3, SERPINE1, ADGRB1, CD82, THBS1, SERPINB5, DDB2, RRMB2, SESN1, SESN2, SESN3, PTEN, RSC2, STEAP3, MDM2, COP1, RCHY1, CCNG1, CCNG2, PPM1D, TP73

Table A.17: Manually curated gene sets.

Patient ID	Use	Genotype
ANKRD26-1	scRNAseq	c.-126T>C
ANKRD26-2	scRNAseq	c.-126T>C
ANKRD26-3	Immunohistochemistry	c.-126T>C
ANKRD26-4	Immunohistochemistry	c.-125T>C
ANKRD26-5	Immunohistochemistry	c.-119C>G
ANKRD26-6	Immunohistochemistry	WAC-ANKRD26

Table A.18: Information of ANKRD26 patient samples used.

References

[1] Kellie R. Machlus and Joseph E. Italiano. *The incredible journey: From megakaryocyte development to platelet formation*. 2013. DOI: 10.1083/jcb.201304054.

[2] Chris S. Vink, Samanta A. Mariani and Elaine Dzierzak. *Embryonic Origins of the Hematopoietic System: Hierarchies and Heterogeneity*. 2022. DOI: 10.1097/HS9.0000000000000737.

[3] Stuart H. Orkin and Leonard I. Zon. *Hematopoiesis: An Evolving Paradigm for Stem Cell Biology*. 2008. DOI: 10.1016/j.cell.2008.01.025.

[4] Ryan Mack et al. *The Fetal-to-Adult Hematopoietic Stem Cell Transition and its Role in Childhood Hematopoietic Malignancies*. 2021. DOI: 10.1007/s12015-021-10230-x.

[5] Patricia Davenport, Zhi Jian Liu and Martha Sola-Visner. 'Fetal vs adult megakaryopoiesis'. In: *Blood* 139.22 (2022). DOI: 10.1182/blood.2020009301.

[6] Hongtao Wang et al. 'Decoding Human Megakaryocyte Development'. In: *Cell Stem Cell* 28.3 (2021). DOI: 10.1016/j.stem.2020.11.006.

[7] Faiyaz Notta et al. 'Distinct routes of lineage development reshape the human blood hierarchy across ontogeny'. In: *Science* 351.6269 (2016). DOI: 10.1126/science.aab2116.

[8] Zhi Jian Liu et al. 'Developmental differences in megakaryocytopoiesis are associated with up-regulated TPO signaling through mTOR and elevated GATA-1 levels in neonatal megakaryocytes'. In: *Blood* 117.15 (2011). DOI: 10.1182/blood-2010-07-293092.

[9] O. Bluteau et al. 'Developmental changes in human megakaryopoiesis'. In: *Journal of Thrombosis and Haemostasis* 11.9 (2013). DOI: 10.1111/jth.12326.

[10] Gianfranco Mattia et al. 'Different ploidy levels of megakaryocytes generated from peripheral or cord blood CD34+ cells are correlated with different levels of platelet release'. In: *Blood* 99.3 (2002). DOI: 10.1182/blood.V99.3.888.

[11] Sam Watcham, Iwo Kucinski and Berthold Gottgens. *New insights into hematopoietic differentiation landscapes from single-cell RNA sequencing*. 2019. DOI: 10.1182/blood-2018-08-835355.

[12] Lars Velten et al. 'Human haematopoietic stem cell lineage commitment is a continuous process'. In: *Nature Cell Biology* 19.4 (2017). DOI: 10.1038/ncb3493.

[13] Bethan Psaila and Adam J Mead. *Single-cell approaches reveal novel cellular pathways for megakaryocyte and erythroid differentiation*. Tech. rep. 2019.

[14] Jörgen Adolfsson et al. 'Identification of Flt3+ Lympho-Myeloid Stem Cells Lacking Erythro-Megakaryocytic Potential: A Revised Road Map for Adult Blood Lineage Commitment'. In: *Cell* 121.2 (Apr. 2005), pp. 295–306. DOI: 10.1016/j.cell.2005.02.013.

[15] Joana Carrelha et al. 'Hierarchically related lineage-restricted fates of multipotent haematopoietic stem cells'. In: *Nature* 554.7690 (2018). DOI: 10.1038/nature25455.

[16] Jianlong Sun et al. 'Clonal dynamics of native haematopoiesis'. In: *Nature* 514.7522 (2014). DOI: 10.1038/nature13824.

[17] Alejo E. Rodriguez-Fraticelli et al. 'Clonal analysis of lineage fate in native haematopoiesis'. In: *Nature* 553.7687 (2018). DOI: 10.1038/nature25168.

[18] Leif S. Ludwig et al. 'Lineage Tracing in Humans Enabled by Mitochondrial Mutations and Single-Cell Genomics'. In: *Cell* 176.6 (2019). DOI: 10.1016/j.cell.2019.01.022.

[19] Chen Weng et al. 'Deciphering cell states and genealogies of human haematopoiesis'. In: *Nature* 627.8003 (2024), pp. 389–398. DOI: 10.1038/s41586-024-07066-z.

[20] Michael Scherer et al. 'Clonal tracing with somatic epimutations reveals dynamics of blood ageing'. In: *Nature* 643.8071 (2025), pp. 478–487. DOI: 10.1038/s41586-025-09041-8.

[21] Jonathan A Furniss, Nathalie Tarassova and Alastair W Poole. *Platelet generation in vivo and in vitro*. Tech. rep.

[22] Joseph E Italiano. 'Megakaryopoiesis and Platelet Biogenesis'. In: *Molecular and Cellular Biology of Platelet Formation: Implications in Health and Disease*. Ed. by Harald Schulze and Joseph Italiano. Cham: Springer International Publishing, 2016, pp. 3–22. DOI: 10.1007/978-3-319-39562-3{_}1.

[23] Shen Y Heazlewood et al. 'High ploidy large cytoplasmic megakaryocytes are hematopoietic stem cells regulators and essential for platelet production'. In: *Nature Communications* 14.1 (2023), p. 2099. DOI: 10.1038/s41467-023-37780-7.

[24] Tobias Junt et al. 'Dynamic Visualization of Thrombopoiesis Within Bone Marrow'. In: *Science* 317.5845 (Sept. 2007), pp. 1767–1770. DOI: 10.1126/science.1146304.

[25] Goro Kosaki. 'Platelet production by megakaryocytes: protoplatelet theory justifies cytoplasmic fragmentation model'. In: *International Journal of Hematology* 88.3 (2008), pp. 255–267. DOI: 10.1007/s12185-008-0147-7.

[26] Satoshi Nishimura et al. 'IL-1α induces thrombopoiesis through megakaryocyte rupture in response to acute platelet needs'. In: *Journal of Cell Biology* 209.3 (2015). DOI: 10.1083/jcb.201410052.

[27] Kathryn S. Potts et al. 'Membrane budding is a major mechanism of in vivo platelet biogenesis'. In: *Journal of Experimental Medicine* 217.9 (2020). DOI: 10.1084/JEM.20191206.

[28] Joseph E. Italiano et al. *Microvesicles, but not platelets, bud off from mouse bone marrow megakaryocytes*. 2021. DOI: 10.1182/blood.2021012496.

[29] Marc L. Ellis et al. *Megakaryocyte buds are distinct from microvesicles and likely to represent platelet precursors*. 2023. DOI: 10.1182/bloodadvances.2022008850.

[30] Erinke van Grinsven and Irina A Udalova. 'You reap what you sow: Neutrophils plucking platelets harvest prothrombotic effects'. In: *Immunity* 55.12 (Dec. 2022), pp. 2217–2219. DOI: 10.1016/j.immuni.2022.11.012.

[31] Tobias Petzold et al. 'Neutrophil plucking on megakaryocytes drives platelet production and boosts cardiovascular disease'. In: *Immunity* 55.12 (Dec. 2022), pp. 2285–2299. DOI: 10.1016/j.immuni.2022.10.001.

[32] Alison C. Livada, Daphne N. Pariser and Craig N. Morrell. 'Megakaryocytes in the lung: History and future perspectives'. In: *Research and Practice in Thrombosis and Haemostasis* 7.2 (2023). DOI: 10.1016/j.rpth.2023.100053.

[33] Emma Lefrançais et al. 'The lung is a site of platelet biogenesis and a reservoir for haematopoietic progenitors'. In: *Nature* 544.7648 (2017). DOI: 10.1038/nature21706.

[34] Nathan L. Asquith et al. 'The bone marrow is the primary site of thrombopoiesis'. In: *Blood* 143.3 (2024). DOI: 10.1182/blood.2023020895.

[35] Karen Guo, Kellie R Machlus and Virginia Camacho. 'The many faces of the megakaryocytes and their biological implications'. In: *Current Opinion in Hematology* 31.1 (2024).

[36] Ayako Nakamura-Ishizu et al. 'Megakaryocytes are essential for HSC quiescence through the production of thrombopoietin'. In: *Biochemical and Biophysical Research Communications* 454.2 (2014), pp. 353–357. DOI: https://doi.org/10.1016/j.bbrc.2014.10.095.

[37] Pierre Cunin and Peter A Nigrovic. 'Megakaryocytes as immune cells'. In: *Journal of Leukocyte Biology* 105.6 (June 2019), pp. 1111–1121. DOI: 10.1002/JLB.MR0718-261RR.

[38] Ingmar Bruns et al. 'Megakaryocytes regulate hematopoietic stem cell quiescence through CXCL4 secretion'. In: *Nature Medicine* 20.11 (2014), pp. 1315–1320. DOI: 10.1038/nm.3707.

[39] Meng Zhao et al. 'Megakaryocytes maintain homeostatic quiescence and promote post-injury regeneration of hematopoietic stem cells'. In: *Nature Medicine* 20.11 (2014), pp. 1321–1326. DOI: 10.1038/nm.3706.

[40] Shen Y Heazlewood et al. 'Megakaryocytes co-localise with hemopoietic stem cells and release cytokines that up-regulate stem cell proliferation'. In: *Stem Cell Research* 11.2 (2013), pp. 782–792. DOI: https://doi.org/10.1016/j.scr.2013.05.007.

[41] Shu Sun et al. 'Single-cell analysis of ploidy and the transcriptome reveals functional and spatial divergency in murine megakaryopoiesis'. In: *Blood* 138.14 (2021). DOI: 10.1182/blood.2021010697.

[42] Anthony K. Yeung et al. 'Lung megakaryocytes display distinct transcriptional and phenotypic properties'. In: *Blood Advances* 4.24 (2020). DOI: 10.1182/bloodadvances.2020002843.

[43] Daphne N. Pariser et al. 'Lung megakaryocytes are immune modulatory cells'. In: *Journal of Clinical Investigation* 131.1 (2021). DOI: 10.1172/JCI137377.

[44] William Vainchenker and Hana Raslova. 'The megakaryocyte: a cell with 3 faces as a mythic god?' In: *Blood* 138.14 (Oct. 2021), pp. 1199–1200. DOI: 10.1182/BLOOD.2021012760.

[45] Marc A. Vittoria, Ryan J. Quinton and Neil J. Ganem. *Whole-genome doubling in tissues and tumors*. Dec. 2023. DOI: 10.1016/j.tig.2023.08.004.

[46] Romain Donne et al. 'Polyploidy in liver development, homeostasis and disease'. In: *Nature Reviews Gastroenterology & Hepatology 2020 17:7* 17.7 (Apr. 2020), pp. 391–405. DOI: 10.1038/s41575-020-0284-x.

[47] Nicolas G. Brukman et al. *How cells fuse*. 2019. DOI: 10.1083/jcb.201901017.

[48] George Vassilopoulos, Pei Rong Wang and David W. Russell. 'Transplanted bone marrow regenerates liver by cell fusion'. In: *Nature* 422.6934 (2003). DOI: 10.1038/nature01539.

[49] Manuel Alvarez-Dolado et al. 'Fusion of bone-marrow-derived cells with Purkinje neurons, cardiomyocytes and hepatocytes'. In: *Nature* 425.6961 (2003), pp. 968–973. DOI: 10.1038/nature02069.

[50] Frederic Lluis and Maria Pia Cosma. *Cell-fusion-mediated somatic-cell reprogramming: A mechanism for tissue regeneration*. 2010. DOI: 10.1002/jcp.22003.

[51] Zhiqiang Shu, Sarayu Row and Wu Min Deng. *Endoreplication: The Good, the Bad, and the Ugly*. 2018. DOI: 10.1016/j.tcb.2018.02.006.

[52] Zakir Ullah et al. 'Differentiation of trophoblast stem cells into giant cells is triggered by p57/Kip2 inhibition of CDK1 activity'. In: *Genes and Development* 22.21 (2008). DOI: 10.1101/gad.1718108.

[53] Hui Zi Chen et al. 'Canonical and atypical E2Fs regulate the mammalian endocycle'. In: *Nature Cell Biology* 14.11 (2012). DOI: 10.1038/ncb2595.

[54] Susanne M.A. Lens and René H. Medema. 'Cytokinesis defects and cancer'. In: *Nature Reviews Cancer 2018 19:1* 19.1 (Dec. 2018), pp. 32–45. DOI: 10.1038/s41568-018-0084-6.

[55] Stefania Mazzi et al. 'Megakaryocyte and polyploidization'. In: *Experimental Hematology* 57 (Jan. 2018), pp. 1–13. DOI: 10.1016/J.EXPHEM.2017.10.001.

[56] Séverine Celton-Morizur et al. 'The insulin/Akt pathway controls a specific cell division program that leads to generation of binucleated tetraploid liver cells in rodents'. In: *Journal of Clinical Investigation* 119.7 (2009). DOI: 10.1172/jci38677.

[57] Shusil K Pandit et al. 'E2F8 is essential for polyploidization in mammalian cells'. In: *Nature Cell Biology* 14.11 (2012), pp. 1181–1191. DOI: 10.1038/ncb2585.

[58] Tim Koopmans and Eva van Rooij. 'Molecular gatekeepers of endogenous adult mammalian cardiomyocyte proliferation'. In: *Nature Reviews Cardiology* (2025). DOI: 10.1038/s41569-025-01145-y.

[59] K. J. Gjelsvik, R. Besen-McNally and V. P. Losick. *Solving the Polyploid Mystery in Health and Disease*. 2019. DOI: 10.1016/j.tig.2018.10.005.

[60] Terry L Orr-Weaver. 'When bigger is better: the role of polyploidy in organogenesis'. In: *Trends in Genetics* 31.6 (June 2015), pp. 307–315. DOI: 10.1016/j.tig.2015.03.011.

[61] Anne C Rios et al. 'Essential role for a novel population of binucleated mammary epithelial cells in lactation'. In: *Nature Communications* 7.1 (2016), p. 11400. DOI: 10.1038/ncomms11400.

[62] Uri Ben-David and Angelika Amon. 'Context is everything: aneuploidy in cancer'. In: *Nature Reviews Genetics 2019 21:1* 21.1 (Sept. 2019), pp. 44–62. DOI: 10.1038/s41576-019-0171-x.

[63] M L Richter et al. 'Single-nucleus RNA-seq2 reveals functional crosstalk between liver zonation and ploidy'. In: *Nature Communications* 12.1 (2021), p. 4264. DOI: 10.1038/s41467-021-24543-5.

[64] Brianna R Watson et al. 'Spatial transcriptomics of healthy and fibrotic human liver at single-cell resolution'. In: *Nature Communications* 16.1 (2025), p. 319. DOI: 10.1038/s41467-024-55325-4.

[65] Tomonori Matsumoto et al. 'In Vivo Lineage Tracing of Polyploid Hepatocytes Reveals Extensive Proliferation during Liver Regeneration'. In: *Cell Stem Cell* 26.1 (Jan. 2020), pp. 34–47. DOI: 10.1016/j.stem.2019.11.014.

[66] Kristine H. Østergaard et al. 'Left ventricular morphology of the giraffe heart examined by stereological methods.' In: *Anatomical record (Hoboken, N.J. : 2007)* 296.4 (2013). DOI: 10.1002/ar.22672.

[67] Wouter Derks and Olaf Bergmann. 'Polyploidy in Cardiomyocytes'. In: *Circulation Research* 126.4 (Feb. 2020), pp. 552–565. DOI: 10.1161/CIRCRESAHA.119.315408.

[68] Rebecca Windmueller et al. 'Direct Comparison of Mononucleated and Binucleated Cardiomyocytes Reveals Molecular Mechanisms Underlying Distinct Proliferative Competencies'. In: *Cell Reports* 30.9 (2020). DOI: 10.1016/j.celrep.2020.02.034.

[69] Michail Yekelchyk et al. 'Mono- and multi-nucleated ventricular cardiomyocytes constitute a transcriptionally homogenous cell population'. In: *Basic Research in Cardiology* 114.5 (2019). DOI: 10.1007/s00395-019-0744-z.

[70] H. W. Vliegen et al. 'Polyploidy of myocyte nuclei in pressure overloaded human hearts: a flow cytometric study in left and right ventricular myocardium.' In: *The American journal of cardiovascular pathology* 5.1 (1995).

[71] Patricia Cabeza Meckert et al. 'Endomitosis and polyploidization of myocardial cells in the periphery of human acute myocardial infarction'. In: *Cardiovascular Research* 67.1 (2005). DOI: 10.1016/j.cardiores.2005.02.017.

[72] Joe Kodama and Takashi Kaito. 'Osteoclast Multinucleation: Review of Current Literature'. In: *International Journal of Molecular Sciences* 21.16 (2020). DOI: 10.3390/ijms21165685.

[73] Kent Søe. 'Osteoclast Fusion: Physiological Regulation of Multinucleation through Heterogeneity—Potential Implications for Drug Sensitivity'. In: *International Journal of Molecular Sciences* 21.20 (2020). DOI: 10.3390/ijms21207717.

[74] Jarred M Whitlock et al. 'Cell surface-bound La protein regulates the cell fusion stage of osteoclastogenesis'. In: *Nature Communications* 14.1 (2023), p. 616. DOI: 10.1038/s41467-023-36168-x.

[75] Ryotaro Iwasaki et al. 'Cell fusion in osteoclasts plays a critical role in controlling bone mass and osteoblastic activity'. In: *Biochemical and Biophysical Research Communications* 377.3 (2008). DOI: 10.1016/j.bbrc.2008.10.076.

[76] Nora G Peterson and Donald T Fox. 'Communal living: the role of polyploidy and syncytia in tissue biology'. In: *Chromosome Research* 29.3 (2021), pp. 245–260. DOI: 10.1007/s10577-021-09664-3.

[77] Natacha Vitrat et al. 'Endomitosis of human megakaryocytes are due to abortive mitosis'. In: *Blood* 91.10 (1998). DOI: 10.1182/blood.v91.10.3711.

[78] Amy E Geddis et al. 'Cell Cycle Endomitotic Megakaryocytes that Form a Bipolar Spindle Exhibit Cleavage Furrow Ingression Followed by Furrow Regression'. In: *Cell Cycle* 6 (2007), pp. 455–460. DOI: 10.4161/cc.6.4.3836.

[79] Larissa Lordier et al. 'Megakaryocyte endomitosis is a failure of late cytokinesis related to defects in the contractile ring and Rho/Rock signaling'. In: *Blood* 112.8 (2008). DOI: 10.1182/blood-2008-03-144956.

[80] Nicholas Papadantonakis et al. 'Direct visualization of the endomitotic cell cycle in living megakaryocytes: Differential patterns in low and high ploidy cells'. In: *Cell Cycle* 7.15 (2008). DOI: 10.4161/cc.6325.

[81] Larissa Lordier et al. 'Presence of a defect in karyokinesis during megakaryocyte endomitosis'. In: *Cell Cycle* 11.23 (2012). DOI: 10.4161/cc.22712.

[82] S Gemble et al. 'Mitotic slippage causes nuclear instability in polyploid cells'. In: *bioRxiv* (Jan. 2025), p. 2025.07.21.665898. DOI: 10.1101/2025.07.21.665898.

[83] Marianna Trakala et al. 'Functional Reprogramming of Polyploidization in Megakaryocytes'. In: *Developmental Cell* 32.2 (2015). DOI: 10.1016/j.devcel.2014.12.015.

[84] Yuan Gao et al. 'Role of RhoA-Specific Guanine Exchange Factors in Regulation of Endomitosis in Megakaryocytes'. In: *Developmental Cell* 22.3 (2012). DOI: 10.1016/j.devcel.2011.12.019.

[85] Larissa Lordier et al. 'RUNX1-induced silencing of non-muscle myosin heavy chain IIB contributes to megakaryocyte polyploidization'. In: (2012). DOI: 10.1038/ncomms1704.

[86] Benjamin L. Ebert et al. 'Identification of RPS14 as a 5q- syndrome gene by RNA interference screen'. In: *Nature* 451.7176 (2008). DOI: 10.1038/nature06494.

[87] Rebekka K. Schneider et al. 'Role of casein kinase 1A1 in the biology and targeted therapy of del(5q) MDS'. In: *Cancer Cell* 26.4 (2014). DOI: 10.1016/j.ccr.2014.08.001.

[88] Maureen McNulty and John D. Crispino. 'Acute megakaryocytic leukemia'. In: *Cold Spring Harbor Perspectives in Medicine* 10.2 (2020). DOI: 10.1101/cshperspect.a034884.

[89] Valentina Fabiola Ilenia Sangiorgio et al. 'GATA1 downregulation in prefibrotic and fibrotic stages of primary myelofibrosis and in the myelofibrotic progression of other myeloproliferative neoplasms'. In: *Leukemia Research* 100 (2021). DOI: 10.1016/j.leukres.2020.106495.

[90] Laure Gilles et al. 'Downregulation of GATA1 drives impaired hematopoiesis in primary myelofibrosis'. In: *Journal of Clinical Investigation* 127.4 (2017). DOI: 10.1172/JCI82905.

[91] M. R. Tijssen and C. Ghevaert. *Transcription factors in late megakaryopoiesis and related platelet disorders*. 2013. DOI: 10.1111/jth.12131.

[92] Takeshi Fujiwara et al. 'Cytokinesis failure generating tetraploids promotes tumorigenesis in p53-null cells'. In: *Nature* 437.7061 (2005). DOI: 10.1038/nature04217.

[93] Teresa Davoli and Titia de Lange. 'Telomere-Driven Tetraploidization Occurs in Human Cells Undergoing Crisis and Promotes Transformation of Mouse Cells'. In: *Cancer Cell* 21.6 (2012). DOI: 10.1016/j.ccr.2012.03.044.

[94] Yosuke Ichijima et al. 'DNA lesions induced by replication stress trigger mitotic aberration and tetraploidy development'. In: *PLoS ONE* 5.1 (2010). DOI: 10.1371/journal.pone.0008821.

[95] Daniela A. Brito and Conly L. Rieder. 'Mitotic Checkpoint Slippage in Humans Occurs via Cyclin B Destruction in the Presence of an Active Checkpoint'. In: *Current Biology* 16.12 (2006). DOI: 10.1016/j.cub.2006.04.043.

[96] Revati Darp et al. 'Oncogenic BRAF induces whole-genome doubling through suppression of cytokinesis'. In: *Nature Communications* 13.1 (2022). DOI: 10.1038/s41467-022-31899-9.

[97] Andreas Panagopoulos et al. 'Multigenerational cell tracking of DNA replication and heritable DNA damage'. In: *Nature* 642.8068 (2025), pp. 785–795. DOI: 10.1038/s41586-025-08986-0.

[98] Dominik M. Duelli et al. 'A Virus Causes Cancer by Inducing Massive Chromosomal Instability through Cell Fusion'. In: *Current Biology* 17.5 (2007). DOI: 10.1016/j.cub.2007.01.049.

[99] Scott L Carter et al. 'Absolute quantification of somatic DNA alterations in human cancer'. In: *Nature Biotechnology* 30.5 (2012), pp. 413–421. DOI: 10.1038/nbt.2203.

[100] Craig M. Bielski et al. 'Genome doubling shapes the evolution and prognosis of advanced cancers'. In: *Nature Genetics* 50.8 (2018). DOI: 10.1038/s41588-018-0165-1.

[101] Travis I Zack et al. 'Pan-cancer patterns of somatic copy number alteration'. In: *Nature Genetics* 45.10 (2013), pp. 1134–1140. DOI: 10.1038/ng.2760.

[102] Sally M. Dewhurst et al. 'Tolerance of whole- genome doubling propagates chromosomal instability and accelerates cancer genome evolution'. In: *Cancer Discovery* 4.2 (2014). DOI: 10.1158/2159-8290.CD-13-0285.

[103] Peter Priestley et al. 'Pan-cancer whole-genome analyses of metastatic solid tumours'. In: *Nature* 575.7781 (2019). DOI: 10.1038/s41586-019-1689-y.

[104] Samuel F Bakhoum et al. 'Chromosomal instability drives metastasis through a cytosolic DNA response'. In: *Nature* 553.7689 (2018), pp. 467–472. DOI: 10.1038/nature25432.

[105] Susana A. Godinho et al. 'Oncogene-like induction of cellular invasion from centrosome amplification'. In: *Nature* 510.7503 (2014). DOI: 10.1038/nature13277.

[106] G. Yahya et al. 'Sublinear scaling of the cellular proteome with ploidy'. In: *Nature Communications* 13.1 (2022). DOI: 10.1038/s41467-022-33904-7.

[107] Klaske M. Schukken and Jason M. Sheltzer. 'Extensive protein dosage compensation in aneuploid human cancers'. In: *Genome research* 32.7 (2022). DOI: 10.1101/gr.276378.121.

[108] Ryan J Quinton et al. 'Whole-genome doubling confers unique genetic vulnerabilities on tumour cells'. In: *Nature* 590.7846 (2021), pp. 492–497. DOI: 10.1038/s41586-020-03133-3.

[109] Neil J. Ganem, Susana A. Godinho and David Pellman. 'A mechanism linking extra centrosomes to chromosomal instability'. In: *Nature* 460.7252 (2009). DOI: 10.1038/nature08136.

[110] Kavya Prasad et al. 'Whole-Genome Duplication Shapes the Aneuploidy Landscape of Human Cancers'. In: *Cancer Research* 82.9 (2022). DOI: 10.1158/0008-5472.CAN-21-2065.

[111] Simon Gemble et al. 'Genetic instability from a single S phase after whole-genome duplication'. In: *Nature* 604 (2022). DOI: 10.1038/s41586-022-04578-4.

[112] Maddalena Nano et al. 'Cell-Cycle Asynchrony Generates DNA Damage at Mitotic Entry in Polyploid Cells'. In: *Current Biology* 29.22 (2019). DOI: 10.1016/j.cub.2019.09.041.

[113] Simon Gemble and Renata Basto. 'CHRONOCRISIS: When Cell Cycle Asynchrony Generates DNA Damage in Polyploid Cells'. In: *BioEssays* 42.10 (2020). DOI: 10.1002/bies.202000105.

[114] Ruxandra A. Lambuta et al. 'Whole-genome doubling drives oncogenic loss of chromatin segregation'. In: *Nature* 615.7954 (2023). DOI: 10.1038/s41586-023-05794-2.

[115] Lauren T Evans et al. 'ANKRD26 recruits PIDD1 to centriolar distal appendages to activate the PIDDosome following centrosome amplification'. In: *The EMBO Journal* 40.4 (2021). DOI: 10.15252/embj.2020105106.

[116] Laura Senovilla et al. 'An immunosurveillance mechanism controls cancer cell ploidy'. In: *Science* 337.6102 (2012). DOI: 10.1126/science.1224922.

[117] Neil J. Ganem et al. 'Cytokinesis failure triggers hippo tumor suppressor pathway activation'. In: *Cell* 158.4 (2014). DOI: 10.1016/j.cell.2014.06.029.

[118] Luca L. Fava et al. 'The PIDDosome activates p53 in response to supernumerary centrosomes'. In: *Genes and Development* 31.1 (2017). DOI: 10.1101/gad.289728.116.

[119] Matteo Burigotto et al. 'Centriolar distal appendages activate the centrosome-PIDDosome-p53 signalling axis via ANKRD26'. In: *The EMBO Journal* 40.4 (2021). DOI: 10.15252/embj.2020104844.

[120] Gavin D. Grant et al. 'Accurate delineation of cell cycle phase transitions in living cells with PIP-FUCCI'. In: *Cell Cycle* 17.21-22 (Nov. 2018), pp. 2496–2516. DOI: 10.1080/15384101.2018.1547001.

[121] Sara Vanessa Bernhard et al. 'Experimental Approaches to Generate and Isolate Human Tetraploid Cells'. In: *Polyploidy: Methods and Protocols*. Springer Nature, 2023. Chap. 20, pp. 391–399. DOI: 10.1007/978-1-0716-2561-3{_}20.

[122] Markus Spindler et al. 'Rapid isolation of mature murine primary megakaryocytes by size exclusion via filtration'. In: *Platelets* 34.1 (2023). DOI: 10.1080/09537104.2023.2192289.

[123] Abdullah O. Khan et al. 'Post-translational polymodification of β1-tubulin regulates motor protein localization in platelet production and function'. In: *Haematologica* 107.1 (Dec. 2020), pp. 243–259. DOI: 10.3324/haematol.2020.270793.

[124] Camélia Benlabiod et al. 'Calreticulin del52 and ins5 knock-in mice recapitulate different myeloproliferative phenotypes observed in patients with MPN'. In: *Nature Communications* 11.1 (Sept. 2020), p. 4886. DOI: 10.1038/s41467-020-18691-3.

[125] Johannes Schindelin et al. 'Fiji: an open-source platform for biological-image analysis'. In: *Nature Methods* 9.7 (July 2012), pp. 676–682. DOI: 10.1038/nmeth.2019.

[126] Michael Hagemann-Jensen et al. 'Single-cell RNA counting at allele and isoform resolution using Smart-seq3'. In: *Nature Biotechnology* 38.6 (2020). DOI: 10.1038/s41587-020-0497-0.

[127] Michael Hagemann-Jensen et al. *Smart-seq3 Protocol v3*. Feb. 2020. DOI: 10.17504/protocols.io.bcq4ivyw.

[128] Wei Xu et al. 'A plate-based single-cell ATAC-seq workflow for fast and robust profiling of chromatin accessibility'. In: *Nature Protocols* (). DOI: 10.1038/s41596-021-00583-5.

[129] Darlan C. Minussi et al. 'Breast tumours maintain a reservoir of subclonal diversity during expansion'. In: *Nature* 592.7853 (2021). DOI: 10.1038/s41586-021-03357-x.

[130] Swati Parekh et al. 'zUMIs - A fast and flexible pipeline to process RNA sequencing data with UMIs'. In: *GigaScience* 7.6 (June 2018). DOI: 10.1093/gigascience/giy059.

[131] Yuhan Hao et al. 'Dictionary learning for integrative, multimodal and scalable single-cell analysis'. In: *Nature Biotechnology* 42.2 (Feb. 2024), pp. 293–304. DOI: 10.1038/s41587-023-01767-y.

[132] Yuhan Hao et al. 'Integrated analysis of multimodal single-cell data'. In: *Cell* 184.13 (2021). DOI: 10.1016/j.cell.2021.04.048.

[133] Lukas Heumos et al. 'Best practices for single-cell analysis across modalities'. In: *Nature Reviews Genetics* 24.8 (2023). DOI: 10.1038/s41576-023-00586-w.

[134] Saket Choudhary and Rahul Satija. 'Comparison and evaluation of statistical error models for scRNA-seq'. In: *Genome Biology* 23.1 (Jan. 2022), p. 27. DOI: 10.1186/s13059-021-02584-9.

[135] Ilya Korsunsky et al. 'Fast, sensitive and accurate integration of single-cell data with Harmony'. In: *Nature Methods* 16.12 (Dec. 2019), pp. 1289–1296. DOI: 10.1038/s41592-019-0619-0.

[136] Etienne Becht et al. 'Dimensionality reduction for visualizing single-cell data using UMAP'. In: *Nature Biotechnology* 37.1 (Jan. 2019), pp. 38–44. DOI: 10.1038/nbt.4314.

[137] Shijie C Zheng et al. 'Universal prediction of cell-cycle position using transfer learning'. In: *Genome Biology* 23.1 (2022), p. 41. DOI: 10.1186/s13059-021-02581-y.

[138] Arthur Liberzon et al. 'The Molecular Signatures Database Hallmark Gene Set Collection'. In: *Cell Systems* 1.6 (Dec. 2015), pp. 417–425. DOI: 10.1016/j.cels.2015.12.004.

[139] Minoru Kanehisa et al. 'KEGG: biological systems database as a model of the real world'. In: *Nucleic Acids Research* 53.D1 (Jan. 2025), pp. D672–D677. DOI: 10.1093/nar/gkae909.

[140] Dominik Saul et al. 'A new gene set identifies senescent cells and predicts senescence-associated pathways across tissues'. In: *Nature Communications* 13.1 (Aug. 2022), p. 4827. DOI: 10.1038/s41467-022-32552-1.

[141] Junyue Cao et al. 'The single-cell transcriptional landscape of mammalian organogenesis'. In: *Nature* 566.7745 (2019). DOI: 10.1038/s41586-019-0969-x.

[142] Michael I Love, Wolfgang Huber and Simon Anders. 'Moderated estimation of fold change and dispersion for RNA-seq data with DESeq2'. In: *Genome Biology* 15.12 (Dec. 2014), p. 550. DOI: 10.1186/s13059-014-0550-8.

[143] Heng Li and Richard Durbin. 'Fast and accurate long-read alignment with Burrows-Wheeler transform.' In: *Bioinformatics (Oxford, England)* 26.5 (Mar. 2010), pp. 589–95. DOI: 10.1093/bioinformatics/btp698.

[144] Heng Li et al. 'The Sequence Alignment/Map format and SAMtools'. In: *Bioinformatics* 25.16 (Aug. 2009), pp. 2078–2079. DOI: 10.1093/bioinformatics/btp352.

[145] *Picard toolkit*. 2019.

[146] Bjorn Bakker et al. 'Single-cell sequencing reveals karyotype heterogeneity in murine and human malignancies'. In: *Genome Biology* 17.1 (Dec. 2016), p. 115. DOI: 10.1186/s13059-016-0971-7.

[147] Broad. *DepMap Public 24Q3*. 2024.

[148] Bruce Wang et al. 'Self-renewing diploid Axin2 + cells fuel homeostatic renewal of the liver'. In: *Nature* 524.7564 (2015). DOI: 10.1038/nature14863.

[149] Andrew W Duncan et al. 'The ploidy conveyor of mature hepatocytes as a source of genetic variation'. In: *Nature* 467.7316 (2010), pp. 707–710. DOI: 10.1038/nature09414.

[150] Kristin A Knouse et al. 'Single cell sequencing reveals low levels of aneuploidy across mammalian tissues'. In: *Proceedings of the National Academy of Sciences* 111.37 (Sept. 2014), pp. 13409–13414. DOI: 10.1073/pnas.1415287111.

[151] Patrick D Wilkinson et al. 'Polyploid Hepatocytes Facilitate Adaptation and Regeneration to Chronic Liver Injury'. In: *The American Journal of Pathology* 189.6 (June 2019), pp. 1241–1255. DOI: 10.1016/j.ajpath.2019.02.008.

[152] Kristin A. Knouse et al. 'Chromosome Segregation Fidelity in Epithelia Requires Tissue Architecture'. In: *Cell* 175.1 (2018). DOI: 10.1016/j.cell.2018.07.042.

[153] Roberta L. Hannibal et al. 'Copy Number Variation Is a Fundamental Aspect of the Placental Genome'. In: *PLoS Genetics* 10.5 (2014). DOI: 10.1371/journal.pgen.1004290.

[154] Roberta L. Hannibal and Julie C. Baker. 'Selective Amplification of the Genome Surrounding Key Placental Genes in Trophoblast Giant Cells'. In: *Current Biology* 26.2 (2016). DOI: 10.1016/j.cub.2015.11.060.

[155] Kazuki Hayashi et al. 'Polyploidy mitigates the impact of DNA damage while simultaneously bearing its burden'. In: *Cell Death Discovery* 10.1 (2024), p. 436. DOI: 10.1038/s41420-024-02206-w.

[156] Peiwen Fei, Eric J. Bernhard and Wafik S. El-Deiry. 'Tissue-specific induction of p53 targets in vivo'. In: *Cancer Research* 62.24 (2002).

[157] Shusil K Pandit, Bart Westendorp and Alain de Bruin. 'Physiological significance of polyploidization in mammalian cells'. In: *Trends in Cell Biology* 23.11 (2013), pp. 556–566. DOI: https://doi.org/10.1016/j.tcb.2013.06.002.

[158] Zeinab Eftekhar, Mojtaba Aghaei and Najmaldin Saki. 'DNA damage repair in megakaryopoiesis: molecular and clinical aspects'. In: *Expert Review of Hematology* 17.10 (Oct. 2024), pp. 705–712. DOI: 10.1080/17474086.2024.2391102.

[159] Lise O. Andrieux et al. 'GATA-1 is essential in EGF-mediated induction of nucleotide excision repair activity and ERCC1 expression through ERK2 in human hepatoma cells'. In: *Cancer Research* 67.5 (2007). DOI: 10.1158/0008-5472.CAN-06-3821.

[160] Chelsia Qiuxia Wang et al. 'Disruption of Runx1 and Runx3 leads to bone marrow failure and leukemia predisposition due to transcriptional and DNA repair defects'. In: *Cell Reports* 8.3 (2014). DOI: 10.1016/j.celrep.2014.06.046.

[161] Bérengère De Laval et al. 'Thrombopoietin-increased DNA-PK-dependent DNA repair limits hematopoietic stem and progenitor cell mutagenesis in response to dna damage'. In: *Cell Stem Cell* 12.1 (2013). DOI: 10.1016/j.stem.2012.10.012.

[162] Bérengère De Laval et al. 'Thrombopoietin promotes NHEJ DNA repair in hematopoietic stem cells through specific activation of Erk and NF-kB pathways and their target, IEX-1'. In: *Blood* 123.4 (2014). DOI: 10.1182/blood-2013-07-515874.

[163] Firas El-Mortada et al. 'Megakaryocytes possess a STING pathway that is transferred to platelets to potentiate activation'. In: *Life Science Alliance* 7.2 (2024). DOI: 10.26508/lsa.202302211.

[164] Joshua Moss et al. 'Megakaryocyte- and erythroblast-specific cell-free DNA patterns in plasma and platelets reflect thrombopoiesis and erythropoiesis levels'. In: *Nature Communications* 14.1 (2023). DOI: 10.1038/s41467-023-43310-2.

[165] Lauren Murphy et al. 'Platelets Sequester Extracellular DNA, Capturing Tumour-Derived and Free Fetal DNA'. In: *Blood* 142.Supplement 1 (2023). DOI: 10.1182/blood-2023-182697.

[166] Daniel Schraivogel et al. 'High-speed fluorescence image-enabled cell sorting'. In: *Science* 375.6578 (2022). DOI: 10.1126/science.abj3013.

[167] Pierre Cunin and Peter A. Nigrovic. *Megakaryocyte emperipolesis: a new frontier in cell-in-cell interaction*. 2020. DOI: 10.1080/09537104.2019.1693035.

[168] Federica Martorana et al. *Everything Comes with a Price: The Toxicity Profile of DNA-Damage Response Targeting Agents*. 2022. DOI: 10.3390/cancers14040953.

[169] Roelof H Bekendam et al. 'Induction of Moderate DNA Damage Enhances Megakaryopoiesis and Platelet Production'. In: *bioRxiv* (Jan. 2025), p. 2025.05.08.652525. DOI: 10.1101/2025.05.08.652525.

[170] Neil T. Umbreit et al. 'Mechanisms generating cancer genome complexity from a single cell division error'. In: *Science* 368.6488 (2020). DOI: 10.1126/science.aba0712.

[171] Mijung Kwon, Mitchell L. Leibowitz and Jae Ho Lee. *Small but mighty: the causes and consequences of micronucleus rupture*. 2020. DOI: 10.1038/s12276-020-00529-z.

[172] Karen Crasta et al. *DNA breaks and chromosome pulverization from errors in mitosis*. 2012. DOI: 10.1038/nature10802.

[173] Stamatis Papathanasiou et al. 'Heritable transcriptional defects from aberrations of nuclear architecture'. In: *Nature* 619.7968 (2023). DOI: 10.1038/s41586-023-06157-7.

[174] Andrew W Duncan et al. 'Aneuploidy as a mechanism for stress-induced liver adaptation'. In: *The Journal of Clinical Investigation* 122.9 (Sept. 2012), pp. 3307–3315. DOI: 10.1172/JCI64026.

[175] Peter Ly et al. 'Selective y centromere inactivation triggers chromosome shattering in micronuclei and repair by non-homologous end joining'. In: *Nature Cell Biology* 19.1 (2017). DOI: 10.1038/ncb3450.

[176] Shihao Zhang et al. 'Hippo Signaling Suppresses Cell Ploidy and Tumorigenesis through Skp2'. In: *Cancer Cell* 31.5 (2017). DOI: 10.1016/j.ccell.2017.04.004.

[177] Todd Heallen et al. 'Hippo signaling impedes adult heart regeneration'. In: *Development (Cambridge)* 140.23 (2013). DOI: 10.1242/dev.102798.

[178] Garrison Buss et al. 'Postmitotic centriole disengagement and maturation leads to centrosome amplification in polyploid trophoblast giant cells'. In: *Molecular Biology of the Cell* 33.13 (2022). DOI: 10.1091/mbc.E22-05-0182.

[179] Trishita Basak and Rupasri Ain. 'Molecular regulation of trophoblast stem cell self-renewal and giant cell differentiation by the Hippo components YAP and LATS1'. In: *Stem Cell Research and Therapy* 13.1 (2022). DOI: 10.1186/s13287-022-02844-w.

[180] V. Soloveva and D. I.H. Linzer. 'Differentiation of placental trophoblast giant cells requires downregulation of p53 and Rb'. In: *Placenta* 25.1 (2004). DOI: 10.1016/S0143-4004(03)00215-7.

[181] Anita Roy et al. 'Uncoupling of the hippo and rho pathways allows megakaryocytes to escape the tetraploid checkpoint'. In: *Haematologica* 101.12 (2016). DOI: 10.3324/haematol.2016.149914.

[182] Valentina C. Sladky and Andreas Villunger. 'Uncovering the PIDDosome and caspase-2 as regulators of organogenesis and cellular differentiation'. In: *Cell Death & Differentiation* 27.7 (July 2020), pp. 2037–2047. DOI: 10.1038/s41418-020-0556-6.

[183] Valentina C. Sladky et al. 'E2F-Family Members Engage the PIDDosome to Limit Hepatocyte Ploidy in Liver Development and Regeneration'. In: *Developmental Cell* 52.3 (2020). DOI: 10.1016/j.devcel.2019.12.016.

[184] Valentina C. Sladky et al. 'Centriole signaling restricts hepatocyte ploidy to maintain liver integrity'. In: *Genes and Development* 36.13-14 (2022). DOI: 10.1101/gad.349727.122.

[185] M Leone et al. 'The PIDDosome controls cardiomyocyte polyploidization during postnatal heart development'. In: *bioRxiv* (Jan. 2025), p. 2024.08.27.609375. DOI: 10.1101/2024.08.27.609375.

[186] Isabelle C Becker et al. 'Cell cycle–dependent centrosome clustering precedes proplatelet formation'. In: *Science Advances* 10.25 (Aug. 2024), eadl6153. DOI: 10.1126/sciadv.adl6153.

[187] Rika Miyazaki et al. 'Comparative analyses of megakaryocytes derived from cord blood and bone marrow'. In: *British Journal of Haematology* 108.3 (Mar. 2000), pp. 602–609. DOI: https://doi.org/10.1046/j.1365-2141.2000.01854.x.

[188] Zhi-Jian Liu et al. 'CDK8/19 inhibition triggers a switch from mitosis to endomitosis in cord blood megakaryocytes'. In: *British Journal of Haematology* 205.6 (Dec. 2024), pp. 2481–2486. DOI: https://doi.org/10.1111/bjh.19836.

[189] Kaelin A Akins et al. 'Runx1 is sufficient but not required for cardiomyocyte cell-cycle activation'. In: *American Journal of Physiology-Heart and Circulatory Physiology* 327.2 (June 2024), H377–H389. DOI: 10.1152/ajpheart.00782.2023.

[190] Mia J. Sullivan, Elizabeth L. Palmer and Juliana Perez Botero. *ANKRD26-Related Thrombocytopenia and Predisposition to Myeloid Neoplasms*. 2022. DOI: 10.1007/s11899-022-00666-4.

[191] Hrushikesh Vyas et al. 'Prevalence and natural history of variants in the ANKRD26 gene: a short review and update of reported cases'. In: *Platelets* 33.8 (Nov. 2022), pp. 1107–1112. DOI: 10.1080/09537104.2022.2071853.

[192] Tommaso Pippucci et al. 'Mutations in the 5-prime UTR of ANKRD26, the ankirin repeat domain 26 gene, cause an autosomal-dominant form of inherited thrombocytopenia, THC2'. In: *American Journal of Human Genetics* 88.1 (2011). DOI: 10.1016/j.ajhg.2010.12.006.

[193] Patrizia Noris et al. 'Mutations in ANKRD26 are responsible for a frequent form of inherited thrombocytopenia: Analysis of 78 patients from 21 families'. In: *Blood* 117.24 (2011). DOI: 10.1182/blood-2011-02-336537.

[194] Saad A. Al Daama et al. 'A missense mutation in ANKRD26 segregates with thrombocytopenia'. In: *Blood* 122.3 (July 2013), pp. 461–462. DOI: 10.1182/blood-2013-03-489344.

[195] Lara Wahlster et al. 'Familial thrombocytopenia due to a complex structural variant resulting in a WAC-ANKRD26 fusion transcript'. In: *Journal of Experimental Medicine* 218.6 (June 2021). DOI: 10.1084/jem.20210444.

[196] Congfei Pang et al. 'Analysis of clinical characteristics and treatment efficacy in two pediatric cases of ANKRD26 -related thrombocytopenia'. In: *Platelets* 34.1 (Dec. 2023). DOI: 10.1080/09537104.2023.2262607.

[197] Dominique Bluteau et al. 'Thrombocytopenia-associated mutations in the ANKRD26 regulatory region induce MAPK hyperactivation'. In: *The Journal of Clinical Investigation* 124.2 (Feb. 2014), pp. 580–591. DOI: 10.1172/JCI71861.

[198] Leila K. Mosavi et al. 'The ankyrin repeat as molecular architecture for protein recognition'. In: *Protein Science* 13.6 (June 2004), pp. 1435–1448. DOI: 10.1110/ps.03554604.

[199] Anna Sofie Englisch et al. 'Ankrd26 is a retinoic acid-responsive plasma membrane-binding and -shaping protein critical for proper cell differentiation'. In: *Cell Reports* 43.3 (Mar. 2024). DOI: 10.1016/j.celrep.2024.113939.

[200] Francesca Basso-Valentina et al. 'ANKRD26 is a new regulator of type I cytokine receptor signaling in normal and pathological hematopoiesis'. In: *Haematologica* 108.8 (2023). DOI: 10.3324/haematol.2022.282049.

[201] Andrew McPherson et al. 'Ongoing genome doubling shapes evolvability and immunity in ovarian cancer'. In: *Nature* (2025). DOI: 10.1038/s41586-025-09240-3.

[202] Jun Li et al. 'Non-cell-autonomous cancer progression from chromosomal instability'. In: *Nature* 620.7976 (2023), pp. 1080–1088. DOI: 10.1038/s41586-023-06464-z.

[203] Melody Di Bona and Samuel F. Bakhoum. *Micronuclei and Cancer*. 2024. DOI: 10.1158/2159-8290.CD-23-1073.

[204] Christy Hong et al. 'cGAS–STING drives the IL-6-dependent survival of chromosomally instable cancers'. In: *Nature* 607.7918 (2022), pp. 366–373. DOI: 10.1038/s41586-022-04847-2.

[205] Pani A. Apostolidis et al. 'Role of tumor suppressor p53 in megakaryopoiesis and platelet function'. In: *Experimental Hematology* 40.2 (2012). DOI: 10.1016/j.exphem.2011.10.006.

[206] Marcin Poreba et al. 'Potent and selective caspase-2 inhibitor prevents MDM-2 cleavage in reversine-treated colon cancer cells'. In: *Cell Death & Differentiation* 26.12 (Dec. 2019), pp. 2695–2709. DOI: 10.1038/s41418-019-0329-2.

[207] Saioa López et al. 'Interplay between whole-genome doubling and the accumulation of deleterious alterations in cancer evolution'. In: *Nature Genetics* 52.3 (2020). DOI: 10.1038/s41588-020-0584-7.

[208] Paul R. Andreassen et al. 'Tetraploid State Induces p53-dependent Arrest of Nontransformed Mammalian Cells in G1'. In: *Molecular Biology of the Cell* 12.5 (May 2001), pp. 1315–1328. DOI: 10.1091/mbc.12.5.1315.

[209] Timour Baslan et al. 'Ordered and deterministic cancer genome evolution after p53 loss'. In: *Nature* 608.7924 (Aug. 2022), pp. 795–802. DOI: 10.1038/s41586-022-05082-5.

[210] A Crockford et al. 'Cyclin D mediates tolerance of genome-doubling in cancers with functional p53'. In: *Annals of oncology : official journal of the European Society for Medical Oncology* 28.1 (Jan. 2017), pp. 149–156. DOI: 10.1093/annonc/mdw612.

[211] Tamara A. Potapova et al. 'Transcriptome analysis of tetraploid cells identifies cyclin D2 as a facilitator of adaptation to genome doubling in the presence of p53'. In: *Molecular Biology of the Cell* 27.20 (Oct. 2016), pp. 3065–3084. DOI: 10.1091/mbc.e16-05-0268.

[212] Jingkun Zeng et al. 'Cyclin E-induced replicative stress drives p53-dependent whole-genome duplication'. In: *Cell* 186.3 (2023). DOI: 10.1016/j.cell.2022.12.036.

[213] Marc A. Vittoria et al. 'Inactivation of the Hippo tumor suppressor pathway promotes melanoma'. In: *Nature Communications* 13.1 (June 2022), p. 3732. DOI: 10.1038/s41467-022-31399-w.

[214] Vincent Z. Braun et al. 'Extra centrosomes delay DNA damage–driven tumorigenesis'. In: *Science Advances* 10.13 (Mar. 2024). DOI: 10.1126/sciadv.adk0564.

[215] Claudia Galofré et al. 'Tetraploidy-Associated Genetic Heterogeneity Confers Chemo-Radiotherapy Resistance to Colorectal Cancer Cells'. In: *Cancers* 12.5 (Apr. 2020), p. 1118. DOI: 10.3390/cancers12051118.

[216] Anastasia Y Kuznetsova et al. 'Chromosomal instability, tolerance of mitotic errors and multidrug resistance are promoted by tetraploidization in human cells.' In: *Cell cycle (Georgetown, Tex.)* 14.17 (2015), pp. 2810–20. DOI: 10.1080/15384101.2015.1068482.

[217] Zuzana Storchová et al. 'Genome-wide genetic analysis of polyploidy in yeast'. In: *Nature* 443.7111 (2006). DOI: 10.1038/nature05178.

[218] Pok Man Hau et al. 'Polyploidization increases the sensitivity to DNA-damaging agents in mammalian cells'. In: *FEBS Letters* 580.19 (Aug. 2006), pp. 4727–4736. DOI: 10.1016/j.febslet.2006.07.059.

[219] Zhenye Yang et al. 'Extra centrosomes and/or chromosomes prolong mitosis in human cells'. In: *Nature Cell Biology* 10.6 (2008). DOI: 10.1038/ncb1738.

[220] LA Allan et al. *The mitotic stopwatch limits the proliferation of whole genome doubled cells*. Sept. 2025. DOI: 10.1101/2025.09.18.676992.

[221] Franz Meitinger et al. 'Control of cell proliferation by memories of mitosis'. In: *Science* 383.6690 (Mar. 2024), pp. 1441–1448. DOI: 10.1126/science.add9528.

[222] Carolyn Marquis et al. 'Chromosomally unstable tumor cells specifically require KIF18A for proliferation'. In: *Nature Communications* 12.1 (Feb. 2021), p. 1213. DOI: 10.1038/s41467-021-21447-2.

[223] Jin Zhu et al. 'Cellular Stress Associated with Aneuploidy'. In: *Developmental Cell* 44.4 (Feb. 2018), pp. 420–431. DOI: 10.1016/j.devcel.2018.02.002.

[224] Tsz Yin Lau and Randy Y C Poon. 'Whole-Genome Duplication and Genome Instability in Cancer Cells: Double the Trouble'. In: *International journal of molecular sciences* 24.4 (Feb. 2023). DOI: 10.3390/ijms24043733.

[225] Jordi Barretina et al. 'The Cancer Cell Line Encyclopedia enables predictive modelling of anticancer drug sensitivity'. In: *Nature* 483.7391 (Mar. 2012), pp. 603–607. DOI: 10.1038/nature11003.

[226] Antoine Tinel and Jürg Tschopp. 'The PIDDosome, a Protein Complex Implicated in Activation of Caspase-2 in Response to Genotoxic Stress'. In: *Science* 304.5672 (May 2004), pp. 843–846. DOI: 10.1126/science.1095432.

[227] Valentina Sladky et al. 'The resurrection of the PIDDosome – emerging roles in the DNA-damage response and centrosome surveillance'. In: *Journal of Cell Science* 130.22 (Nov. 2017), pp. 3779–3787. DOI: 10.1242/jcs.203448.

[228] Lenno Krenning, Jonne A Raaijmakers and René H Medema. 'Centrosomes: Please keep your social distance!' In: *The EMBO Journal* 40.4 (2021). DOI: 10.15252/embj.2020107525.

[229] Lavinia Spain et al. 'Late-Stage Metastatic Melanoma Emerges through a Diversity of Evolutionary Pathways'. In: *Cancer Discovery* 13.6 (June 2023), pp. 1364–1385. DOI: 10.1158/2159-8290.CD-22-1427.

[230] Tanja A. Gruber and James R. Downing. 'The biology of pediatric acute megakaryoblastic leukemia'. In: *Blood* 126.8 (Aug. 2015), pp. 943–949. DOI: 10.1182/blood-2015-05-567859.

[231] Valentina C. Sladky et al. *Polyploidy control in hepatic health and disease*. 2021. DOI: 10.1016/j.jhep.2021.06.030.

[232] Shuyuan Zhang et al. 'The Polyploid State Plays a Tumor-Suppressive Role in the Liver'. In: *Developmental Cell* 44.4 (Feb. 2018), pp. 447–459. DOI: 10.1016/j.devcel.2018.01.010.

[233] Ludmil B. Alexandrov et al. 'Signatures of mutational processes in human cancer'. In: *Nature* 500.7463 (Aug. 2013), pp. 415–421. DOI: 10.1038/nature12477.

[234] Jarno Drost et al. 'Use of CRISPR-modified human stem cell organoids to study the origin of mutational signatures in cancer'. In: *Science* 358.6360 (Oct. 2017), pp. 234–238. DOI: 10.1126/science.aao3130.

[235] Francesc Muyas et al. 'De novo detection of somatic mutations in high-throughput single-cell profiling data sets'. In: *Nature Biotechnology* 42.5 (2024). DOI: 10.1038/s41587-023-01863-z.

[236] Gaëlle Marteil et al. 'Over-elongation of centrioles in cancer promotes centriole amplification and chromosome missegregation'. In: *Nature Communications* 9.1 (Mar. 2018), p. 1258. DOI: 10.1038/s41467-018-03641-x.

[237] Susana A Godinho and Renata Basto. 'Centrosomes and cancer: balancing tumor-promoting and inhibitory roles'. In: *Trends in Cell Biology* 35.6 (June 2025), pp. 515–526. DOI: 10.1016/j.tcb.2025.02.009.

[238] Sjoerd J. Klaasen et al. 'Nuclear chromosome locations dictate segregation error frequencies'. In: *Nature* 607.7919 (July 2022), pp. 604–609. DOI: 10.1038/s41586-022-04938-0.

[239] Eléonore Toufektchan and John Maciejowski. 'Purification of micronuclei from cultured cells by flow cytometry'. In: *STAR Protocols* 2.1 (Mar. 2021), p. 100378. DOI: 10.1016/j.xpro.2021.100378.

[240] Xiaowei Yan, Paul Mischel and Howard Chang. 'Extrachromosomal DNA in cancer'. In: *Nature Reviews Cancer* 24.4 (Apr. 2024), pp. 261–273. DOI: 10.1038/s41568-024-00669-8.

[241] Chris Bailey et al. 'Origins and impact of extrachromosomal DNA'. In: *Nature* 635.8037 (Nov. 2024), pp. 193–200. DOI: 10.1038/s41586-024-08107-3.

[242] Jinxin Phaedo Chen et al. 'scCircle-seq unveils the diversity and complexity of extrachromosomal circular DNAs in single cells'. In: *Nature Communications* 15.1 (Feb. 2024), p. 1768. DOI: 10.1038/s41467-024-45972-y.

[243] Lara Wahlster et al. 'ANKRD26-related thrombocytopenia 2 with a baseline increase in blasts: implications for clinical surveillance'. In: *Blood* 146.2 (July 2025), pp. 254–259. DOI: 10.1182/blood.2024027368.

[244] Kristbjorn Orri Gudmundsson and Yang Du. 'Quiescence regulation by normal haematopoietic stem cells and leukaemia stem cells'. In: *The FEBS Journal* 290.15 (Aug. 2023), pp. 3708–3722. DOI: 10.1111/febs.16472.

[245] Liang Zheng et al. 'Modelling ANKRD26 5-prime-UTR mutation-related thrombocytopenia'. In: *Disease Models & Mechanisms* 18.4 (Apr. 2025). DOI: 10.1242/dmm.052222.

[246] Tapan K. Bera et al. 'A model for obesity and gigantism due to disruption of the Ankrd26 gene'. In: *Proceedings of the National Academy of Sciences* 105.1 (Jan. 2008), pp. 270–275. DOI: 10.1073/pnas.0710978105.

[247] Ori Hassin and Moshe Oren. 'Drugging p53 in cancer: one protein, many targets'. In: *Nature Reviews Drug Discovery* 22.2 (Feb. 2023), pp. 127–144. DOI: 10.1038/s41573-022-00571-8.

[248] Lyubomir T. Vassilev et al. 'In Vivo Activation of the p53 Pathway by Small-Molecule Antagonists of MDM2'. In: *Science* 303.5659 (Feb. 2004), pp. 844–848. DOI: 10.1126/science.1092472.

[249] Camelia Iancu-Rubin et al. 'Activation of p53 by the MDM2 inhibitor RG7112 impairs thrombopoiesis'. In: *Experimental Hematology* 42.2 (Feb. 2014), pp. 137–145. DOI: 10.1016/j.exphem.2013.11.012.

[250] John Mascarenhas et al. 'Oral idasanutlin in patients with polycythemia vera'. In: *Blood* 134.6 (Aug. 2019), pp. 525–533. DOI: 10.1182/blood.2018893545.

[251] John Mascarenhas et al. 'Safety and Efficacy of Idasanutlin in Patients (pts) with Hydroxyurea (HU)-Resistant/Intolerant Polycythemia Vera (PV): Results of an International Phase II Study'. In: *Blood* 136.Supplement 1 (Nov. 2020), pp. 29–31. DOI: 10.1182/blood-2020-135868.

[252] Xucheng Hou et al. 'Lipid nanoparticles for mRNA delivery'. In: *Nature Reviews Materials* 6.12 (Aug. 2021), pp. 1078–1094. DOI: 10.1038/s41578-021-00358-0.

[253] Jerry Leung et al. 'Genetically engineered transfusable platelets using mRNA lipid nanoparticles'. In: *Science Advances* 9.48 (Dec. 2023). DOI: 10.1126/sciadv.adi0508.